Deutsches Biomasseforschungszentrum
gemeinnützige GmbH

DBFZ

Tagungsband 4

# 2nd Workshop CFD

## Computational Fluid Dynamics and biomass thermochemical Conversion

9 September 2016 | Leipzig

# 2nd Workshop CFD

*Computational Fluid Dynamics and biomass thermochemical Conversions, 9 September 2016, Leipzig*

- Conference Proceeding -

## *Imprint*

**Published by:**
DBFZ Deutsches Biomasseforschungszentrum
gemeinnützige GmbH
Torgauer Straße 116
04347 Leipzig
Germany
Phone: +49 (0)341 2434-112
Fax: +49 (0)341 2434-133
info@dbfz.de
www.dbfz.de

With support from

Federal Ministry of Food and Agriculture

by decision of the German Bundestag

**General Management:**
Prof. Dr. Michael Nelles
(Scientific Managing Director)
Daniel Mayer
(Administrative Managing Director)

**Tagungsband, Nr. 4**
2nd Computational Fluid Dynamics (CFD) and biomass thermochemical Conversion
Leipzig: DBFZ, 2016
**ISSN:** 2199-9384
**ISBN:** 978-3-946629-07-8

**Editorial deadline:** September 7, 2016
**Date of Publication:** December 19, 2016

Responsibility for the content lies with the publishers.

**Pictures:** DBFZ, © davis - Fotolia.com (Title)
**Editing & DTP:** Daniela Prauß
**Frontpage:** Stefanie Bader



**Organizer:**

DBFZ Deutsches Biomasseforschungszentrum gemeinnützige GmbH
Torgauer Straße 116
04347 Leipzig, Germany
Phone: +49 (0)341 2434 - 112
Fax: +49 (0)341 2434 - 133
info@dbfz.de
Internet: www.dbfz.de

**Scientific Contact:**

Fouzi Tabet
Phone: +49 (0)341 2434-495
E-Mail: fouzi.tabet@dbfz.de

# Words of welcome

## *Dear Participants of the 2nd CFD-Workshop,*

*Fouzi Tabet (DBFZ)*

DBFZ Deutsches Biomasseforschungzentrum gemeinnützige GmbH is actively involved in several areas of CFD (Computational Fluid Dynamics) with an emphasis on biomass thermochemical conversion.

Given the high importance of CFD applications to biomass thermochemical conversion, DBFZ has decided to organize every two years an international workshop on this topic with the aim to provide a forum for researchers and industrials around the world to share practical experiences and address the current opportunities and limitations of CFD in the field of biomass thermochemical conversion.

The 2nd edition of the workshop took place at DBFZ in September the 9th, 2016 at Hotel de Pologne, Leipzig.

The workshop gave an exposure to the major areas of research in CFD applications to biomass thermochemical conversion with special focus on the following topics:

- Small scale combustion
- Medium and large scale combustion
- Co-firing
- Gasification

Several sessions covering the above topics including guest plenary lectures were organized.

The workshop was a great success with high level of participation from countries over the world like Germany, Austria, the Netherlands, France, Belgium, Denmark, Norway, Algeria, etc. The presenters did an outstanding job of sharing their expertise

During this 2nd edition, 13 contributed papers were presented including the plenary lectures. The papers corresponding to the workshop contributions are being published in this proceedings.
Following the recommendations of the participants, the next edition will include more topics within biomass conversion technologies.
I would like to thank the participants (committees members and authors) for their contribution to the 2nd international workshop on CFD (Computational Fluid Dynamics) and biomass thermochemical conversion.

Sincerely,

F. TABET





# *Table of content*

## KEYNOTES



## PRESENTATIONS



## POSTER



## ANNEX

# KEYNOTES





*Dirk Roekaerts (TU Delft, The Netherlands)*

## Development and validation of CFD Models for liquid biofuel combustion

*Dirk Roekaerts*
*Delft University of Technology, Department of Process and Energy*
*Leeghwaterstraat, 39, 2628 CB, Delft, The Netherlands*
*Eindhoven University of Technology, Department of Multiphase and Reacting Flows,*
*Eindhoven, The Netherlands*
*D.J.E.M.Roekaerts@tudelft.nl*

*Likun Ma*
*National University of Defense Technology, College of Aerospace Science and Engineering,*
*Changsha, China*
*malikun-2005@hotmail.com*

*Jeroen van Oijen*
*Eindhoven University of Technology, Department of Multiphase and Reacting Flows,*
*Eindhoven, The Netherlands*
*J.A.v.Oijen@tue.nl*

**KEYWORDS:** Liquid biofuel, ethanol, MILD combustion, CFD, Flamelet Generated Manifolds

**ABSTRACT**

In this paper we present an overview of CFD modeling of spray combustion of liquid biofuels, with focus on the application of Flamelet Generated Manifolds (FGM) on modeling of MILD combustion. Most attention is paid to the case of experimentally well-documented ethanol flames. For each of the model components (atomization, evaporation, dispersion, turbulence, combustion, turbulence-chemistry interaction) a model with best level of accuracy at affordable cost is considered and validated by comparison with experiment. Additional complexity to be taken into account in other biofuels is considered briefly, in the form of a review of recent literature.

### 1. INTRODUCTION

Liquid biofuel comes in several forms from different sources: ethanol from sugar containing crops, directly from plants that contain high amounts of vegetable oil, pyrolysis oil from rapid heating in the absence of oxygen of wood, diesel fuel from Fischer-Tropsch synthesis after gasification of biomass. Also blends of biofuel and fossil fuel are used in practice and their combustion has to be understood.

Depending on the type and application CFD modeling of the combustion of the fuel faces different problems. Clearly the easiest case is ethanol, a single component fuel with known properties and chemical kinetics of combustion. Most other biofuels have in common with fossil fuels that they are multicomponent and then the evaporation is more complex. Furthermore the chemical composition might be varying or to a large extent unknown. Then the formulation of effective properties becomes an essential problem. The case of ethanol will be taken here as example showing the ingredients of a CFD simulation are and the accuracy that can be achieved. More information on the modeling of light fuel spray flames can be found in [1-4]. Next some of the recent applications of CFD to more complex biofuels are reviewed.

Achieving low pollutant emissions while maintaining high efficiency and the required heat flux is a key goal for innovation in combustion research [5-6]. The MILD (Moderate or Intense Low-oxygen Dilution) combustion or "flameless oxidation" [7-9], has been such innovation. This type of combustion also known as flameless combustion arises when fuel and/or oxidizer streams are diluted with products of combustion, leading to avoidance of peak

temperatures and lower NOx formation. An early study on MILD combustion of biofuel was made by Reddy et al [10]. They performed an experimental study of biodiesel fuel MILD combustion in a high swirl combustor, and found that the emission is drastically reduced when the pure biodiesel is blended with conventional diesel. MILD combustion of another biofuel --- Butyl Nonanoate (BN) was investigated by Khalil and Gupta [11] under gas turbine condition. 15% reduction in NO emission compared to JP8 was observed, and CO emission was also lower than JP8. These studies have demonstrated the promising performance of the MILD combustion technology for liquid biofuels. The ethanol flames described below are also taken from a database of flames mimicking MILD combustion conditions, but focusing on local flame measurements rather than emissions.

## 2. MODEL COMPONENTS

Spray combustion involves many phenomena and processes and the strong coupling between them makes modeling of it very difficult [12]. Fig.1 illustrates the key processes in the *dilute* region of spray combustion and the interactions between them. Here *dilute* refers to the situation that the liquid volume fraction is less than $10^{-3}$. For the gas phase, the turbulence, dispersion, micro-mixing and combustion have to be considered. And for the liquid phase, the atomization, dispersion and evaporation require to be modeled. Fuel jet break up and atomization in general take place in the dense region close to the injector. The two phases are closely coupled through momentum, heat and mass transfer. In this section we describe the main model components for modeling turbulent spray combustion.

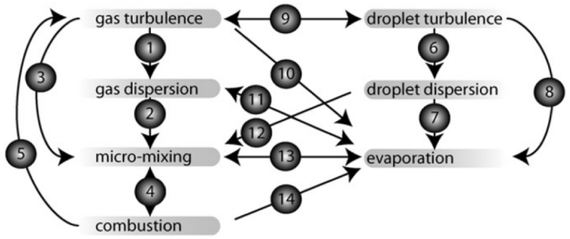


*Figure 1: Phenomena and their interactions in dilute turbulent spray combustion[12]*

### 2.1. Atomization model

The atomization process can be divided into primary breakup and secondary breakup. The primary breakup is the process that liquid jet or sheet disintegrates into irregular-shaped ligaments or large droplets. The secondary breakup refers to the process of the further disintegration of these large droplets and ligaments into even smaller fragments. Gorokhovski and Herrmann [13] give a review on the modeling of primary atomization.
Disintegration of a liquid jet may be caused by many factors, for instance, the turbulence in the liquid jet, cavitation in the nozzle and the interfacial forces between the liquid jet and the surrounding medium [14]. Owing to the rich physics involved and strong configuration and operation condition dependence, the mechanism of atomization is still far from been fully understood. Although DNS is a very attractive tool to create understanding of this complicated process [15], it is too computationally expensive and practical simulations of spray combustion still rely on correlations and simple models. The LISA (Linearized Instability Sheet Atomization) model [16] and the ELSA (Eulerian-Lagrangian Spray Atomization) model [17-19] are examples. Provided detailed experimental information on the spray just after atomization is known, atomization modeling is not needed and simple mechanistic models for droplet injection can be used. An example of this is the conditional droplet injection model (CDIM) [1].

### 2.2. Dispersion model in Eulerian-Lagrangian framework

In the Eulerian-Lagrangian CFD framework for dispersed multiphase flow the gas phase is described by the usual transport equations for momentum, energy and mass fractions. The droplets are considered as entities exchanging mass momentum and energy with the continuum. Evolution of droplet position and velocity is often described





based on the assumption of spherical droplets and no internal flow pattern (based on high liquid to gas density ratio and inertial forces balanced by surface tension and viscosity). Then dominant for droplets are the drag and gravitational forces, and therefore the particle momentum equation, also known as BBO (Basset-Boussinesq-Oseen) equation [20], is greatly simplified. The droplet motion can be described as:

$$\frac{d\mathbf{X}}{dt} = \mathbf{U}_p, \tag{1}$$

$$\frac{d\mathbf{U}_p}{dt} = \frac{\mathbf{U}_{seen} - \mathbf{U}_p}{\tau_\mathrm{p}} + \mathbf{g}, \tag{2}$$

where $\mathbf{X}$ and $\mathbf{U}_p$ are the droplet position and velocity vectors, and $\mathbf{U}_{seen}$ is the gas phase velocity "seen" by the droplets. $\tau_\mathrm{p}$ is the droplet relaxation time for Stokes flow:

$$\tau_\mathrm{p} = \frac{\tau_p^{St}}{C_D}, \quad \tau_p^{St} = \frac{\rho_{liq} D_p^2}{18\mu_\mathrm{m}}. \tag{3}$$

The deviation from Stokes drag $(C_D)$ in most cases is given by the Schiller-Naumann correlation:

$$C_D = \begin{cases} 1 + 0.15 Re_p^{0.687}, & Re_p \le 1000 \\ 0.44 Re_p / 24, & Re_p > 1000 \end{cases} \tag{4}$$

The droplet Reynolds number $\mathrm{Re}_p$ is defined as:

$$\mathrm{Re}_\mathrm{p} = \frac{\rho_\mathrm{g} |\mathbf{U}_\mathrm{seen} - \mathbf{U}_\mathrm{p}| D_\mathrm{p}}{\mu_\mathrm{m}}, \tag{5}$$

$D_p$ is the droplet diameter, $\rho_g$ the gas phase density and $\mu_m$ the gas phase viscosity evaluated at the film (subscript "m") condition (see Eqs. 8 and 9).
Some other empirical corrections are reported in literature [21]. Sazhin et al. [22] have suggested a modification of $C_D$ for the effect of evaporation on drag :

$$C_{D,evp} = \frac{C_D}{(1+B_M)^\alpha}, \quad \alpha = \begin{cases} 1, & B_M < 0.78 \\ 0.75, & B_M \ge 0.78 \end{cases} \tag{6}$$

where $B_M$ is the Spalding mass transfer number. In order to calculate droplet drag force, the seen gas phase velocity, $\mathbf{U}_{seen}$, has to be provided. It can be decomposed as follows:

$$\mathbf{U}_{seen} = \widetilde{\mathbf{U}}\left(\mathbf{x}_p, t\right) + \mathbf{u}''_{\mathbf{seen}} \tag{7}$$

where $\widetilde{\mathbf{U}}$ is the mean continuous phase velocity, given by solving the Favre-averaged or filtered Navier-Stokes equation. The process of determining the fluctuating component, $\mathbf{u}''_{\mathbf{seen}}$, is called dispersion modeling [23]. Two main groups of dispersion models are the Continuous Random Walk (CRW) model and the Langevin model. In RANS and LES modeling of turbulence, the droplet seen velocity fluctuation $\mathbf{u}''_{\mathbf{seen}}$ are respectively related to the modeled gas phase Reynolds stresses and subgrid stresses [23-24].

### 2.3. Evaporation model

The heat and mass transfer between liquid and gas phase is described by a submodel for evaporation. The baseline models consider the case of a single component liquid, far away from supercritical conditions.

Then a complete single droplet evaporation model includes four parts: Liquid Phase Model (LPM), Droplet Surface Properties (DSP) model, gas side Heat and Mass Transfer (HMT) model and “Seen” Gas Properties (SGP) model, see Fig. 2. In the HMT model for standard heating conditions, radiative transfer can be neglected for small droplets.

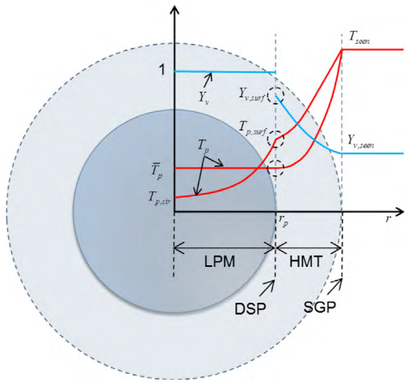


*Figure 2: Illustration of baseline evaporation modelling*

The LPM describes the evolution of droplet temperature. A wide range of droplet heating models have been reported in literature, the infinite conductivity model (uniform droplet temperature) is the most commonly used one. The DSP determines how the mass fraction of fuel vapor at droplet surface, $Y_{v,surf}$, is calculated. The surface fuel mass fraction is obtained from Raoult’s Law, saying that the mole fraction at the droplet surface is equal to the ratio of the partial pressure of fuel vapor to the total pressure of the gas. Various correlations exist to evaluate the partial pressure of fuel vapor at droplet surface. If it is assumed that the equilibrium between gas and droplet surface has been reached at each time step, the mole fraction of fuel vapor $X_{v,surf}$ at the droplet surface can be calculated from the Clausius-Clapeyron equation, this model is referred to as equilibrium model. For rapidly evaporation small droplets the non-equilibrium effect is to be considered, for example by using Langmuir-Knudsen law, the model is then referred to as non-equilibrium model.
Nusselt and Sherwood numbers, Nu and Sh describe the enhancements of heat and mass transfer by the convective flow. The HMT model describes the method of evaluating these two quantities. In the widely used Abramzon and Sirignano model, these two quantities are calculated in an iterative way that takes into account the effects of Stefan flow. A correction proposed by Bird et al. has been found to perform equally well [4].
Within a thin film surrounding the droplets, gas phase conditions change quickly from properties at the droplet surface to properties away from the droplet in the “seen” gas phase. The representative gas phase properties (indicated by subscript “m”) used in the evaporation and dispersion model are evaluated as a weighted averages of droplet surface properties and “seen” gas properties:

$$T_m = (1-\alpha)\,T_{surf} + \alpha\,T_{seen} \quad \text{and} \quad Y_m = (1-\alpha)\,Y_{surf} + \alpha\,Y_{seen} \tag{8}$$

$$\mu_m = \mu(T_m, Y_m), \quad \lambda_m = \lambda(T_m, Y_m), \quad D_m = D(T_m, Y_m), \quad C_{p,m} = C_p(T_m, Y_m). \tag{9}$$

Using $\alpha = 1/3$ (the “1/3 rule”) has been found to perform well in spray combustion simulations.

## 2.4. Turbulent two-way coupling

In turbulence modeling by either RANS or LES unclosed terms have to be modeled. As part of this procedure, the influence of the dispersed phase on gas phase flow is accounted for by the so-called “two-way coupling” terms. For more information on the turbulent two-way coupling, we refer to [12] and [25]. The models can be simply based on summation of effects of individual droplets behavior as described above, but additional effects due to wake effects and flame kernel effects around droplets may be important [26-27].





## 2.5. Combustion models for spray combustion

The local flame structure in turbulent spray flames can be very complex and has been represented in models in a variety of ways as reviewed in [12]. A compromise has to be between accuracy and cost. Flamelet-based models assume that mean (in RANS) or filtered (in LES) composition and/or source terms can be obtained by averaging over properties of laminar local states. They offer the advantage that detailed chemistry (accurate) is included in pre-calculated (low cost) flame properties stored in a lookup table. The challenge is in the selection of the flamelet type and of the parameters describing the local state. Well known examples are Flamelet/Progress Variable (FPV) [28], and Flamelet Generated Manifolds (FGM) [29] models.
Most often, the mixture fraction Z, which represents the extent of mixing between “fuel stream” and “oxidizer stream”, and a progress variable, which denotes the progress of chemical reaction from “pure mixing” to “fully burnt”, are chosen as independent variables. The dimension of the lookup table can be extended to incorporate more physics when required, for example, adding enthalpy to account for the heat loss/gain [1], adding scalar dissipation rate $\chi$ to consider the influence of strain [30] and adding pressure to take into account the effect of pressure variation [31].
Recently the FGM method has been extended towards the use of a multistage FGM. Taking into account that in different regions of a flame, different key processes occur and different progress variables are optimal, this method uses several different progress variables for parameterization of different regions of the flame [32]. This development was especially motivated by the need to accurately describe flames in MILD combustion. In modeling of MILD combustion auto-ignition is to be represented accurately and this implies that the flamelets and the progress variable used in FGM method have to be chosen carefully.
In most studies using flamelet models for spray flames gaseous flamelets have been used to represent the local flame structure of turbulent spray flames. This may not be sufficiently accurate and many studies have also been made on using laminar *spray* flames and the development of spray flamelet models for turbulent spray flames [33-39].
Not only flamelet based but also other turbulent combustion models have been extended to model spray combustion: recent developments include Conditional Moment Closure (CMC) [40], Probability Density Function (PDF) or Filtered Density Function (FDF) [41-42], two phase turbulent combustion model (FSM) [43] and second-order moment (SOM) turbulent combustion model [44].

# 3. VALIDATION STUDIES

Modeling of spray combustion involves many different model components. Careful validation of the numerical results with available experimental data is crucial for the building of reliable modeling approaches. In this section some results of the application of the type of models described above to lab-scale ethanol flames are reported, demonstrating the high level of accuracy that can be achieved.

## 3.1. Target test dataset

The Delft Spray-in-Hot-Coflow (DSHC) burner was designed to study the fundamental aspects of flameless oxidation of representative biofuels --- ethanol and acetone [45]. With different spray and gas phase properties measured and influences of coflow conditions and fuel flexibility studied, the DSHC dataset provides a valuable basis for the development and validation of modeling methods towards the application of MILD spray combustion [45].
The schematic of the DSHC burner is shown in Fig.3. The liquid fuel (ethanol) is injected into the hot-diluted coflow by a pressure-swirl atomizer. A secondary burner matrix generates a hot-diluted coflow. This emulates the air diluted by recirculated combustion products in a large scale MILD combustion furnace. Comprehensive laser diagnostic measurements, including Laser Doppler Anemometry (LDA), Phase Doppler Anemometry (PDA) and Coherent Anti-Stokes Raman Scattering (CARS) have been conducted. Gas phase velocity components, temperature and $O_2$ volume fraction have been measured along the radial direction at coflow exit (Z=0 mm). Droplets properties (velocity, diameter, number concentration and mass flux) have been measured along the radial direction at different axial locations (Z=8, 10, 12, 15, 20, 30, 35, 40, 45 mm).

Gas phase temperature has been measured with CARS technique along the radial direction at different axial locations (Z=15, 20, 30, 40, 50, 60 mm). For further details about the DSHC burner and the database, the readers are referred to [46-47].

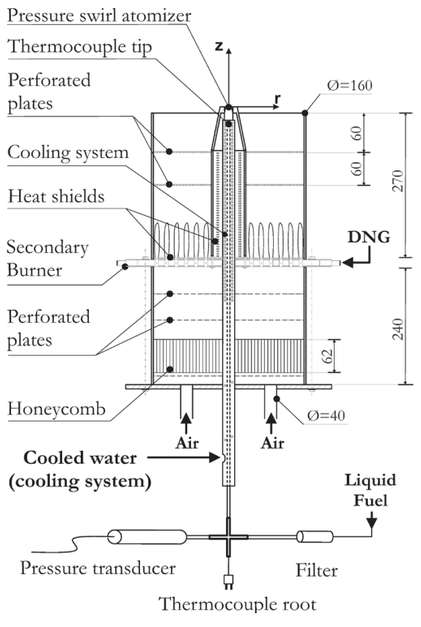


*Figure 3: Schematic of the DSHC burner [46]*

### 3.2. Validation procedure

In refs. [1-4], the following three steps have been taken to develop, validate and apply the modeling approaches:

1. Test performance of different models on a selected test case;
2. Test performance of selected models on a series of test cases;
3. Explore predictions of selected models on other cases.

Many different modeling methods, and model components have been first tested, compared or developed. The target case for all these studies was the same, namely case Hii of the the Delft Spray-in-Hot-Coflow (DSHC) flames, which has the typical MILD condition, and most importantly has an extensive well defined experimental dataset.

### 3.3. Step 1: testing model performance on a selected case

For the selected test case (case Hii), the performance of different models was studied. In all cases the atomization was represented using a newly developed conditional droplet injection model [1]. Performance of different models for evaporation, dispersion, turbulence and combustion was compared. Because sufficiently fine grids (fine: 2.2x10$^6$ cells; coarse 0.3x10$^6$ cells) were used the dispersion model was considered not critical and influence of subgrid velocity fluctuations on droplet dispersion was neglected. Subgrid scalar fluctuations were included using a presumed PDF method, requiring solution of a model for the scalar variance.





*Table 1: Final selection of models for the DSHC simulations*

| Process / phenomena | | Models |
|---|---|---|
| Atomization | | Conditional Droplet Injection Model |
| Evaporation | LPM | Infinite conductivity |
| | DSP | Equilibrium model |
| | HMT | Ranz-Marshall correlation with Bird's correction |
| | SGP | 1/3-rule |
| Dispersion | | Droplets influenced by mean or resolved velocity field only |
| Combustion | | Non-adiabatic FGM |
| Turbulence | | Unsteady-RANS or LES |

Table 1 shows the combination of models producing most satisfactory results for almost all properties when compared with experimental data.

Fig. 4 gives an example of model comparison. Here the results of LES and URANS are compared to experimental results. In this figure, results from three cases have been compared, LES with fine mesh, LES with coarse mesh and URANS with coarse mesh. The latter two cases use the same mesh. The mean gas phase temperature is significantly improved in terms of well-captured peak temperature as well as the radial width of temperature peak in the LES cases compared to the URANS case, regardless the mesh used. This means that the better prediction of temperature field in the LES is mainly due to the better performance of the dynamic algebraic model used for the mixture fraction variance in LES cases as compared to the variance transport equation with fixed model constants used in the RANS case.

### 3.4. Step 2: testing selected model on a series of test cases

The second step of validation was to apply the best combination of models developed or identified in the first step to a wide range of cases in order to further check its capabilities and limitations. For this purpose, two more hot-diluted coflow cases and the cold coflow case were respectively investigated.

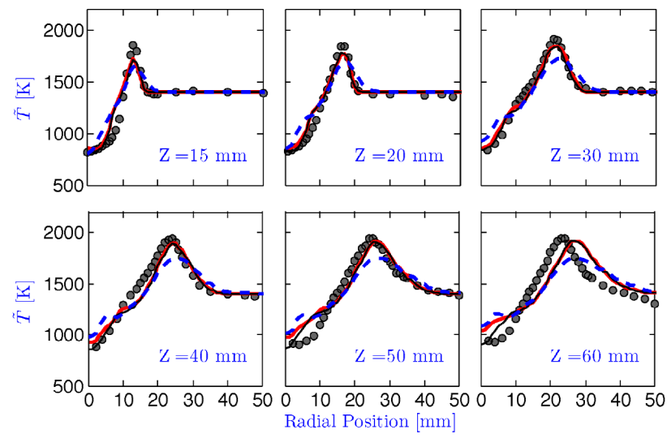


*Figure 4: Radial profiles of mean gas phase temperature, gray dot: experimental data, solid red line: LES with fine mesh, solid black line: LES with coarse mesh, dashed blue line: URANS with coarse mesh*

However, for the cold coflow case a non-adiabatic FGM was used. With little or no influence on the predictions. These results clearly demonstrated that the model approach is not only able to accurately capture important trends

such as the change of flame lift-off heights and flame width with varying coflow conditions, but also correctly reproduced the multi-flame structure in the case Aii. The conditions of the studied cases are shown in Fig. 5.

*Figure 5: DSHC cases that are employed for model validation depending on temperature and coflow oxygen mole fraction of the coflow (Hi, Hii, Hiii cases with hot diluted coflow; Aii case with air coflow)*

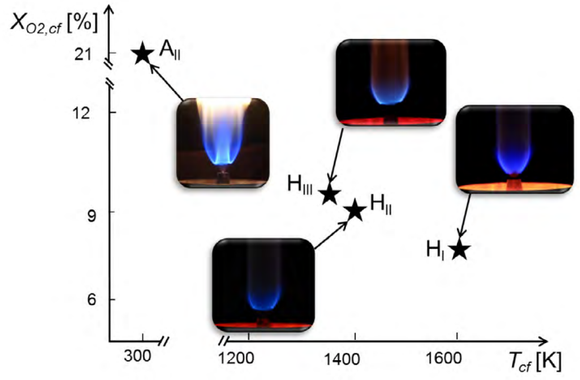


### 3.5. Step 3: explore predictions on other cases

Based on the confidence gained in the previous two steps, some virtual numerical cases have been explored in order to gain deeper insight on the MILD spray combustion [2,4]. For example, due to the limitation of the DSHC burner configuration, the influence of the coflow temperature and $O_2$ concentration, which are two important parameters for the establishment of MILD combustion, cannot be studied independently in the experiment. On the contrary, this can be easily done in the numerical simulation. With this parametric study, the impacts of these two parameters have been identified, and a suitable combination of them for the establishment of a MILD spray combustion was suggested. Another example of the studying of virtual cases is the exploration of the influence of spray polydispersity on the flame structure. Zones of heat release and/or presence of certain species can be identified. Species predictions can be very detailed because of the information contained in the FGM, but are based on an assumed local flamelet structure.

## 4. COMPLEX FUELS AND APPLICATIONS

### 4.1. Evaporation modeling

Most biofuels consists of very many components. Then relative volatility of components is a key feature and a multicomponent formulation of evaporation is required. Two main approaches exist: either using a continuous distribution function of mole fractions of the components characterised by molar mass or using a representation of the mixture using a small number of discrete components, i.e. using a surrogate mixture. The influence of the heat and mass transfer limitations inside the droplet on evaporation of a binary mixture was studied in [48]. Evaporation of a bio-oil drop based on a discrete approach with 10 components, representing pyrolysis oil was studied in [49], and also mixtures with other fuels (diesel, biodiesel, ethanol). Pyrolysis oil drops were found to have a longer lifetime than other fuels. In [50] both a continuous model and a discrete multicomponent model were developed and implemented in OpenFOAM and applied to predict measured properties of swirl stabilised flames of diesel and biodiesel. The impact of relative abundance of species and relative volatility were determined.

### 4.2. Biofuel combustion in engines

In principle reaction mechanisms are needed to handle fuel effects and emissions. But the literature shows examples with a wide range of chemical complexity taken into account, as shown by the next two examples.





In a CFD studies of biodiesel combustion in a light-duty diesel engine presented in [51,52] detailed mechanisms are used. In [51] a reaction mechanism of 80 species and 303 reactions is used, capable of emulating biodiesel-diesel mixtures of different blending levels and biodiesel produced from different feedstock. The simulated cases were validated for in-cylinder pressure profiles and peak pressure values and timings and emissions. The RANS CFD model implemented in OpenFOAM included the unsteady flamelet model. Both ignition and combustion processes are accounted using the same chemical kinetic mechanism. In [52] combustion of fossil diesel and the methyl esters of coconut (CME), palm (PME) and soy (SME) across three engine conditions is studied and the models for physical properties and chemical mechanisms are further elaborated.
In [53] AVL FIRE 3D CFD code was used for the simulation of biodiesel's influence on the injection characteristics and the operating conditions of a heavy-duty diesel engine. Mineral diesel oil and biodiesel from rapeseed were compared. The MCC model is used. It divides the combustion process in a premixed stage and a non-premixed stage and the heat release curve is described by a Vibe function. The rate of NOx formation is based on the Zel'dovich mechanism and a CO formation model calibrated with actual data. Among the aspects discussed are the influence of biodiesel composition on Sauter Mean Diameter, the role of calorific value and oxygen content of the biodiesel.

### 4.3. Pyrolysis oil gasification

Pyrolysis oil can be used as fuel for a gasifier. In order to model this process a chemical mechanism is needed. A large simplification occurs if the combustion or gasification of a complex fuel is represented by the combustion of a model substance. Ethylene glycol has been proposed as model fuel for the study of pyrolysis oil gasification, because of its similar physical properties (viscosity and spray behavior) and equal C/H/O ratio. But also for the model substance a mechanism has to be proposed. Ref. [54] describes development and validation of a detailed chemical kinetic model of ethylene glycol gasification. It contains 80 species and 1243 reactions. The mechanism is validated using ignition delay times, laminar flame speeds and concentration profiles in laminar flames of several fuels (ethanol, acetaldehyde, ethane). A reduced version of the developed mechanism was also developed. It was implemented in ANSYS Fluent 12.0 and used in combination with the Eddy Dissipation Concept model for turbulence-chemistry interaction to predict the reacting flow in an entrained flow gasifier. Predictions of CO and $CO_2$ mole fraction as function of distance from the burner were found to be in acceptable agreement with experimental measurements.

## 5. CONCLUSIONS AND RECOMMENDATIONS

We have given an overview description of the model components that are required for CFD modeling of turbulent spray combustion of liquid biofuel. The study of ethanol combustion in a labscale burner mimicking MILD combustion has been used as an example to demonstrate the validation process for spray combustion simulation. For this simple fuel properties and chemical mechanism are available. To reach good agreement with detailed experimental measurements the following aspects were found most crucial: representation of the initial conditions of the spray, droplet evaporation models, influence of turbulent fluctuations. In case of biodiesel or pyrolysis oil these three aspects remain important, but in addition information on chemical composition and chemical mechanism has to be provided or developed. A wide variety of models for turbulence chemistry interaction are used in CFD simulations of liquid fuel flames. FGM and similar methods offer a powerful tool to keep information from underlying detailed chemistry while working with a limited number of variables to be solved in the turbulent flow calculation. In the simulation of low emission techniques as MILD or flameless combustion special attention is needed for the simulation of the ignition process. This can be done using the newly developed multistage FGM method. A lot of useful information on how to select models and accurately perform CFD simulations of turbulent combustion can be found in Ref. [55]

## 6. ACKNOWLEDGEMENTS

The reported ethanol flame simulations were sponsored by NWO Physical Sciences for the use of supercomputer facilities (Cartesius).

## 7. REFERENCES


[01] L. Ma and D. Roekaerts, Modeling of spray jet flame under MILD condition with non-adiabatic FGM and a new conditional droplet injection model, *Combust. Flame*, vol. 165, pp. 402–423, 2016.

[02] L. Ma and D. Roekaerts, Structure of spray in hot-diluted coflow flames under different coflow conditions: A numerical study, *Combust. Flame*, vol. 172, pp. 20–37, 2016.

[03] L. Ma and D. Roekaerts, Numerical study of the multi-flame structure in spray combustion, *Proc. Combust. Inst.*, in press, 2016.

[04] L. Ma, Computational Modeling of Turbulent Spray Combustion, PhD Thesis, Delft University of Technology, 2016.

[05] H.J. Kim, S.H. Park, K.S. Lee, and C.S. Lee, A study of spray strategies on improvement of engine performance and emissions reduction characteristics in a DME fueled diesel engine, *Energy*, vol. 36, no. 3, pp. 1802–1813, 2011.

[06] G. Valentino, L. Allocca, S. Iannuzzi and A. Montanaro, Biodiesel/mineral diesel fuel mixtures: Spray evolution and engine performance and emissions characterization, *Energy*, vol. 36, no. 6, pp. 3924–3932, 2011.

[07] A. Cavaliere and M. de Joannon, Mild Combustion, *Prog. Energy Combust. Sci.*, vol. 30, no. 4, pp. 329–366, 2004.

[08] J. A. Wünning and J. G. Wünning, Flameless oxidation to reduce thermal NO-formation, *Prog. Energy Combust. Sci.*, vol. 23, no. 1, pp. 81–94, 1997.

[09] S. Kruse, B. Kerschgens, L. Berger, E. Varea, and H. Pitsch, Experimental and numerical study of MILD combustion for gas turbine applications, *Appl. Energy*, vol. 148, pp. 456–465, 2015.

[10] V. Mahendra Reddy, D. Sawant, D. Trivedi and S. Kumar, Studies on a liquid fuel based two stage flameless combustor, *Proc. Combust. Inst.*, vol. 34, no. 2, pp. 3319–3326, 2013.

[11] A. E. E. Khalil and A. K. Gupta, Clean combustion in gas turbine engines using Butyl Nonanoate biofuel, *Fuel*, vol. 116, pp. 522–528, 2014.

[12] P. Jenny, D. Roekaerts and N. Beishuizen, Modeling of turbulent dilute spray combustion, *Prog. Energy Combust. Sci.*, vol. 38, no. 6, pp. 846–887, 2012.

[13] M. Gorokhovski and M. Herrmann, Modeling Primary Atomization, *Annu. Rev. Fluid Mech.*, vol. 40, no. 1, pp. 343–366, 2008.

[14] M. Birouk and I. Gokalp, Current status of droplet evaporation in turbulent flows, *Prog. Energy Combust. Sci.*, vol. 32, no. 4, pp. 408–423, 2006.

[15] J. Shinjo and A. Umemura, Detailed simulation of primary atomization mechanisms in Diesel jet sprays (isolated identification of liquid jet tip effects), *Proc. Combust. Inst.*, vol. 33, no. 2, pp. 2089–2097, 2011.

[16] P. Senecal, D. Schmidt, I. Nouar, C., Rutland, R. Reitz and M. Corradini, Modeling high-speed viscous liquid sheet atomization, *Int. J. Multiph. Flow*, vol. 25, no. 6–7, pp. 1073–1097, 1999.

[17] A. Vallet and R. Borghi, Modélisation eulerienne de l'atomisation d'un jet liquide, *Comput. fluid Mech.*, vol. 327, no. 10, pp. 1015–1020, 1999.

[18] D. Lakehal, M. Meier and M. Fulgosi, Interface tracking towards the direct simulation of heat and mass transfer in multiphase flows, *Int. J. Heat Fluid Flow*, vol. 23, pp. 242–257, 2002.

[19] R. Lebas, T. Menard, P.A. Beau, A. Berlemont and F.X. Demoulin, Numerical simulation of primary break-up and atomization: DNS and modelling study, *Int. J. Multiph. Flow*, vol. 35, no. 3, pp. 247–260, 2009.

[20] J.S. Shirolkar, C.F.M. Coimbra and M.Q. Mcquay, Fundamental aspects of modeling turbulent particle dispersion in dilute flows, *Prog. Energy Combust. Sci.*, vol. 22, no. 96, pp. 363–399, 1996.

[21] R. S. Miller, K. Harstad and J. Bellan, Evaluation of equilibrium and non-equilibrium evaporation models for many-droplet gas-liquid flow simulations, *Int. J. Multiph. Flow*, vol. 24, pp. 1025–1055, 1998.

[22] S. S. Sazhin, W.A. Abdelghaffar, E. M. Sazhina and M.R. Heikal, Models for droplet transient heating: Effects on droplet evaporation, ignition, and break-up, *Int. J. Therm. Sci.*, vol. 44, pp. 610–622, 2005.

[23] E. Amani and M.R.H. Nobari, Systematic tuning of dispersion models for simulation of evaporating sprays, *Int. J. Multiph. Flow*, vol. 48, pp. 11–31, 2013.

[24] B. Naud, Particle dispersion modelling based on the Generalised Langevin Model for the seen velocity, in *Turbulence, Heat and Mass Transfer 7*, 2012, no. 1.

[25] N.A. Beishuizen, PDF modelling and particle-turbulence interaction of turbulent spray flames, PhD Thesis, Delft University of Technology, 2008.

[26] J. Shinjo and A. Umemura, Droplet/turbulence interaction and early flame kernel development in an autoigniting realistic dense spray, *Proc. Combust. Inst.*, vol. 34, no. 1, pp. 1553–1560, 2013.

[27] J. Shinjo, J. Xia and A. Umemura, Droplet/ligament modulation of local small-scale turbulence and scalar mixing in a dense fuel spray, *Proc. Combust. Inst.*, 2014.

[28] C. D. Pierce and P. Moin, Progress-variable approach for large-eddy simulation of non-premixed turbulent combustion, *J. Fluid Mech.*, vol. 504, pp. 73–97, 2004.

[29] J.A. van Oijen and L.P.H. de Goey, Modelling of Premixed Laminar Flames using Flamelet-Generated Manifolds, *Combust. Sci. Technol.*, vol. 161, no. 1, pp. 113–137, 2000.

[30] M. Ihme and Y.C. See, Prediction of autoignition in a lifted methane/air flame using an unsteady flamelet/progress variable model, *Combust. Flame*, vol. 157, no. 10, pp. 1850–1862, 2010.

[31] C. Bekdemir, Tabulated Chemical Kinetics for Efficient and Detailed Simulations of Diesel Engine Combustion, PhD Thesis, Eindhoven University of Technology, 2012.

[32] M.U. Göktolga, J.A. van Oijen, and L.P.H. de Goey, Modeling MILD combustion using a novel multistage FGM method, *Proc. Combust. Inst.*, in press, 2016

[33] E. Gutheil and W. A. Sirignano, Counterflow Spray Combustion Modeling with Detailed Transport and Detailed Chemistry, *Combust. Flame*, vol. 113, no. 1–2, pp. 92–105, 1998.

[34] H. Watanabe, R. Kurose, S. Hwang and F. Akamatsu, Characteristics of flamelets in spray flames formed in a laminar counterflow, *Combust. Flame*, vol. 148, no. 4, pp. 234–248, 2007.

[35] Y. Baba and R. Kurose, Analysis and flamelet modelling for spray combustion, *J. Fluid Mech.*, vol. 612, pp. 45–79, 2008.

[36] B. Franzelli, B. Fiorina and N. Darabiha, A tabulated chemistry method for spray combustion, *Proc. Combust. Inst.*, vol. 34, no. 1, pp. 1659–1666, 2013.

[37] H. Olguin and E. Gutheil, Influence of evaporation on spray flamelet structures, *Combust. Flame*, vol. 161, no. 4, pp. 987–996, 2014.

[38] K. Luo, J. Fan and K. Cen, New spray flamelet equations considering evaporation effects in the mixture fraction space, *Fuel*, vol. 103, pp. 1154–1157, 2013.

[39] B. Franzelli, A. Vié and M. Ihme, On the generalisation of the mixture fraction to a monotonic mixing-describing variable for the flamelet formulation of spray flames, *Combust. Theory Model.*, vol. 7830, no. November, pp. 1–34, 2015.

[40] S. Ukai, A. Kronenburg and O.T.T. Stein, LES-CMC of a dilute acetone spray flame, *Proc. Combust. Inst.*, vol. 34, no. 1, pp. 1643–1650, 2013.

[41] S. Bhattacharjee and D.C. Haworth, Simulations of transient n-heptane and n-dodecane spray flames under engine-relevant conditions using a transported PDF method, *Combust. Flame*, vol. 160, no. 10, pp. 2083–2102, 2013.

[42] W.P. Jones, A.J. Marquis and K. Vogiatzaki, Large-eddy simulation of spray combustion in a gas turbine combustor, *Combust. Flame*, vol. 161, no. 1, pp. 222–239, 2014.

[43] F. Wang, B. Hu and Y. Huang, A two-phase turbulent combustion model and its validation for spray flames, *Fuel*, vol. 113, pp. 280–286, 2013.

[44] K. Luo, Y. Bai, J. Yang, H. Wang, L. Zhou and J. Fan, A-priori validation of a second-order moment combustion model via DNS database, *Int. J. Heat Mass Transf.*, vol. 86, pp. 415–425, 2015.

[45] H. Correia Rodrigues, Spray combustion in moderate and intense low-oxygen conditions - an experimental study, PhD Thesis, Delft University of Technology, 2015.

[46] H. Correia Rodrigues, M.J. Tummers, E.H. van Veen and D.J.E.M. Roekaerts, Spray flame structure in conventional and hot-diluted combustion regime, *Combust. Flame*, vol. 162, pp. 759–773, 2015.

[47] H. Correia Rodrigues, M.J. Tummers, E.H. van Veen and D.J.E.M. Roekaerts, Effects of coflow temperature and composition on ethanol spray flames in hot-diluted coflow, *Int. J. Heat Fluid Flow*, vol. 51, pp. 309–323, 2015.
[48] P. Keller, A. Bader and C. Hasse, The influence of intra-droplet heat and mass transfer limitations in evaporation of binary hydrocarbon mixtures, *Int. J. Heat Mass Transf*, Vol. 67, pp. 1191-1207, 2013.
[49] Lei Zhang and Song-Charng Kong, Multicomponent vaporization modeling of bio-oil and its mixtures with other fuels, *Fuel,* Vol. 95, pp. 471-480, 2012.
[50] M.F. Mohd Yasin, R.S. Cant, C.T. Chong and S. Hochgreb, Discrete multicomponent model for biodiesel spray combustion simulation, *Fuel,* Vol. 126, pp. 44-54, 2014.
[51] Harun Mohamed Ismail, Hoon Kiat Ng, Suyin Gan and Tommaso Lucchini, Computational study of biodiesel–diesel fuel blends on emission characteristics for a light-duty diesel engine using OpenFOAM, *Applied Energy*, Vol. 111, pp. 827–841, 2013.
[52] Hoon Kiat Ng, Suyin Gan, Jo-Han Ng and Kar Mun Pang, Simulation of biodiesel combustion in a light-duty diesel engine using integrated compact biodiesel–diesel reaction mechanism, *Applied Energy,*Vol. 102, pp. 1275-1287, 2013.
[53] Luka Lešnik, Blaz Vajda, Zoran Zunic, Leopold Škerget and Breda Kegl, The influence of biodiesel fuel on injection characteristics, diesel engine performance, and emission formation, *Applied Energy,* Vol. 111, pp. 558–570, 2013.
[54] Simon Hafner, Arash Rashidi , Georgiana Baldea and Uwe Riedel, A detailed chemical kinetic model of high-temperature ethylene glycol gasification, Combust. Theory Model, Vol. 15(4), pp. 517-535, 2011.
[55] ERCOFTAC Best Practice Guidelines Computational Fluid Dynamics of Turbulent Combustion, L. Vervisch and D. Roekaerts (Editors), ERCOFTAC, 2016, www.ercoftac.org





*Miguel A. Gómez (University of Vigo, Spain)*

# Contributions in modelling of biomass combustion for applications in small-scale boilers

*Miguel A. Gómez*
*Defense University Center, Spanish Naval Academy*
*Plaza de España s/n 36900 Marín, Spain*
*miguelgr@uvigo.es*

*Jacobo Porteiro, Sergio Chapela, José Luis Míguez*
*Industrial Engineering School, University of Vigo*
*Lagoas-Marcosende s/n 36310 Vigo, Spain*
*porteiro@uvigo.es, schapela@uvigo.es, jmiguez@uvigo.es*

**KEYWORDS:** CFD modelling, biomass combustion, thermally thin, thermally thick

## ABSTRACT

Two biomass combustion model with thermally thin and thermally thick approaches are presented and applied in the simulation of a commercial biomass domestic boiler. The models are based in several Eulerian variables that define the solid phase in the packed bed which is calculated as a porous zone with a volume-averaged approach. The combustion models are coupled with a fuel-feeding model based on Lagrangian trajectories of particles, which are transformed into the solid phase variables when the particles reach the packed bed. The method is applied to a 27-kW boiler operating in stable conditions with two feeding systems. The model variables are visualized and the boiler behaviour is compared with the experimental measurements. The CFD model gives reasonably good predictions of the heat transferred, flue gases temperatures, air excess index and $CO_2$ emissions as well as the fluctuations of the boiler when the feeding rate is not stable.

## 1. INTRODUCTION

The study of biomass combustion is currently receiving increased interest due to the effects of greenhouse gas emissions and the lack of fossil fuel resources in certain areas of the world. Understanding biomass behaviour in the combustion process is a key factor in designing and improving combustion systems such as boilers, burners and furnaces. Development of CFD techniques have become efficient tools in the search for a better understanding of biomass combustion systems. Commercial CFD codes are mainly developed in the calculation of gas phase processes. However, modelling the complex phenomena involved in the thermal conversion of solid biomass is still a field in development. Several works [1-3] have proposed a wide variety of strategies for implementing several submodels into the commercial CFD codes to couple the thermal conversion of the solid phase with the CFD simulation of the remaining processes. Most published CFD models of biomass combustion systems are based on compact domains wherein the combustion of the packed bed occurs through either a zero- or one-dimensional approach [4-7]. Yang et al. [8] employed a higher level of discretization and modeled a two-dimensional packed bed of thermally thick particles. Most of these works focused on species prediction with temperatures at steady state; however, a few cases determined the transient evolution of the combustion system. Collazo et al. [9] simulated a three-dimensional burner in which the biomass particles were considered to be in a continuous solid phase. The same Eulerian solid-phase approach was used by Gómez et al. [10] to simulate an experimental burner by developing a set of equations which model the packed bed.
This method was applied to the simulation of two different biomass boilers [11, 12] by including fuel-feeding models that replenish the Eulerian variables as they are consumed to reach a steady state. Thunman et al. [13] proposed an Eulerian approach for modeling a thermally thick bed that uses a subgrid scale inside the particles and reduces the number of grid points to the number of stages in biomass thermal conversion. Mehrabian et al. [14] applied the moving-layer methodology proposed by Thunman [13] at the particle scale to represent the thermal conversion of each layer by employing a dense discrete phase model (DPM) to simulate the biomass particles

and their interaction with the gas phase. Ström and Thunman [15] used the same layer model to implement a three-dimensional single-particle model. Gómez et al. [16] also used the thermally thick approach of Thunman [13] to simulate a biomass combustor through an efficient algorithm that solve large amounts of particles in reasonably short calculation times.

In this paper, the different strategies used by the authors in previous papers [10, 16] for the modelling of packed beds are shown. Both models are applied to the transient three-dimensional simulation of an actual biomass domestic. The solid phase of both models is modelled using Eulerian variables that are defined and calculated through transport equations that model the thermal conversion of the solid particles. The first one uses a thermally thin approach and considers homogeneous temperature and composition in the whole particle. The second one discretizes the particle in several layers coincident with the combustion stages. A feeding model is introduced to the combustion model to simulate the fuel feeding of a boiler. A domestic boiler is simulated through both bed models. Experimental tests are used to contrast the response of the boiler to different fuel feeding conditions.

## 2. SOLID PHASE MODELLING

### 2.1. Thermally thin model

The modeling of the solid-phase combustion requires the implementation of several submodels that calculate the evolution of the major variables involved in the thermal conversion of the particles. The authors in previous works [9, 10] proposed a set of variables that modeled the presence of solid biomass particles in the bed region and their interaction with the gas phase during the combustion process. In this work, several scalar variables were defined to represent the major characteristics of biomass conversion. These variables are the enthalpy of the solid (h), the local solid fraction ($\varepsilon$), the volume of the particle, as represented by the third power of its diameter ($d_p$), the local moisture density ($\rho_{moist}$), the local dry wood density ($\rho_{wood}$), local char density ($\rho_{char}$).

The transport equations of these scalars (Eqs. 1-6) and the relationships between the wood component densities and the total density (Eq. 7) represent the transient evolution of the most representative parameters of biomass. In the scalar transport equations (Eqs. 1-6), the first term on the left-hand side denotes the transient term, which represents the temporal variation in the variables. Because there is no mass diffusion between the particles, the diffusive term is only present in the enthalpy equation, thus accounting for the equivalent conductivity between the solids. The term Shs in Eq. 1 and the entire right-hand side of Equations (2 to 6) represent the generation or consumption of each variable.

The source term of Equations 2 and 3 is a function of the relationship between wood consumption and char generation and the consumption with their reference densities. We consider the reference density of a component (wood or char) as the density of a particle completely created from that component; the empirically obtained values for each fuel type were set as constants throughout the model. This formulation calls for shrinkage of the particles during both the devolatilization and char consumption stages, and the resulting fractions of wood and char fulfil the ratios of wood and char densities in both the particles and their respective specific densities.

$$\frac{\partial(\varepsilon\rho_{part}h_s)}{\partial t} = \nabla\left(k_{s,eff}\cdot\nabla T_s\right) + S_{h_s} \quad (1)$$

$$\frac{\partial\varepsilon}{\partial t} = \left(\frac{-\dot{\omega}'''_{wood}}{\rho^s_{wood}} + \frac{\dot{\omega}'''_{G,char}-\dot{\omega}'''_{c,char}}{\rho^s_{char}}\right)\varepsilon \quad (2)$$

$$\frac{\partial d^3_{eq}}{\partial t} = \left(\frac{-\dot{\omega}'''_{wood}}{\rho^s_{wood}} + \frac{\dot{\omega}'''_{G,char}-\dot{\omega}'''_{c,char}}{\rho^s_{char}}\right) d^3_{eq} \quad (3)$$

$$\frac{\partial(\varepsilon\rho_{moist})}{\partial t} = -\dot{\omega}'''_{moist}\,\varepsilon \quad (4)$$

$$\frac{\partial(\varepsilon\rho_{wood})}{\partial t} = -\dot{\omega}'''_{wood}\,\varepsilon \quad (5)$$





$$\frac{\partial(\varepsilon\rho_{char})}{\partial t} = \left(\dot{\omega}'''_{G,char} - \dot{\omega}'''_{c,char}\right)\varepsilon \quad (6)$$

$$\rho_{moist} + \rho_{wood} + \rho_{char} = \rho_{part} \quad (7)$$

The terms $\dot{\omega}'''_i$ that are involved in the source terms of Equations (2-6) represent the generation or consumption rates of the wood components. Equations (8-11) show the terms $\dot{\omega}'''_i$.

$$\dot{\omega}'''_{moist} = \tau\,\frac{\rho_{part}Cp}{LH_{moist}}\frac{\partial T_s}{\partial t}, T_s \geq T_{evap} \quad (8)$$

$$\dot{\omega}'''_{wood} = \rho_{wood}\sum_{i=1}^{3} A_i exp\left(-\frac{E_i}{RT_s}\right) \quad (9)$$

$$\dot{\omega}'''_{G,char} = \rho_{wood}\,A_3 exp\left(-\frac{E_3}{RT_s}\right) \quad (10)$$

$$\dot{\omega}'''_{c,char} = K^{ox}_{glob}\,A_v[O_2]M_C + K^{g,1}_{glob}\,A_v[CO_2]M_C + K^{g,2}_{glob}\,A_v[H_2O]M_C \quad (11)$$

The dry wood consumption is modeled as a thermally controlled conversion into gas, tar and char [17]. Therefore, the devolatilization rate considers three different Arrhenius rates, which correspond to each conversion process (Eq. 9). The char consumption rate (Eq. 10) is modeled as the sum of direct char oxidation [13], and two gasification reactions [18].

### 2.2. Thermally thick model

The thermally thick particle model is considers the same characteristics of the thermally thin model in the modelling of gas phase and the interaction between solid and gas phases. Nevertheless, the segregation of biomass components and temperatures of the internal intraparticle layers gives a more accurate evolution of combustion of the solid phase.

The particle is modelled as three concentric layers representing the main stages of the biomass during its combustion (moist wood, dry wood and char). Each layer is characterised by its volume and temperature as its main representative variables. These variables create two intra-particle subgrids. The temperatures subgrid contains four elements: the temperature of the three layers and an additional element as the char layer is divided into two sublayers to obtain a better prediction of the surface temperature of the particle, which is important in the heat exchange between the particle and the environment [16]. Figure 1 shows a representation of the approach in the particle model.

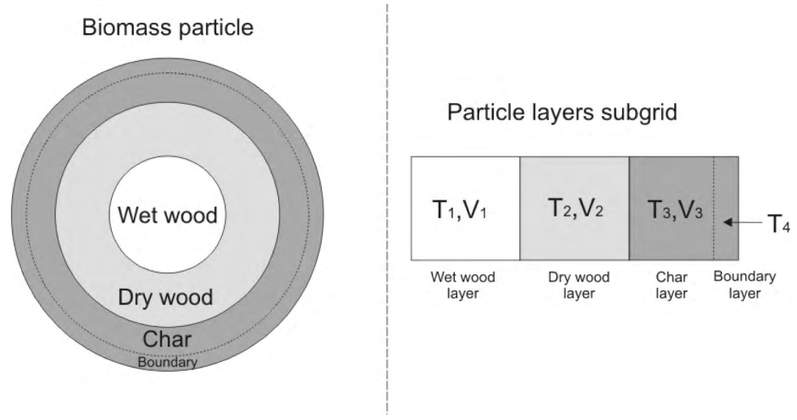


*Figure 1: Representation of the subgrid scale approach [40]*

A radial symmetry is considered for the particle discretization. Therefore, no directional heat propagation is considered in the particle model. One-dimensional unsteady heat conduction is formulated to solve the temperature of the layers. Equation 12 states the heat conduction in a spherical geometry. This equation is integrated over a generic control volume at position (P) (Figure 2), and over a time step (Δt). Equation 13 is obtained by applying discretization techniques as a first-order temporal discretisation and a central differencing scheme. In this equation, the transient and diffusion terms are defined by geometrical parameters and material properties. The source term represents the heat generation of the layer and the heat exchange between the particle and the particle surroundings in the case of the external layer.

$$\frac{\partial(\rho h)}{\partial t} = \frac{1}{r^2}\frac{\partial}{\partial r}\left(kr^2\frac{\partial T}{\partial r}\right) + S_h \tag{12}$$

$$\frac{(\rho Cp)_P T_P - (\rho Cp)_P T_P^0}{\Delta t} V_P = 8\pi k_{P,E} \cdot R_E^2 \frac{T_E - T_P}{R_E^2 - R_I^2} - 8\pi k_{I,P} \cdot R_I^2 \frac{T_P - T_I}{R_P^2 - R_{I,I}^2} + S_{h,P} V_P \tag{13}$$

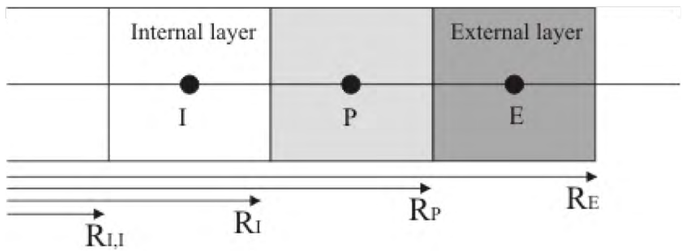


*Figure 2: Representation of the finite element notation in the subgrid-scale approach*

Equation 13 is then linearized as a function of the layer (P) and the neighbour layer temperatures and an independent term depending of the heat sources and the layer temperature in the past time step. This model also considers the heat transport (convective and advective) between neighbour cells, which is included in the source term of the external layer.

As the four temperatures follow the same linear equation estructure (Eq. 14), they can be grouped in a system of four linear equations (Eq. 15). This system can be easily solved and the temperatures of all layers are obtained without an iterative process. The coefficients of this equation system are shown in the authors´ previous paper [40].

$$a_P T_P = a_P^0 T_P^0 + a_I T_I + a_E T_E + b \tag{14}$$

$$\begin{pmatrix} a_{P,1} & -a_{E,1} & 0 & 0 \\ -a_{I,2} & a_{P,2} & -a_{E,2} & 0 \\ 0 & -a_{I,3} & a_{P,3} & -a_{E,3} \\ 0 & 0 & -a_{I,4} & a_{P,4} \end{pmatrix} * \begin{pmatrix} T_1 \\ T_2 \\ T_3 \\ T_4 \end{pmatrix} = \begin{pmatrix} a_{P,1}^0 T_1^0 + b_1 \\ a_{P,2}^0 T_2^0 + b_2 \\ a_{P,3}^0 T_3^0 + b_3 \\ a_{P,4}^0 T_4^0 + b_4 \end{pmatrix} \tag{15}$$





As the combustion process advances, the drying, devolatilization and char combustion fronts move toward the centre of the particle. Thus, the volume of the layers and therefore, the particle subgrid elements continuously change. This volume variation is formulated with a conservation equation consisting in a transient volume source (Eq. 16). This equation can also be linearized as a linear function of the layers volumes (Eq.1 7). As this is applied to the three layers, a system of three linear equations (Eq. 18) can be established. The coefficients of this equation system are also shown in [16].

$$\frac{V_P - V_P^0}{\Delta t} = S_{V_P} \tag{16}$$

$$a_P V_P = a_P^0 V_P^0 + a_I V_I + b \tag{17}$$

$$\begin{pmatrix} a_{P,1} & 0 & 0 \\ -a_{I,2} & a_{P,2} & 0 \\ 0 & -a_{I,3} & a_{P,1} \end{pmatrix} * \begin{pmatrix} V_1 \\ V_2 \\ V_3 \end{pmatrix} = \begin{pmatrix} a_{P,1}^0 V_1^0 + b_1 \\ a_{P,2}^0 V_2^0 + b_2 \\ a_{P,3}^0 V_3^0 + b_3 \end{pmatrix} \tag{18}$$

### 2.3. Boiler additional modelling

In both thermally thin and thermally thick models, the solid phase affected by their environments via convection, radiation and reaction. These processes, which are expressed by the exchange of mass and energy between the gas phase and the solid phase. The terms that affect the gas phase are discussed in [10]. In addition, the feeding system of the simulated boiler, which consists in a continuous drop of pellet particles in a metal box, is modelled as Lagrangian trajectories through a DPM algorithm which considers the interaction between gas and particles. The particles are modelled as combusting spheres and all the combustion stages take place along the trajectories. These Lagrangian trajectories are removed when they reach a packed bed cell and the bed Eulerian variables are updated [12].

## 3. EXPERIMENTAL SYSTEM

### 3.1. Boiler

The simulated experimental boiler is a 27 kW pellet boiler and is represented in Figure 3. The fuel bed of this boiler is located in a metallic box with several holes at its floor and at the lateral walls to allow air to cross the bed. The fuel is dropped onto the bed from a fuel store through a feeding channel. The air inlet is a tube that drives the air to a semi-closed space placed under the bed, which distributed the air that is to enter the bed among the numerous holes in the floor of the bed box. The flame is expected to be located over the bed box, and the hot gases released from the fuel exchange heat with the tubes and the boiler walls, which are cooled by water. Those exhausted gases are driven out from the boiler through an escape tube, which is also cooled by water.

There is a frontal door in front of the flame region that enables visibility of the flame and part of the bed. This door has an important effect on the boiler's behavior because it is the main inlet of air infiltrations. These infiltrations provide an effect of a secondary air inlet. However, the magnitudes of these fluxes are not controlled.
The boiler geometry is discretized in a polyhedral mesh, with a special refinement in the zones where stronger gradients are expected such as the bed region and immediately above, the near wall region and the areas surrounding the air entrances.

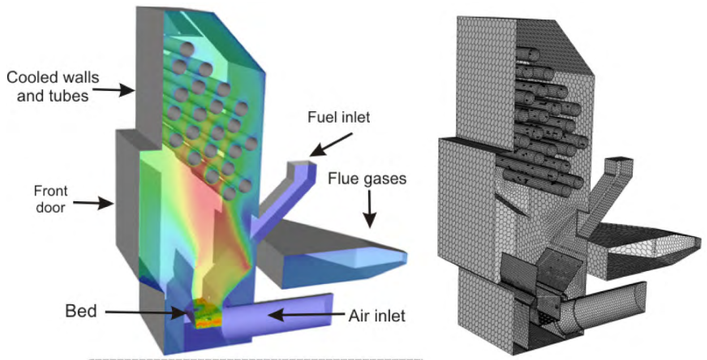


*Figure 3: Scheme of the boiler geometry and the mesh used for the simulations*

### 3.2. Experimental tests

Two experiments (E1 and E2) were performed using this boiler with different feeding methods. In test E1, the fuel was introduced into the boiler through a conveyor belt, which drops the pellets into the fuel inlet at a constant rate. In experiment E2, a hopper with a screw was used to introduce the fuel in random batches. The experimental conditions of the tests are listed in table 1.

*Table 1: Experimental tests performed in the boiler*

| Test | Power (kW) | Feeding rate (g·s$^{-1}$) | Air excess | Feeding method |
|---|---|---|---|---|
| E1 | 27.2 | 1.6 | 1.6 | belt-hopper |
| E2 | 27.2 | 1.6 | 1.6 | screw-hopper |

## 4. SIMULATIONS RESULTS

In this section, the main results obtained in the simulations of the aforementioned boiler are shown and compared with experimental tests. The two models shown above were tested in an experimental batch combustor and the results are shown in [16]. The simulation results of the thermally thin model in the boiler are analysed in the author´s previous paper [12]. Below, the main variables of the thermally thick model are shown in the bed of the boiler. As the model divides the biomass particles into three layers representing the stages of biomass combustion, the scalar fields of these layers gives information about the combustion state in the packed bed. Figure 4 shows the boiler bed with the layers (moist wood, dry wood and char) volumetric fractions. The field of solid fraction (Eq. 1) shows values between 0.4 and 0.6. The moist wood fraction is high in the upper area of the bed in which values of 1 represent the virgin biomass. This location of moist wood is due to the boiler feeding system which drop the virgin biomass particles from above. The dry wood is located in the middle region of the bed. It increases from the surface which means the drying takes place in that area, reaches the maximum fraction and from the middle down of the bed it decreases which means the devolatilization takes place. The lower region of the bed is occupied by char. In this area, the biomass is in an advanced state of degradation and the higher surface temperatures are expected due to the char combustion in the particle surface.

In Figure 5 the temperatures of the three layers and the particle surface inside the bed and the gas temperature in the boiler freeboard are shown as scalar fields. These temperatures are related to the reaction rates of the particle layers and the heat exchange between particles and gas phase as well as the gas reaction kinetics.





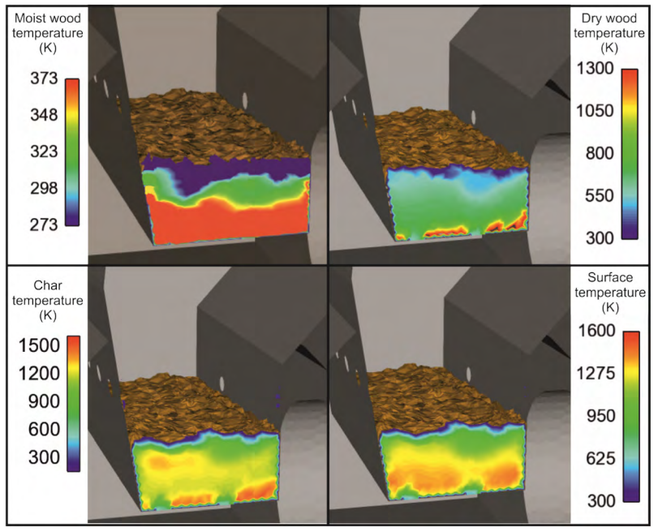


*Figure 4: Fields of solid fraction in the packed bed and the volumetric fractions of the particle layers*

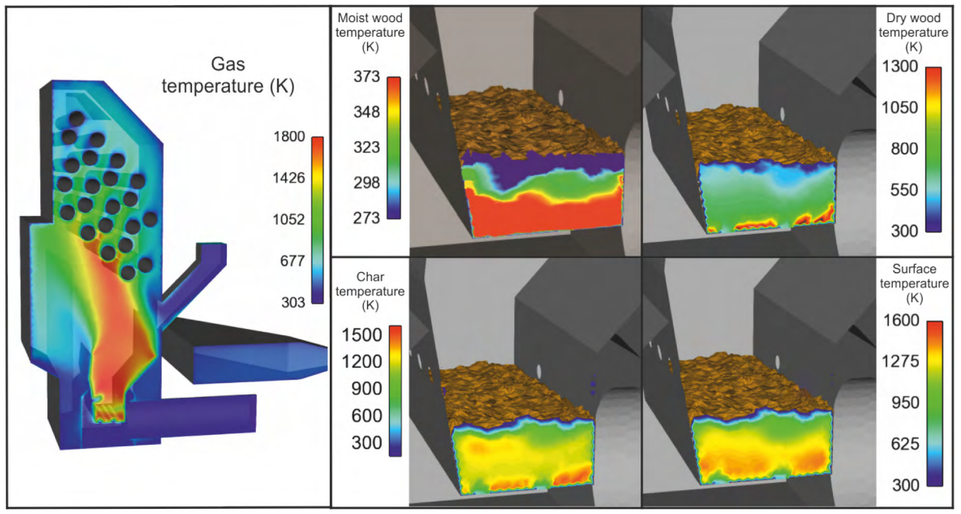


*Figure 5: Temperatures of gas and particle layers inside the bed*

A comparison between both (thermally thin and thermally thick) models and the experiments preformed with the boiler is presented in Figure 6. This figure shows the range and the most probable values of the data collected in the flue gases during the tests and simulations with both feeding systems belt (B) and screw (S). The results of temperature and air excess index and $CO_2$ emissions are reasonably close to the experiments. CO emissions show less accurate predictions which may be caused due to the simplicity in the homogeneous gas reaction scheme. Figure 7 shows the evolution of fuel mas flux and the CO emissions in the simulation of the tests shown in the table 1. This figure show instabilities when the boiler operates with screw feeding in comparison with the belt.

This behaviour may be an effect of the mass fed by batches, which are common with screw systems and create fluctuations due to the abrupt increment of fresh biomass and the consequent release of high amounts of gases that makes insufficient the constant air supply to achieve a complete combustion.

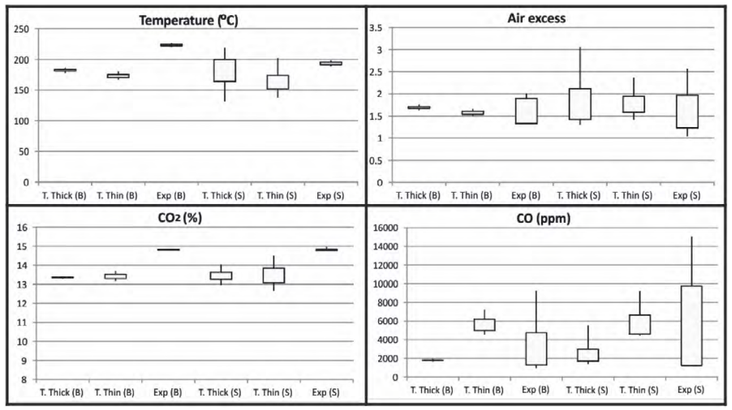


*Figure 6: Comparison of the predictions of both models and experimental results*

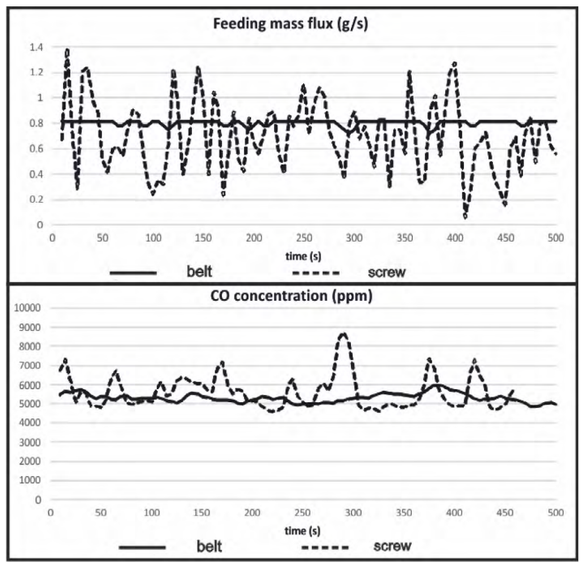


*Figure 7: Transient evolution of fuel mass flux and CO emissions in the simulations of the boiler operating with both feeding systems (belt and screw)*

## 5. CONCLUSION

Two CFD simulation methods were developed by implementing classical techniques and a comprehensive model to consider the main solid variables not considered in the CFD code. Both models were applied to the simulation of a commercial biomass boiler with several sub-models that had been previously presented by the authors. The main variables that affect to the boiler working were visualized and their influence in the combustion performance was discussed. The simulation results were compared with the experimental data and the general boiler behavior is analyzed. The predictions showed a reasonably good behaviour for the flue gases temperatures, air excess index, $CO_2$ emissions and the heat exchanged, and the instability of the emissions caused by a stochastic fuel feeding observed in the experiments was also captured in the simulations.





## 6. ACKNOWLEDGEMENTS

The authors acknowledge financial support from Project ENE2015-67439-R of the Ministry of Economy of Spain.

## 7. REFERENCES

[01] Zhou H, Jensen AD, Glarborg P, Jensen PA, Kavaliauskas A. (2005). Numerical modeling of straw combustion in a fixed bed. Fuel. 84: 389.
[02] Porteiro J, Granada E, Collazo J, Patiño D, Morán JC. (2009) Numerical modeling of a biomass pellet domestic boiler. Energy Fuels. 23: 1067.
[03] Kær SK. (2004). Numerical modelling of a straw-fired grate boiler. Fuel. 83: 1183.
[04] Yin C, Rosendahl L, Kær SK, Clausen S, Hvid SL, Hiller T. (2008). Mathematical modeling and experimental study of biomass combustion in a thermal 108 MW grate-fired boiler. Energy Fuels. 22: 1380.
[05] Cooper J, Hallett WLH. (2000) A numerical model for packed bed combustion of char particles. Chem. Eng. Sci. 55: 4451:
[06] Van der Lans RP, Pedersen LT, Jensen A, Glarborg P, Dam-Johansen K. (2000) Modelling and experiments of straw combustion in a grate furnace. Biomass Bioenerg. 19: 199.
[07] Yang YB, Ryu C, Khor A, Yates NE, Sharifi VN, Swithenbank J. (2005) Fuel size effect on pinewood combustion in a packed bed. Fuel. 84: 2026.
[08] Y.B. Yang, V.N. Sharifi, J. Swithenbank, Numerical simulation of the burning characteristics of thermally-thick biomass fuels in packed beds, Trans IChemE Part B. Process Saf. Environ. Prot., vol. 83, pp. 1–11, 2005.
[09] Collazo J, Porteiro J, Patiño D, Granada E. (2012). Numerical modeling of the combustion of densified wood under fixed-bed conditions. Fuel. 93: 149.
[10] Gómez MA, Porteiro J, Patiño D, Míguez JL. (2014). CFD Modelling of Thermal Conversion and Packed Bed Compaction in Biomass Combustion. Fuel. 117: 716.
[11] Gómez MA, Porteiro J, Patiño D, Míguez JL. (2015). Eulerian CFD Modelling for Biomass Combustion. Transient Simulation of an Underfeed Pellet Boiler. Energ Convers Manage. 101: 666.
[12] Gómez MA, Porteiro J, De la Cuesta D, Patiño D, Míguez JL.(2015). 2015 Numerical Simulation of the Combustion Process of a Pellet-Drop-Feed Boiler. Fuel. In Press.
[13] Thunman H, Leckner B, Niklasson F, Johnsson F. (2002). Combustion of wood particles – a particle model for eulerian calculations. Combust Flame. 129: 30.
[14] Mehrabian R, Zahirovic S, Scharler R, Obernberger I, Kleditzsch S, Wirtz S, Scherer V, Lu H, Baxter LL. (2012). A CFD model for thermal conversion of thermally thick biomass particles. Fuel Process Technol. 95: 96.
[15] Ström H, Thunman H. (2013). CFD simulations of biofuel bed conversion: A submodel for the drying and devolatilization of thermally thick wood particles. Combust Flame. 160: 417.
[16] Gómez MA, Porteiro J, Patiño D, Míguez JL. Fast-solving thermally thick model of biomass particles embedded in a CFD code for the simulation of fixed-bed burners. Energ Convers Manage 2015; 105: 30–44.
[17] Wagenaar BM, Prins W, Swaaij WPM. (1993) Flash pyrolysis kinetics of pine wood. Fuel Process Technol. 36: 291.
[18] Bryden KM, Ragland KW. (1996). Modeling of a deep, fixed bed combustor. Energy Fuel. 10: 269.

*Andrea Dernbecher (DBFZ, Germany)*

# Review on CFD based bed models for biomass conversion in small scale applications

*Andrea Dernbecher, Fouzi Tabet*
*DBFZ Deutsches Biomasseforschungszentrum gemeinnützige GmbH*
*Torgauer Straße 116, D-04347 Leipzig, Germany*
*andrea.dernbecher@dbfz.de, fouzi.tabet@dbfz.de*

**KEYWORDS:** Biomass combustion, bed model, small-scale application, thermo-chemical conversion

## ABSTRACT

In this paper a short summary about commonly used models for the simulation of the biomass bed in biomass grate firing systems is given. The processes of thermo-chemical conversion in the fuel bed are summarized and commonly used models to describe heat transfer, drying, pyrolysis gasification and combustion are presented. Four different approaches to simulate the biomass bed in grate firing biomass combustion applications are discussed based on selected examples for the different types of bed models.

## 1. INTRODUCTION

Biomass heating in small scale applications has to tackle several challenges to further evolve and to continue to offer a valuable alternative for conventional heating devices. The main objective in the design of biomass heating devices is to reduce the emission of particulate matter, CO and NOx. Furthermore, the usage of alternative fuels should be advanced. This issue is closely connected to the emissions, as alternative fuels like straw lead to higher emissions than virgin wood. Another objective is to decrease the nominal power output of biomass heating systems to make them applicable for low energy houses, which are well insulated and have a low energy demand.
Recent progress in numerical techniques and computing efficiency has advanced Computational Fluid Dynamics (CFD) as a widely used approach in biomass combustion. Numerical simulation is an excellent supplement to the experiment-based design of heating systems. The calculation of the combustion chamber is usually divided into three parts, the modelling of biomass conversion in the fuel bed, the simulation of the gas phase reactions and additional models. The simulation of the biomass bed is challenging and crucial for the further simulation of gas phase reactions in the free board, since the precursors for the gas phase reactions are formed in the biomass bed. In this article a short summary about commonly used models for the simulation of the biomass bed is given. The thermo-chemical processes in the biomass bed are summarized and selected examples for different types of bed models are presented. Some of the examples do not describe small scale applications, but they illustrate possibilities to simulate the thermo-chemical conversion of the biomass bed. All shown approaches are transferrable to small scale applications.

## 2. BIOMASS CONVERSION – PROCESSES DURING THERMO-CHEMICAL COMBUSTION OF BIOMASS AND MATHEMATICAL MODELS

Thermo-chemical conversion of biomass in a fixed-bed consists of the steps: heating up, drying, pyrolysis, gasification and combustion. Furthermore, shrinking, compaction of the bed, cracking and release of precursors for pollution formation can be observed during the process.

### 2.1. Heat transfer

To describe the heating-up of a biogenic fuel, the different phases, which can be found in biomass, have to be considered. Biomass consists of cell wall substance, bound water, liquid water, water vapour, air and other gases. All present materials have individual properties, from which the effective material properties for the heat transfer inside the bulk material are calculated.





Additionally, it is important to consider, that heat transfer along and perpendicular to fibres is different. An effective heat transfer coefficient based on heat transfer in both directions is used in many publications, which deal with biomass with oriented fibres [1].
In a whole bed of biomass, heat transfer is influenced by the shape of the particles, which form the bulk material. Intra-particle gradients of heat lead to a broad reaction front, which travels through the biomass bed. In some models, the intra-particle gradients are neglected, since the particles are considered to be thermally thin. For simulations with small particles compared to the bed size, this assumption is valid [2].

### 2.2. Drying

Three models for drying are widely used in the literature, the kinetic approach, the thermal approach and the equilibrium approach. The kinetic approach describes the evaporation rate with an Arrhenius equation as it is used to describe chemical reaction rates. In the thermal approach a thin drying front travels through the biomass. Evaporation is limited to the region, in which the temperature of the biomass reaches the boiling point of water. In the drying front all thermal energy is used for the evaporation of water and no further temperature increase is allowed before the biomass is dry. The equilibrium approach considers the difference of concentration of water vapour in the biomass and the surrounding gas phase. The evaporation rate is proportional to the driving difference of concentrations [3]. A combination of thermal and equilibrium approach is often used to cover a broader temperature range.

### 2.3. Pyrolysis

Pyrolysis is a very important step of thermo-chemical conversion of biomass. Dry biomass decomposes to volatiles and char due to increasing temperature and without any reacting agent. Many models were developed by experts in biomass thermochemical conversion to describe pyrolysis. A comprehensive review about various models for pyrolysis was published recently [5]. Three models of those are frequently used for the simulation of whole biomass beds in literature. The simplest approach is the one-step model presented in equation (1).

dry biomass → volatiles + char (1)

A more complex model was introduced by Shafizadeh and Chin [4]. It includes individual kinetic rates for the production of volatiles, tar and char. It is sometimes extended to cover the secondary reactions of tar cracking. Another possibility is to describe pyrolysis with three parallel reactions, which represent the decomposition of the biomass components cellulose, hemicellulose and lignin.

### 2.4. Gasification and combustion of char

For gasification and combustion of char, char is considered to be pure carbon. The following reactions are used to characterize gasification:

$$C + H_2O \rightarrow CO + H_2 \quad (2)$$
$$C + CO_2 \rightarrow 2\,CO \quad (3)$$
$$C + 2\,H_2 \rightarrow CH_4 \quad (4)$$

Since the reactions are slow in comparison to other processes during biomass combustion, they are partially or fully neglected in some simulations [6]. The char oxidation is shown in equation (5), in which $\phi$ is a factor depending on the local temperature [7].

$$C + 1/\phi\, O_2 \rightarrow 2\,(1-1/\phi)\,CO + (2/\phi-1)\,CO_2 \quad (5)$$

### 2.5. Homogeneous gas phase reactions in the fuel bed

Compared to gas phase reactions in the free board, homogeneous reactions in the fuel bed have small influence on the results of a comprehensive simulation of a biomass combustion system. Therefore, they are often neglected in the bed model. When gas phase reactions in the fuel bed are taken into account, they are represented by a global reaction scheme. The few reactions of the global scheme describe the oxidation of volatiles, which leave the biomass during pyrolysis and gasification. Mixing of volatiles and oxidizing air can be described by an additional equation [8].

### 2.6. Additional models

Besides the basic processes in the biomass bed, other phenomena occur, which are covered by additional models for the bed model. Especially mechanical and structural changes like shrinking of particles, compaction of the bed, channeling and formation of cracks are covered with additional models in the bed model. An example for the simulation of compaction of a bed is shown in Figure 1.

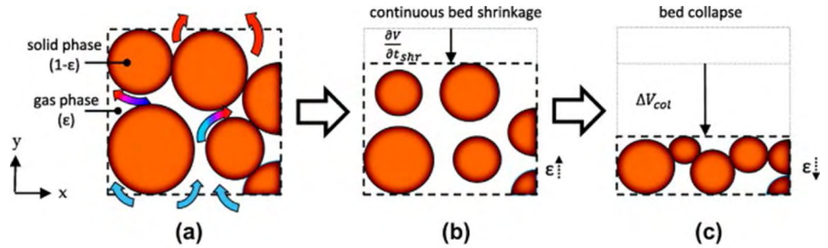


*Figure 1: Shrinking and collapsing of a fuel bed [9]*

The formation of precursors from the biomass bed is very important step for the simulation of pollutants in the gas phase. Suitable models to simulate the formation of polycyclic aromatic hydrocarbons (PAH), tars, inorganic salts and NOx-precursors can be applied to the bed model.

## 3. EXAMPLES FOR FIXED-BED MODELS

For the modelling of fixed-beds, various approaches can be found in literature. The choice of the model depends on the system, which is simulated and the type of biomass, which is used in this systems.

### 3.1. Empirical models

If the focus of the combustion simulation lies on the gas phase reactions in the freeboard, an empirical bed model can be used. In this case, the inlet conditions of the free board simulation concerning gas phase composition, temperature and velocity of the combustible gases are taken from measurements. Some data are difficult to obtain and may be derived from experimental data by calculations [10]. This approach is also called semi-empirical bed model.
An example for an empirical bed model was published by Scharler and Obernberger in 2000 [11]. They simulated a boiler for the combustion of waste wood with travelling grate. The concentration of species leaving the fuel bed and their velocity were measured and used as inlet conditions for the calculations in the free board. The concentration of the gases was measured along the grate and profiles of the gas concentrations were used in the following simulation.





### 3.2. Separate bed models

In a commonly used modelling approach, the bed model is calculated separately from the free board combustion. The results of the separate calculation are used as inlet conditions for the gas phase reaction simulation. The bed model can be zero- to three-dimensional, depending on the simulated case. A one- or two-way coupling can be applied by exchange of heat and mass flows between biomass bed and free board.

Galgano et al. published an example for a 1d separate bed model in 2006 [12]. The combustion of a wood log was simulated. The wood log was represented by a one-dimensional bed model, using the radius of the log as spatial coordinate. Reactions in the free board were calculated in a two-dimensional CFD-simulation. Drying was calculated by a thermal approach, pyrolysis as a simple one-step reaction and the heterogeneous reactions of char with $H_2O$, $CO_2$ and $O_2$ were simulated. Gas phase reactions were not accounted for in the solid phase. The reactions and evaporation were considered to be located on a thin reacting surface moving through the wood log. The wood log was separated in various layers by the reacting surfaces, as it can be seen in Figure 2. Heat transfer was calculated for each individual layer with the components occurring in the layer. Coupling between solid and gaseous phase was realized by heat and mass exchange at the surface of the wood log.

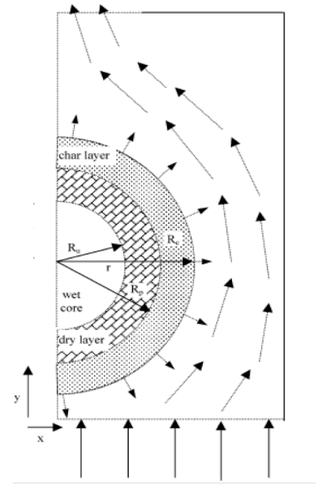


*Figure 2: Simulation of a wood log with layers [12]*

An example for a two-dimensional bed model can be found at Yang et al. 2007 [8]. A 38 $MW_{el}$ power plant for the combustion of straw was simulated. The combustion took place on a moving grate, for the simulation the height of the bed and the length of the grate were the two spatial coordinates. The two-way coupling of bed model and free board simulation was performed according to the scheme shown in Figure 3. Drying was modelled with a combination of thermal and equilibrium approach, pyrolysis was modelled with a simple one-step reaction and the heterogeneous reaction of char with oxygen was simulated. Additionally, a global reaction mechanism was applied to simulate the homogeneous gas phase reactions inside the biomass bed. The particles in the bed were assumed to be thermally thin and heat transfer was calculated accordingly. Additionally, inter-particle radiation was taken into account in the equation for effective heat transport through the solid phase.

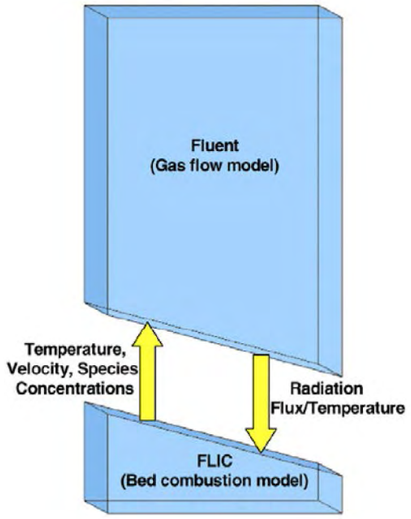


*Figure 3: Interaction of separate bed model and CFD domain [8]*

### 3.3. Discrete particle models

The discrete particle model (DPM) offers several advantages for the simulation of a biomass bed consisting of particles like pellets, wood chips or municipal solid waste. Each particle undergoes drying, pyrolysis, gasification and combustion and also the movement of every particle is calculated. The simulation allows a detailed prediction of the behaviour of the biomass bed.

An example for this approach was introduced by Simsek et al. in 2009 [13], in which a fuel bed of municipal solid waste on a moving grate was simulated. Drying was modelled with a thermal approach, pyrolysis with a simple one-step reaction and the heterogeneous reaction of char with oxygen was considered. Gas phase combustion was not modelled in the fuel bed.

The particles were assumed to be thermally small and exchange heat by contact conduction and radiation among each other. Heat transfer between gaseous and solid phase was based on convection and radiation of the flame to the upper layer of particles. In figure 4 results for the simulation can be seen. The mass fraction of char in particles is shown and indicates the dispersion of particles by the moving grate. The individual calculation of thermo-chemical conversion for each particle is computationally expensive.

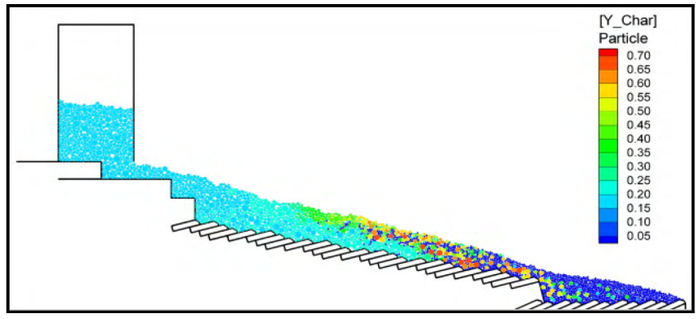


*Figure 4: Mass fraction of char in a bed of municipal solid waste modeled with DPM [13]*





### 3.4. Porous medium approach

In the porous medium approach the biomass bed is described as a porous zone inside the CFD domain. A simulation with this approach was presented by Chaney et al. in 2012 [7]. They analyzed a 50 kW pellet boiler, with the bed as a porous medium. Drying was modelled by an Arrhenius approach and pyrolysis was described by a simple one-step reaction. The pyrolysis reaction was limited to devolatilization zones in the biomass bed, since this approach achieved the most reasonable results. The pyrolysis zones can be seen in figure 5. Heterogeneous reactions of char with oxygen were considered and homogeneous reactions in the gas phase in the fuel bed were simulated by a global reaction mechanism. Heat and mass transfer inside the fuel bed and between solid and gaseous phase were based on the default equations for porous medium in the commercial simulation code. In figure 5 results of the simulation are shown, the temperature of the gas phase is illustrated by the colors.

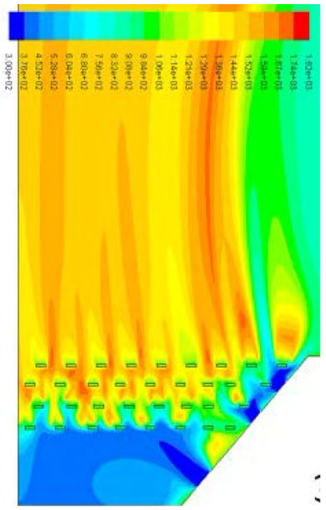

*Figure 5: Results of simulation with porous medium as bed model, temperature of the gas phase [7]*

## 4. CONCLUSIONS

From the selected examples described above, it can be seen that CFD is already widely used to simulate small scale biomass combustion and various models for the biomass bed exist. A suitable setup has to be chosen according to the examined technology and biomass type. Due to increasing availability of CPU, more comprehensive and complex simulations become realizable. This should be exploited to advance optimisation of combustion chambers by means of CFD. Numerical methods will be of special benefit to improve the reduction of emissions, to increase efficiency and to make a broad range of solid fuels available for small scale combustion. CFD should be further developed to enable the use as a virtual platform to achieve the mentioned objectives.

## 5. REFERENCES

[01] Grønli MG. (1996). A Theoretical and Experimental Study of the Thermal Degradation of Biomass, PhD thesis, Norwegian University of Science and Technology
[02] Johansson R et al. (2007). Influence of intraparticle gradients in modeling of fixed bed combustion. Combust. Flame 149: 1–2, 49–62
[03] Jalili M. (2015). Multi-scale modeling of fixed-bed drying of woody fuel particles. PhD thesis, TU Berlin
[04] Shafizadeh F, Chin PPS. (1977). Thermal Deterioration of Wood. In: Goldstein, IS (Editor): Wood Technology: Chemical Aspects. Vol. 43. Washington, D. C.: American Chemical Society (ISBN 0-8412-0373-3). 57–81

[05] Anca-Couce A. (2016). Reaction mechanisms and multi-scale modelling of lignocellulosic biomass pyrolysis. Prog. Energy Combust. Sci. 53: 41–79
[06] Thunman, H et al. (2002). Combustion of wood particles - a particle model for eulerian calculations. Combust. Flame 129: 1–2, 30–46
[07] Chaney J et al. (2012). An overview of CFD modelling of small-scale fixed-bed biomass pellet boilers with preliminary results from a simplified approach. Energ. Convers. Manage. 63: 149–156
[08] Yang YB et al. (2007). Mathematical modelling of straw combustion in a 38 MWe power plant furnace and effect of operating conditions. Fuel 86: 1–2, 129–142
[09] Duffy NTM, Eaton JA. (2013). Investigation of factors affecting channelling in fixed-bed solid fuel combustion using CFD. Combust. Flame 160: 10
[10] Thunman, H et al. (2001). Composition of Volatile Gases and Thermochemical Properties of Wood for Modeling of Fixed or Fluidized Beds. Energy Fuels 15: 6, 1488–1497
[11] Scharler R, Obernberger I. (2000). Numerical Modelling of Biomass Grate Furnaces. Proceedings of the 5th European Conference on Industrial Furnaces and Boilers. Porto, (ISBN 972-8034-04-0)
[12] Galgano A et al. (2006). Experimental Validation of a Coupled Solid- and Gas-Phase Model for Combustion and Gasification of Wood Logs; Energy Fuels, 20: 5, 2223–2232
[13] Simsek E et al. (2009). Numerical simulation of grate firing systems using a coupled CFD/discrete element method (DEM). Powder Technol. 193: 3, 266–273





*Kamil Kwiatkowski (University of Warsaw, Poland)*

## Thermochemical conversion of wood – modelling with OpenFOAM

*Kamil Kwiatkowski*
*Institute of Theoretical Physics, Faculty of Physics, University of Warsaw*
*Pasteura 5, 02-093 Warsaw, Poland*
*Interdisciplinary Centre for Mathematical and Computational Modeling, University of Warsaw*
*Prosta 69, 00-838 Warsaw, Poland*
*kamil.kwiatkowski@fuw.edu.pl*

*Pawel Jan Zuk*
*Institute of Theoretical Physics, Faculty of Physics, University of Warsaw*
*Pasteura 5, 02-093 Warsaw, Poland*
*Institute for Fundamental Technological Research, Polish Academy of Sciences*
*02-106 Warsaw, Poland*
*pawel.zuk@fuw.edu.pl*

**KEYWORDS:** Evaporation, pyrolysis, gasification, openFoam, biomassGasificationFoam, wood

**ABSTRACT**

The thermal conversion of wood ia modelled with the *biomassGasificationFoam*, the library and solver developed in OpenFOAM, an open-source CFD packages. We focus on thee slow conversion of wood, when the processes involved in thermal conversion of wood are clearly distinguishable, namely evaporation, pyrolysis and gasification. The main focus in on the kinetics and pathways of the processes and on the amount of heat required to drive them. To analyze and compare schemes of kinetics we developed oversimplified one-cell test case. The results are compared with the results of the TGA analysis.

## 1. INTRODUCTION

Thermochemical conversion of wood refers to the variety of pathways of thermal decomposition of wood into gaseous, liquid or solid products. Thermal conversion of wood includes evaporation of water embedded within wood, pyrolysis of holocellulose and lignin, and gasification of remaining char. These processes take place in different ranges of temperature, thus when wood sample is small and when this sample is heated relatively slowly, processes of drying, pyrolysis and gasification proceed one after another. Such conditions can be easily fulfilled in well-controlled thermogravimetric analysis (TGA). In this robust experimental technique mass loss of small isotropic sample of wood is constantly measured during decomposition.

In present paper we model evaporation and pyrolysis of small isotropic sample of wood with code *biomassGasificationFoam* [1,2], relatively new openFOAM [3,4] solver developed to model biomass gasification in fixed-bed. The code *biomassGasificationFoam* contains solver and a library that allows for defining chemical and physical properties of feedstock, and its evolution with temperature and conversion ratio. Library includes different pathways of conversion, homogeneous and heterogeneous reactions between gases and sold material and basic radiation. We present an oversimplified case developed to test and cross-check different pathways of thermal conversion. In this one-cell test only the effects of heat transfer and thermal conversion are included, the effects of fluid flow are neglected. Although oversimplified, this case is suitable to simulate decomposition of small sample in thermogravimetric reactor. Drying with two different ways of defining heat of evaporation is analyzed: directly provided and computed based on enthalpies of formation of liquid water and water vapor. The results are in good agreement with TGA data. Next we present the results of pyrolysis for two different schemes of kinetics: so-called multi-component [5] and multi-stage [6] schemes.

## 2. CODE BIOMASSGASIFICATIONFOAM

The OpenFOAM code [3] is an open source C++ package for solving partial differential equations with finite volume method. The code, and its variant foam [4] is widely used in various fields of fluid mechanics and provides robust, standardized libraries and tools for solving partial differential equations. Solver *biomassGasificationFoam* [1,2] is based on an algorithm used in the unsteady solver *reactingFoam* for reacting flows, laminar or turbulent. The *reactingFoam* solves flow, heat transfer and reactions only in the gas phase. In the following list we summarize functionalities of the *biomassGasificationFoam* which allow for modeling of thermal conversion of solid and porous materials:

- flow of gaseous mixture (e.g. $N_2$, CO, $H_2$, $CH_4$, $CO_2$, vapours, etc.);
- flow inside and outside porous media;
- chemical reactions with gaseous and solid substrates (homogeneous and heterogeneous reactions) with defined heat of reaction;
- potentially complex definition of porous media (cellulose, hemicellulose and lignin, etc.), anisotropic, inhomogeneous, irregular shape, partially decomposed, etc.;
- various pathways of potential decomposition, including endo- and exothermic ones;
- exchange of mass and energy between gases and solid phases;
- evolving properties of porous material (porosity, permeability, composition, heat capacity, etc.).

Readers interested in mathematical model behind the solver and in implementation details are referred to the following references [1,2]. In present analysis we used second version of the *biomassGasificationFoam* code (version 2.0), based on foam 3.1 [2].

## 3. THERMOGRAVIMETRIC ANALYSIS

Thermogravimetric analysis (TGA) quantifies thermal decomposition of wood under well controlled conditions. The experiment was done using the TA Instrument Q500 thermogravimeter with the following heating protocol: initial temperature of 300 K, constant heating rate of 10 K/min. The experiment was carried out until the temperature reached 1300 K. We provided a nitrogen environment, only the processes of drying and pyrolysis took place. Wood sample has 24 mg, with water constant of approximately 8 %wt. The experiment is described in more details in our previous paper [5].
The mass loss due to sequential stages of decomposition is plotted in Fig. 1.

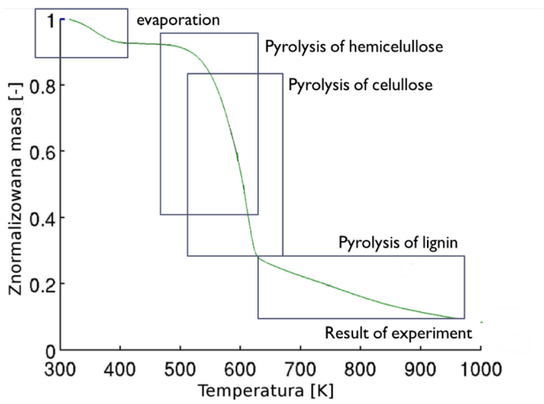


*Figure 1: Mass loss due to evaporation and pyrolysis measured during TGA analysis*





When the temperature reaches 400 K (which correspond to 600 s) wood is completely dry, then pyrolysis begins around 500 K (1200 s) slowing down rapidly around 600 K (1800 s). Finally, when temperature is increasing small amount of mass is still being devolatized.

## 4. EVAPORATION

Evaporation is an initial stage of thermal conversion, when moisture embedded in wood structure is released as a water vapor. The endothermicity of evaporation and amount of heat that is needed to evaporate moisture are well known. Thus, we can simulate evaporation to test and verify two mechanisms specifying heat of evaporation, or more generally, heat of reaction, including pyrolysis, gasification or combustion: The first mechanism, which is already implemented in solver reactingFoam, is typical for the gas phase reactions. In this approach the heat of reaction is determined based on difference in formation enthalpies of subtracts and products. Unfortunately, the enthalpies of formation of solid components, like lignin, are difficult to determine. In such case the heat of process or reaction has to be specified directly based on experimental results. The first methods is well known and used in gas-phase reactions, while the latter is common for solid decomposition. In *biomassGasificationFoam* both approaches are included for gas-phase and solid-phase heterogeneous reactions.
In Fig. 2a and 2b we show the results of drying of 24 mg wood sample with 8% of moisture with heating rate equal 10 K/min and initial temperature 300 K. Note that due to constant heating rate temperature and time axes from left and right plots correspond to each other: 600 s = 100 K. Thus predicted time of evaporation corresponds well with experimental results from thermogravimetric analysis presented in Fig. 1.

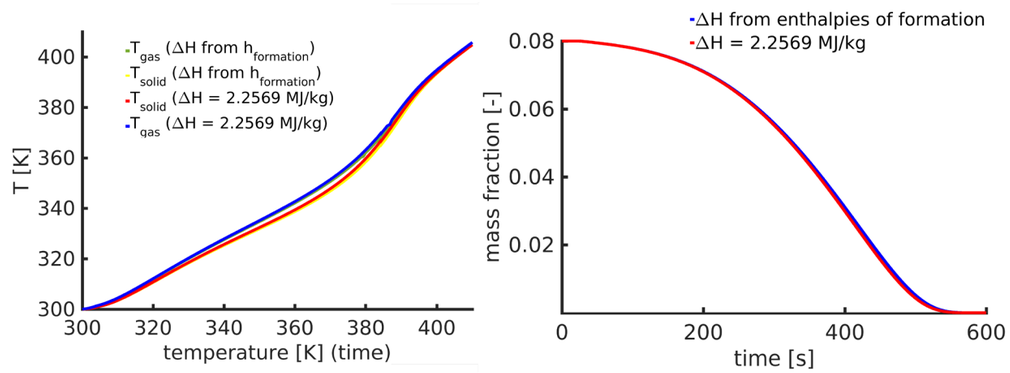


*Figure 2: Temperature profiles for gas and solid during evaporation (left) and evolution of mass fraction of moisture (right)*

Heating by electric heater ensures constant heating rate 10 K/min. At first heat is used to dry wood, thus temperature profile shown in Fig. 2 (left) is lower than linear. In Fig 2 (right) we show that evaporation proceeds at almost the same rate for both methods. Moisture evaporates negligibly faster when the heat of evaporation is directly provided. It is because the heat of evaporation of water (2.2569 MJ/kg) is defined for 373.15 K. When moisture evaporates in lower temperature additional energy is needed to heat water to 373.15 K, as it does when the approach based on the enthalpies of formation is used.

## 5. PYROLYSIS

To demonstrate the functionalities of the *biomassGasificationFoam* solver to simulate pyrolysis, we analyze two different schemes of pyrolysis kinetics presented in Fig. 3: so-called multicomponent approach [5] and more common multistage approach [6]. More complex schemes can be applied as well.

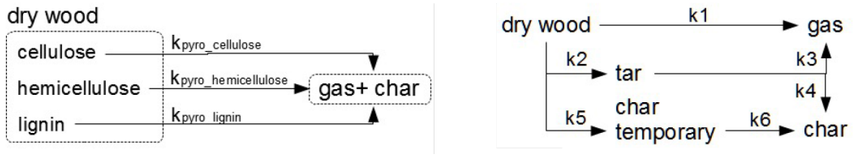


*Figure 3: Two schemes of wood pyrolysis: multicomponent scheme (left) and multistage scheme (right)*

In the multicomponent scheme wood is defined as a set of different components, usually hemicellulose, cellulose and lignin, each of them is decomposed to gas and char (tar yield is neglected). with different rate. Since enthalpies of formation of hemicellulose, cellulose and lignin can be, at least to some extend, approximated by the enthalpies of formation of glucose or similar compounds, we can calculate heat of each reactions.

In the multistage scheme heat of each elementary reaction is individually specified, usually based on analysis of experimental data. However, despite the expensive research on this topic, the uncertainty of experimental data and its analysis is relatively high. The well known scheme developed by Park et al [6] is analyzed in order to demonstrate the exothermic properties pyrolysis. We discuss results and present the improvement of Park's scheme.

## 5.1. Multi-component scheme

In the multi-component analysis, we assume that wood is composed from hemicellulose, cellulose and lignin, which are decomposed according to the following set of reactions [5]:

hem = 3.98 CH4 + 20.84 H2 + 8.46 CO + 7.81 CO2 + 0.058791 char (9.5e8 2.25e4) (R1)
cel = 1.84 CH4 + 5.84 H2 + 9.91 CO + 6.58 CO2 + 0.108791 char (7.0e8 2.35e4) (R2)
lig = 1.57 CH4 + 8.75 H2 + 5.73 CO + 9.72 CO2 + 0.258791 char (1.5e1 1.8e4) (R3)

Reaction R1 is interpreted in the following way: 1 kg of hemicellulose is decomposed into 0.05 kg of char and 0.95 kg of gases, according to given proportion. The first number denotes Arrhenius constant, while the second is activation temperature. The results of simulation performed with multi-component schemes are presented in Fig. 4.

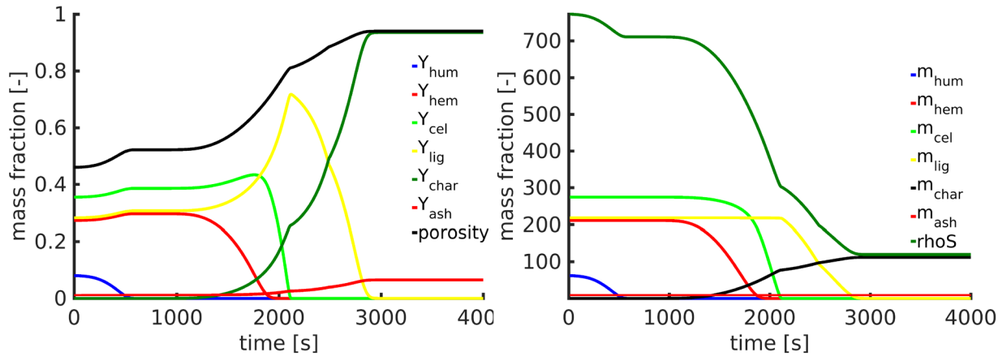


*Figure 4: Evolution of mass fractions of wood components and porosity (left). Evolution of densities of wood and its components (right)*

Note that the increase of mass fractions of wood components visible in Fig. 4 (left) is due to the fact that total mass of wood (denominator in mass fractions) is decreasing. As we show in Fig. 4 (right) the mass of each components is decreasing.





## 5.2. Multi-stage schemes

The multi-stages mechanism presented in Fig. 3 (right) is analyzed, where the wood is decomposed into gas, tar and char through intermediate stages of temporary char. We test two sets of kinetic constants, original set proposed by Park's et al [6] and its modification. The parameters of kinetic used in *biomassGasificationFoam* are summarized in Table 1. Note that Arrhenius constants in pyrolysis schemes often differ from each by several orders of magnitude [6].

*Table 1: Kinetic constants for multi-stage kinetics*

| reactions | kinetic constants from [6]<br>Arrhenius constat [1/s],<br>activation temperature [K],<br>heat of reaction [J/kg] | modified kinetic constants<br>Arrhenius constat [1/s],<br>activation temperature [K],<br>heat of reaction [J/kg] |
|---|---|---|
| wood = gas | 4.38e9, 1.837e4, 8.0e4 | 2.38e5, 1.98e4, 8.0e4 |
| wood = tar solid (part of solid) | 1.08e10, 1.78e4, 8.0e4 | 2.08e4, 2.08e4, 8.0e4 |
| wood = char1 (temporary char) | 3.75e6, 1.343e4, 8.0e4 | 1.05e4, 1.88e4, 8.0e4 |
| tarsolid = gas + 0.1 tar (gaseous tar) | 4.28e4, 1.299e4, -4.02e4 | 1.28e3, 1.71e4, -4.02e4 |
| tarsolid = char (final char) | 1.00e5, 1.299e4, -4.02e4 | 1.00e3, 1.299e4, -4.02e4 |
| char1 (temporary) = char (final) | 1.38e10, 1.936e5, -30.e4 | 8.08e1, 1.7e4, -30e4 |

In Fig. 5 we present the evolution of mass fractions and densities of wood and pyrolysis products, when kinetics scheme developed by Park's et al. [6] is used. The whole process takes less than 600 s, when sample is still colder than 400 K. Moreover, wood is transformed into final char so rapidly, that only small amount of gas and tar is produced. Thus, the overall mass loss is negligible. Kinetics developed in [6] overshoots rates of all reactions when applied to the *biomassGasificationFoam*. The most probable reason is that non-equilibrium approach for heat transfer adopted in the *biomassGasificationFoam* [1,2] works more effectively than usually used equilibrium approach.

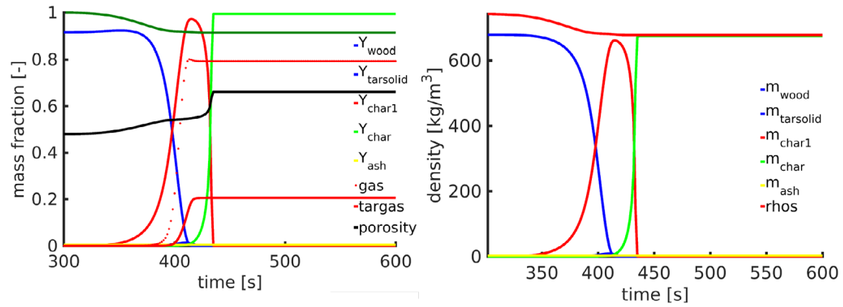


*Figure 5: Results with kinetics developed by Park's et al. [6]. Evolution of mass fractions of wood, pyrolysis products and porosity (left). Evolution of densities of wood and products of pyrolysis (right)*

The improved kinetics is presented in Table 1. Note that Arrhenius constants are smaller and more coherent than in [6], with significantly slower rate of char production from temporary char and from wood. Slowing down wood carbonization has two effects: it increases pyrolysis time and it gives enough time for gas and tar to be devolatized. In Fig. 6. we present results performed with improved kinetics.
Simulated process slows down rapidly around 1800 s, when temperature exceeds 600 K, which corresponds with experimental results presented in Fg. 1. The slow mass loss visible for high temperature is partially reproduced, but it does not last as long as in during the TGA experiment. It has to stressed that presented corresponds to simplified one-cell test case, when hydrodynamical effects are neglected.

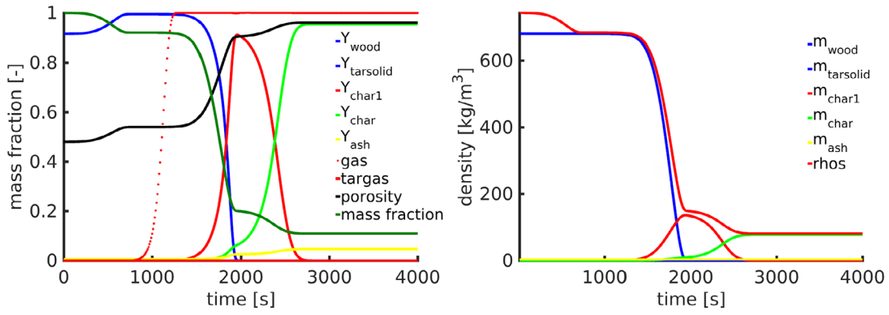


*Figure 6: Improved kinetics. Evolution of mass fractions of wood, pyrolysis products and porosity (left). Evolution of densities of wood and products of pyrolysis (right)*

## 6. CONCLUSION

We shortly demonstrated simulation of evaporation and pyrolysis done with the *biomassGasificationFoam i*n oversimplified test case. Two approaches providing heat of reactions implemented in the solver were verified in the evaporation case. Two different schemes for describing complex process of pyrolysis were compared: multi-component and multi-stage schemes. Both of them give reasonable results when kinetic constants are adequate. Standard kinetics has to be verified before using in *biomassGasificationFoam*.

## 7. ACKNOWLEDGEMENTS

This work has been funded by the Polish Ministry of Science and Higher Education (Ministerstwo Nauki i Szkolnictwa Wyższego) under program Iuventus Plus IP2014 729 024373.

## 8. REFERENCES

[01] OpenFOAM, The OpenFOAM Foundation (2016). www.openfoam.org [last access 30.09.2016]
[02] foam 3.1 (former foem-extenede), www.openfoamwiki.net/ [last access 30.09.2016]
[03] K Kwiatkowski, PJ Zuk, M Dudyński, K Bajer (2014). Pyrolysis and gasification of single biomass particle–new openFoam solver, J. Phys.: Conf. Ser. 530 012015
[04] K Kwiatkowski, PJ Zuk, biomassGasififcationFoam project, https://www.researchgate.net/project/biomass-GasificationFoam [last access 30.09.2016]
[05] K Kwiatkowski, B Górecki, J Korotko, W Gryglas, M Dudyński, K Bajer (2014). Numerical Modeling of Biomass Pyrolysis—Heat and Mass Transport Models, Num. Heat Transfer A. 64,
[06] WC Park, A Atreya, HR Baum (2010). Experimental and theoretical investigation of heat and mass transfer processes during wood pyrolysis, Comb Flame, 157, 481-494.





*Mateusz Szubel (AGH University of Science and Technology, Poland)*

# Selected aspects of straw combustion in straw batch boilers - numerical and experimental approach

*Mateusz Szubel, Grzegorz Basista, Mariusz Filipowicz*
*AGH University of Science and Technology*
*al. Mickiewicza 30, 30-059 Krakow, Poland*
*mszubel@agh.edu.pl, basistag@agh.edu.pl, filipow@agh.edu.pl*

*Wojciech Adamczyk*
*Institute of Thermal Technology, Silesian University of Technology*
*Konarskiego 22, 44-100 Gliwice, Poland*
*wojciech.adamczyk@polsl.pl*

**KEYWORDS:** Biomass, combustion, boilers, experiments, CFD simulations

## ABSTRACT

The selection and design of any biomass combustion system is mainly determined by the characteristics of the fuel to be used, local environmental legislation, the costs and performance of the equipment necessary or available as well as the energy and capacity needed [1]. Not all of the biomass residues can be used for energy production. In many cases it would be economically unjustified, i.e. when stock is too distracted (then low energy density does not allow for recovery or transportation) or when storage is too cost expensive [2]. Due to the high content of the volatiles in biomass, in case of the analysis of combustion of this type of fuel, gasification as well as combustion of its products are often considered as the most significant stages of the biomass combustion process. Besides the above mentioned problems concerning fuel properties, serious difficulties arising from the use of biomass-fired boilers are related with control of the post-combustion of products of the gasification (especially carbon monoxide). Solution for many problems mentioned above is to use biomass in relatively small dedicated units - in distributed generation. From this point of view, straw batch boilers are very promising and give opportunity to consume fuel in place of production. The paper is short review of selected aspects of the studies devoted to operation and optimization of the straw-fired batch boilers. Described studies are performed on Faculty of Energy and Fuels, AGH University of Science and technology in Krakow (Poland). Series of the experimental and the numerical analyses have been carried out, mainly to determine critical factors which are responsible for efficient combustion in the secondary combustion chamber of heating units.

## 1. INTRODUCTION

Some countries such as Denmark have extensive experiences in the field of practical and theoretical studies regarding low-power biomass batch boilers [3]. In Poland, many heating units such as straw-fired boilers are based on Danish designs. Despite the robust structure, reliability and simple handling, improvement in the field of CO emission is still necessary. Increase of total efficiency of the unit as well as reduction of the CO emission is possible mainly by separation of the primary combustion and the secondary combustion. Figure 1 shows differences between the simple, classic batch boiler and the modified modern construction which is currently popular on the polish market. The most significant change is modification of direction of the gases flow and separation of the secondary combustion in vertical rear section of the chamber, as well as change in range of the air staging system configuration.

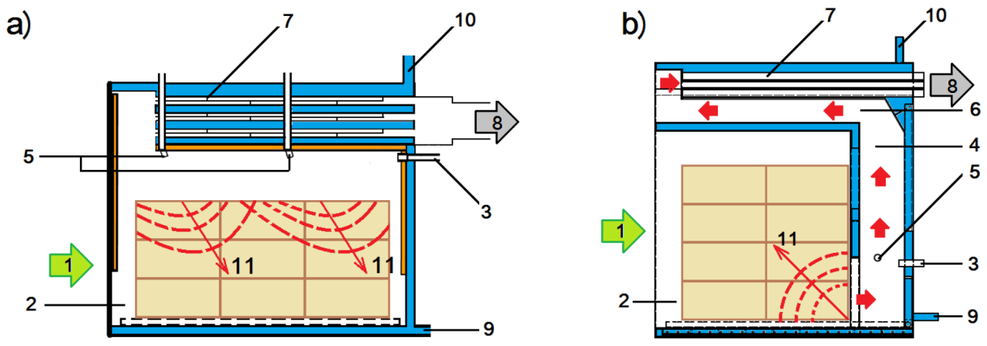


*Figure 1: Cross section of the simple batch boiler [3] (a) and the modern batch boiler [4] (b): 1) direction of the fuel loading (door), 2) primary combustion chamber, 3) primary air nozzles connected through the air manifold with the fan, 4) secondary combustion chamber, 5) secondary air nozzle on the side wall of the secondary combustion chamber, 6) dust separator, 7) heat exchanger, 8) outlet of the exhaust, 9) inlet of the cold water, 10) outlet of the hot water, 11) arrows showing general direction of the flame propagation*

However, even in the case of units with the primary and the secondary combustion section, possibility of reduction of CO concentration in exhaust is limited. It is especially problematic in big units, in which volume of the secondary combustion chamber is larger. In case of the small - scale straw - fired batch boiler few major reasons of incomplete combustion in the secondary combustion section have to be listed: too low excess air ratio, too low temperature level in the area of combustion, insufficient mixing of combustible gases and an oxidizer and incorrect localisation of the air nozzles.

Numerous studies devoted to possibilities of optimization of operation of above mentioned type of heating units in range of the emissions and total efficiency are carried out by scientists from AGH University of Science and Technology (AGH UST), supported by specialists from Silesian University of Technology with support of the producer of the biomass - fired batch boilers. Selected aspects of the research are described in further chapters of this paper.

## 2. EXPERIMENTAL VARIANT ANALYSIS OF IMPACT OF THE AIR DIRECTIONAL NOZZLES ON THE POST COMBUSTION OF CARBON MONOXIDE

In case of the most popular type of the straw - fired batch boilers the air distribution system consists of two parts responsible for the primary and the secondary air feeding. Figure 2a shows the air manifold installed behind the rear wall of the 180 kW boiler which has been examined on the Faculty of Energy and Fuels of AGH UST. Two secondary air nozzles are installed on the side walls, opposite each other, perpendicular to the series of seven primary air nozzles (on the rear wall).

Two additional terminations of the secondary air inlets (Fig. 2b) has been applied to reach better mixing of the gasification products and air. Design of the nozzles was based on the promising results of the numerical simulation of the air staging system in straw - fired boiler, what has been described in [4]. Special nozzles were designed as the diffusors (to increase the air velocity and to provide a wider air flux) deflected vertically and horizontally. Two types of the nozzles have been produced - first pair deflected by 5°, second one deflected by 10°. To examine new elements of the air feeding system, experiments have been carried out for the variants of application of each type of the nozzles (each angle of the deflection), as well as for the boiler in the state-of-the-art (lack of directional nozzles).





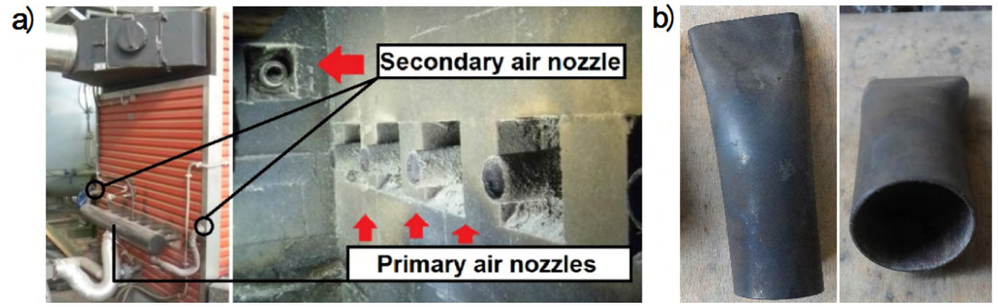


*Figure 2: a) Location of the air manifold at the rear wall of the boiler and the view of the air pipes from the inside of the combustion chamber; b) the nozzles produced for the experimental tests removed from the combustion chamber after the measurements*

To perform measurements of the temperature inside the combustion chambers, PTTK thermocouples have been applied. Four sensors have been selected to control the temperature during the operation of the boiler. The locations of the temperature measurement points has been provided below: $T_{right}$ – the centre of the right wall of the primary combustion chamber, $T_{left}$ – the centre of the left wall of the primary combustion chamber, $T_{in}$ – the rear wall of the boiler, at about 1/3rd of the height of the vertical area of the secondary combustion chamber (inlet of the syngas to the secondary combustion chamber), $T_{out}$ – top part of the right wall of the secondary combustion chamber. MRU ECO 3000 exhaust analyzer has been applied during the experimental tests to determine CO content in the exhaust lifted to the chimney.

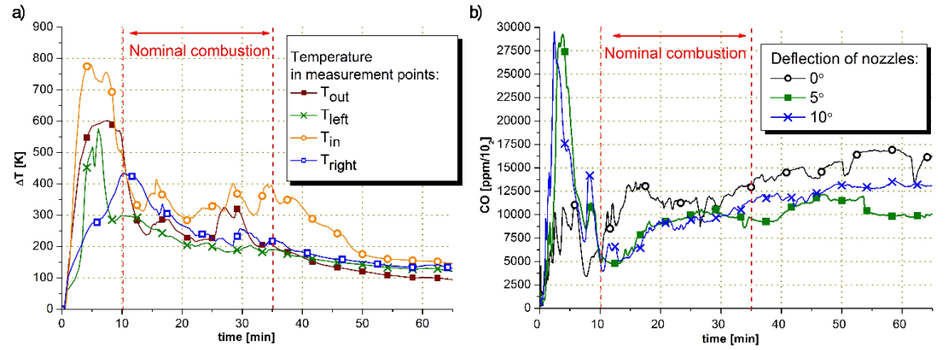


*Figure 3: Selected result of the experiments: a) temperature variation in measurement points during the combustion process; b) comparison of three examined cases of the secondary air directioning*

Number of straw boxes for the individual test was 4 (30% of the nominal load). Three experiments for each case of the nozzle angle have been carried out. Before comparison of CO emission, analysis of the dynamics of temperature variation has been performed to determine stages of the combustion. Ignition, nominal combustion and smouldering of the charcoal have been distinguished (Fig. 3a). Significant reduction of CO content in the exhaust has been noted both in case of 5° as well as 10° of the nozzles deflection (Fig. 3b). However, average emission in the second and third step of combustion was the lowest for the second case (5°).

## 3. NUMERICAL VARIANT ANALYSIS OF IMPACT OF AIR STAGING SYSTEM CONFIGURATION ON SELECTED PARAMETERS OF THE BOILER

Based on numerous tests carried out on the experimental stand of the boiler designed according to description from previous chapter, it was possible to develop a prototype of the unit equipped with advanced air staging system (Fig. 4). The boiler is currently under installation on the test stand on AGH UST. Before first run of the device, based on previous experiences as well as technical specification of the new boiler it was possible to develop simplified numerical model of the operation of the unit.

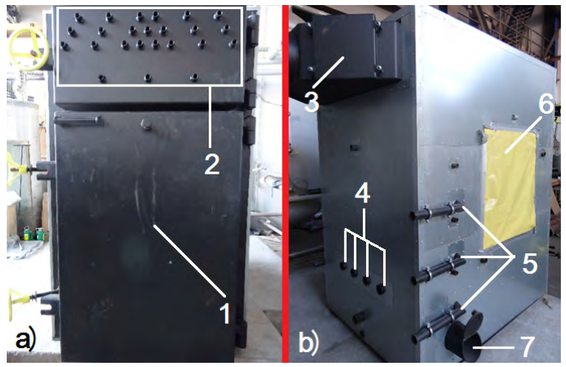


*Figure 4: Newly designed prototype of the straw-fired batch boiler, adapted to application of automatic fuel feeding; a) front view: 1) door, 2) series of the measuring connectors located on the support door; b) rear corner view: 3) flue, 4) primary air inlets, 5) secondary air inlets, 6) connection of the fuel feeder, 7) ignition orifice*

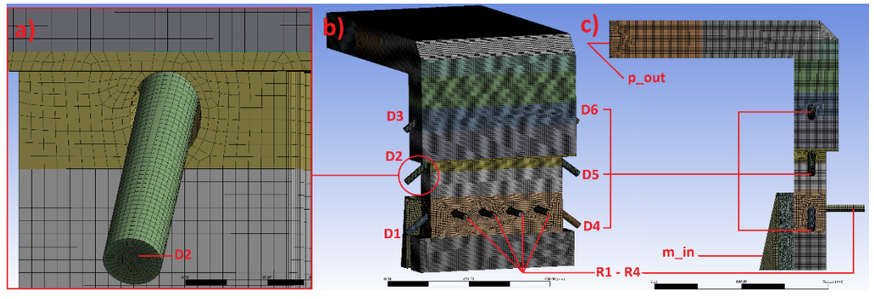


*Figure 5: Spatial geometry of the secondary chamber (vertical part) and the ash separator (top horizontal part) after the process of discretization of the computational domain – zoom presenting computational grid (a), 3D view (b): R1 – R4–primary air nozzles, D1 – D2–secondary air nozzles, and side view (c): m_in–inlet of products of the gasification to the chamber (separated triangle element is part of the primary chamber filled by straw), p_out–outlet of exhaust from the computational domain*

A numerical CFD RANS model has been developed to analyse the phenomenon occurring at the beginning of the combustion in the area of the secondary combustion chamber. Fluid dynamics as well as the combustion model allowed to determine impact of the configuration of the air feeding system on the key elements of the heat balance of the device.

Figure 5 presents spatial geometry, as well as result of the discretisation process ($1{,}75 \cdot 10^6$ of control volumes). Inlet of the syngas to the secondary combustion chamber through the area of porous zone (piece of the straw cube) has been determined as the boundary condition. Simulations have been carried out for few variants of the air feeding configuration, what is included in Table 1. The transport equation were based on the k-eps realizable model of turbulence. Impact of absorption of the energy by three-atom molecules ($H_2O$, $CO_2$) has been took into account using "weighted sum of gray gases model" in radiation modelling. Eight chemical reactions were determined and given reagents have been took into account: $H_2$, $O_2$, CO, $CH_4$, $NH_3$, NO, HCN and products $H_2O$, $CO_2$, CO, $H_2$, NO, $N_2$ [5].





*Table 1: Inlet boundary conditions in analyzed variants of air feeding*

| Variant | R1 | R2 | R3 | R4 | D1 | D2 | D3 | D4 | D5 | D6 |
|---|---|---|---|---|---|---|---|---|---|---|
| | [g/s] | | | | | | | | | |
| 1 | 15,5 | 18,5 | 18,5 | 15,5 | 16,6 | x | x | 16,6 | x | x |
| 2 | | | | | x | 16,6 | x | x | 16,6 | x |
| 3 | | | | | x | x | 16,6 | x | x | 16,6 |
| 4 | | | | | 8,4 | 8,4 | x | 8,4 | 8,4 | x |
| 5 | | | | | 5,53 | 5,53 | 5,53 | 5,53 | 5,53 | 5,53 |
| 6 | | | | | 16,6 | 16,6 | x | 16,6 | 16,6 | x |
| 7 | | | | | 16,6 | 16,6 | 16,6 | 16,6 | 16,6 | 16,6 |

Based on results of simulations, selected elements of the heat balance of the boiler have been determined. Temperature of exhaust and concentration of CO in examined variants are showed in Figure 5a. Figure 5b presents value of loss related with heat which is lifted up with exhaust through the outlet of the secondary chamber. It has to be noted, that hot gas leaving the chamber flows through the heat exchanger, which allows to reduce exhaust temperature. Second parameter included on the chart is incomplete combustion loss, related with presence of combustible compounds in the exhaust.

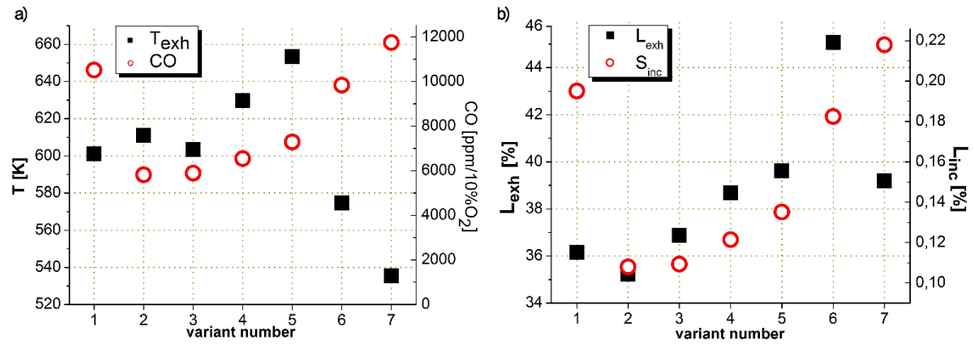


*Figure 6: Exhaust temperature and concentration of CO in exhaust (a), as well as the flue gas loss $L_{exh}$ and incomplete combustion loss $L_{inc}$ depending on the variant of air feeding*

Despite that in second variant the exhaust temperature as well as concentration of CO are not the lowest, the greatest reduction of studied losses has been achieved. It can be concluded, that it is result of impact of the location of the secondary air nozzles as well as the air mass flow rate on the efficiency of the post - combustion.

## 4. CONCLUSION

The robust structure, reliability, simple handling and low cost of operation, especially in case of own fuel are the most important advantages of the biomass - fired batch boilers. Improvement in range of the emission levels as well as total efficiency of the units is possible by studies using both of experimental and numerical methods. Implementation of the CFD modelling with governing equations adapted to simulations of combustion gives complex information concerning the impact of design of the heating unit and control of operation on important parameters of the combustion process. Selected examples of studies carried out on the AGH UST described in the paper prove that it is possible to significantly improve series of features of the batch boilers by implementation of relatively

simple modifications. It is recommended to expand air feeding system in range of number, position and shape of the air nozzles to optimize conditions of the post - combustion in the secondary combustion chamber. Promising results of the previous works allow to conclude that it is possible to adapt parameters of the straw - fired batch boilers to the most restrictive environmental regulations.

## 5. ACKNOWLEDGEMENTS

The studies performed on the experimental stand and the CFD analyses were carried out under the project “BioORC: Construction of cogeneration system with small to medium size biomass boilers” project. The construction of the measurement stand with the straw – fired batch boiler was possible thanks to the METALERG company (Oława, Poland).

## 6. REFERENCES

[01] Van Loo S, Koppejan J. (2008). The Handbook of Biomass Combustion and Co-firing, Earthscan (ISBN 978-1-84407-249-1).
[02] Johansson T. B, Kelly H, Reddy A. K. N, Williams R. H. (1993). Renewable Energy Sources for Fuels and Electricity, Island Press (ISBN 1-55936-139-2).
[03] Kristensen E. F., Kristensen J. K, (2004) Development and test of small-scale batch-fired straw boilers in Denmark. Biomass and Bioenergy. 26: 561-569
[04] Szubel M. (2015). Analysis of selected problems of biomass combustion process in batch boilers – experimental and numerical approach, Experimental Fluid Mechanics 2015: proceedings of the international conference: November 17.–20. 2015, Prague, Czech Republic: 778-787
[05] Miltner M, Makaruk A, Harasek M, Friedl A. (2008) Computational fluid dynamic simulation of a solid biomass combustor: modelling approaches. Clean Technologies in Environmental Policy. 10: 165-174





# PRESENTATIONS

*Shekhar R. Kulkarni (Ghent University, Belgium)*

# Numerical investigation of process intensification of biomass fast pyrolysis in a Gas-Solid Vortex Reactor

*Shekhar R. Kulkarni, Laurien A. Vandewalle, Arturo González Quiroga, Pieter A. Reyniers, Kevin M. Van Geem*, Guy B. Marin*
*Laboratory for Chemical Technology (LCT), Ghent University,*
*914 Technologiepark-Zwijnaarde - 9052 Ghent, Belgium*
**corresponding author: Kevin.VanGeem@UGent.be*

**KEYWORDS:** Gas-Solid Vortex Reactor, fast pyrolysis, process intensification, lignocellulosic biomass

## ABSTRACT

Bio-oil, generated from fast pyrolysis of biomass, is emerging as an alternative energy carrier, complimentary to traditional fossil fuels. Fast pyrolysis requires certain reactor characteristics to be fulfilled in order to achieve a high biomass conversion and selectivity towards the desired compounds: i.e. high interfacial heat transfer; rapid removal and quenching of generated bio-oil vapours and precise temperature control. None of the currently employed reactor configurations simultaneously fulfill all of these criteria. A new reactor concept is presented called the Gas-Solid Vortex Reactor (GSVR), which can be beneficial for obtaining high yields of high-quality bio-oil [1] from lignocellulosic biomass A detailed gas-flow analysis of the GSVR at various operating conditions desired for fast pyrolysis of biomass is presented in this work.

## 1. INTRODUCTION

Biomass fast pyrolysis has the potential to become one of the main contributors to renewable energy. The process can harvest energies in biomass and directly produce a fuel-grade liquid, commonly known as bio-oil. Additionally, commercially valuable chemicals such as 4-ethylguaiacol, furfural, creosol and catechol, are observed to be present in bio-oil fraction, making fast pyrolysis all the more valuable and attractive. Though bio-oil mass yields as high as 75% are reported, it is highly dependent on the vapour residence time inside the reactor, the heat transfer rate to the solid particles and the rapid cooling of the generated vapours.

The Gas-Solid Vortex Reactor (GSVR) can be considered as a fluidized bed reactor in which rotating particle beds are generated due to the actions of centrifugal and drag forces. Centrifugal force in these devices is typically generated by introducing the fluidization gas at high velocity via small, circumferentially distributed slots. One such vortex reactor, intended for generating bio-oil by fast pyrolysis of lignocellulosic biomass is being constructed at the Laboratory for Chemical Technology of Ghent University. As shown in Figure 1, this GSVR consists of two concentric cylinders in which the fluidization gas is distributed around the annulus and enters tangentially into the inner chamber via eight rectangular, 1 mm width slots, positioned at 10° with respect to the tangent. The axial length and the internal diameter of the reactor are 15 mm and 80 mm, respectively. Biomass is fed at one point next to the gas inlet slots through a circular conduit of 10 mm diameter connected to the top plate of the inner chamber, located at an 18° inclination with respect to the horizontal plane. Mass and energy balances show that the lower and upper limit for the biomass mass flow rate are $1.4\ 10^{-4}$ and $8.3\ 10^{-4}$ kg $s^{-1}$ respectively. The corresponding operating windows for the gas ($N_2$) mass flow rate and inlet temperature are $5.0\ 10^{-3}$ - $1.0\ 10^{-2}$ kg $s^{-1}$ and 800 - 923 K. As also indicated, the bottom wall and the outlet walls are profiled to minimize axial recirculation , which would unfavourably increase the residence time of unwanted particles and the pyrolysis vapours.

The GSVR exhibits fluidization in a centrifugal field and hence operates at inertial forces higher than the gravitational force. This results in a sustained, rotating, and moderately dense packed bed of biomass along the circumferential wall beyond the slots [2]. Such a solid bed is characterized by higher width-to-height ratios and by slip velocities much larger than those of a gravitational fluidized bed.





Better heat transfer is thus achieved in this reactor configuration, allowing a more precise control of the reaction temperature compared to conventional fluidized bed reactors [3]. Also, using high velocity gas to maintain bed rotation reduces the space time of vapour phase in the GSVR. Owing to these properties, the GSVR becomes suitable for the fast pyrolysis of lignocellulosic biomass.

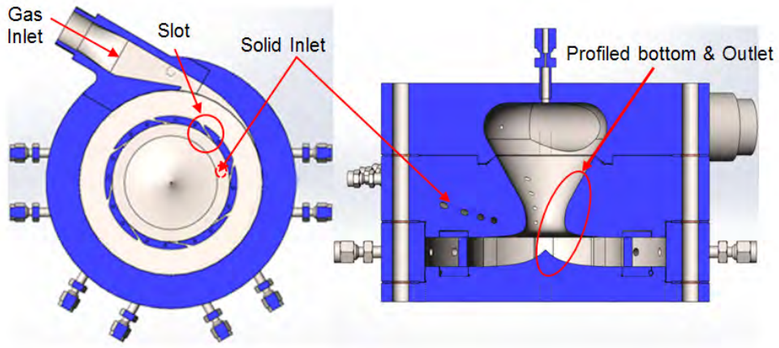


*Figure 1: Top view and side view of the Gas-Solid Vortex Reactor designed at the Laboratory for Chemical Technology of Ghent University*

## 2. RESULTS AND DISCUSSIONS

### 2.1. Simulation Conditions

Computational fluid dynamic simulations were performed in order to get a better insight in the gas flow properties and fluid dynamics inside the GSVR. These simulations were performed in the commercial CFD software package ANSYS Fluent 15.0. The general simulation conditions are listed in Table 1.

*Table 1 : General simulation conditions*

| | |
|---|---|
| Gas | Nitrogen |
| Density Model | Ideal Gas |
| Thermal Conductivity Model | Kinetic Theory |
| Viscosity Model | Kinetic Theory |
| Gas Inlet Temperature | 842 K |
| Inlet Gas Pressure | 50 kPa (g) |
| Outlet Gas Pressure | 10 kPa (g) |
| Near-Wall Treatment | Standard |
| Gravity | Enabled |

### 2.2. Computational domain size

Due to the design of the tangential inlet, the rotational symmetry of the GSVR is broken. However, to reduce the computational domain for the simulations, the effect of omitting the tangential inlet is investigated, thus restoring rotational symmetry and allowing to reduce the computational domain to 1/8th of its original size. A comparative study on the three obtained reactor geometries was performed, see Figure 2: full geometry with the tangential gas inlet (~$2.3\ 10^6$ cells); full geometry with circumferential gas inlet (~$1.7\ 10^6$ cells) and 1/8th pie section with circumferential inlet (~$0.25\ 10^6$ cells). In case of the pie-shape domain, periodic boundary conditions were used on the tangential domain boundaries. These steady-state gas-only simulations were performed with the realizable k-ε turbulence model at equivalent boundary conditions.

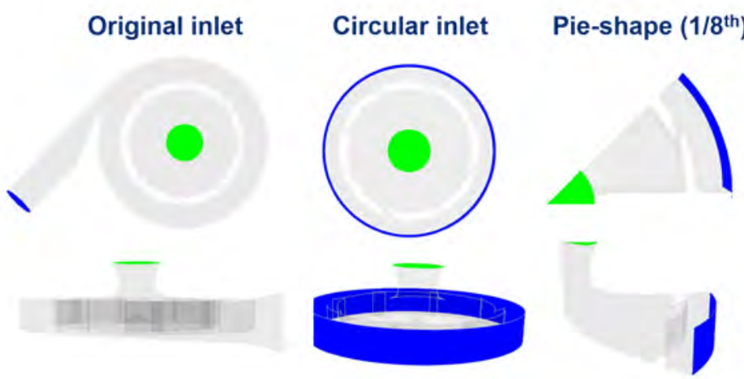


*Figure 2 : Three Geometries of the reactive GSVR studied*

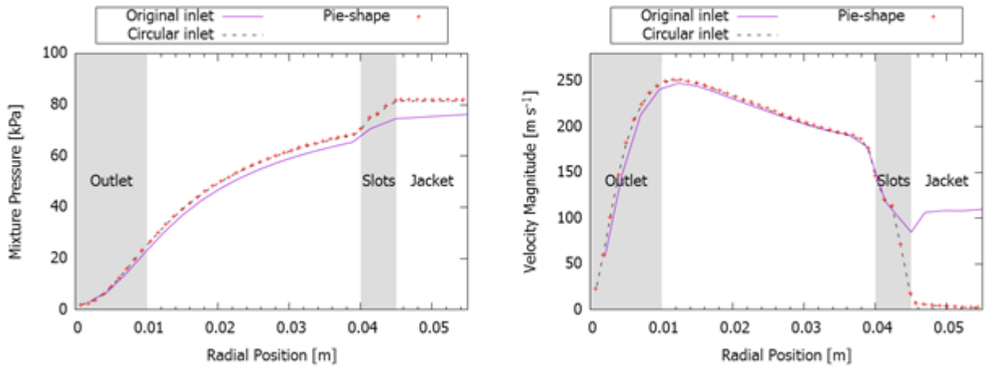


*Figure 3 : Pressure and Velocity comparisons in various reactor geometries*

As can be seen in Figure 3, both the pressure and velocity show very similar trends in all three configurations. Noticeable differences in these profiles are visible only in the jacket and in the slots as the velocity, in particular the tangential velocity, there is much lower in case of a circumferential inlet. The radial component on the other hand behaves quite similar for all geometries, also in the slots. Nevertheless, since the differences in the inner chamber are negligible, it was deemed acceptable to reduce the computational domain to 1/8$^{th}$ of its original size to decrease the computational cost.

### 2.3. Turbulence Model Comparisons

The realizable k-ε (rk-ε) model and Reynolds Stress Model (RSM) were compared for a constant gas flow of $10^{-2}$ kg $s^{-1}$ under the hot flow inlet conditions. Based on the pressure and velocity profiles for both these cases, the results obtained with both turbulence models are very similar, as shown in Figure 4.

The anisotropy of stresses inside these reactors can be captured to a satisfying level with an inherently isotropic model such as the realizable k-ε model. However, as the simulations with the rk-ε model are faster and more stable than those with the RSM model, this model is selected.





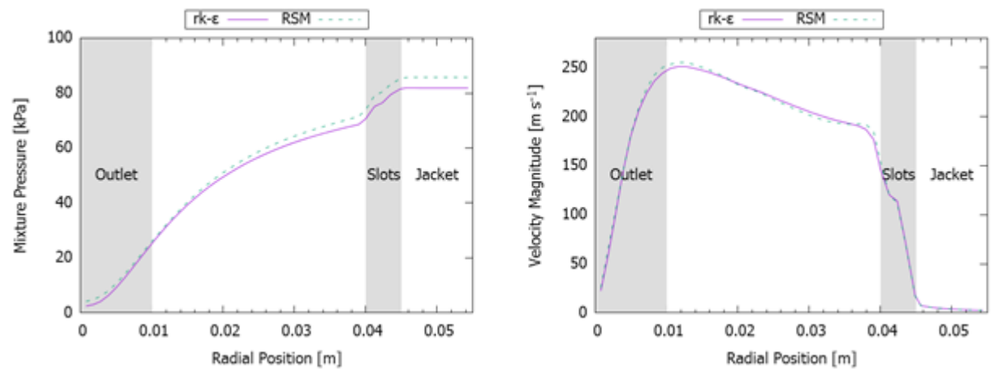


*Figure 4 : Comparison of realizable-k-ε and RSM turbulence model for gas-only simulations in GSVR*

### 2.4. Gas-only simulations

These simulations are performed with realizable k-ε turbulence model for gas flow $10^{-2}$ kg $s^{-1}$ and inlet temperature of 842 K. The pressure profiles at z=10 mm plane for hot flow is displayed in Figure 5. The pressure drop across the slots and between the slots & the outlet of the reactor is 12 kPa and 40 kPa respectively. These values are in agreement to the order of magnitude with similar works published in the literature [1].

As seen in the velocity field in Figure 6, a strongly swirling flow is developed inside the reactor. As is characteristic of a swirling flow, the velocity increases as the radius decreases. Towards the centre of the reactor, an axial recirculation zone is created which reduces the velocity to near-zero values.

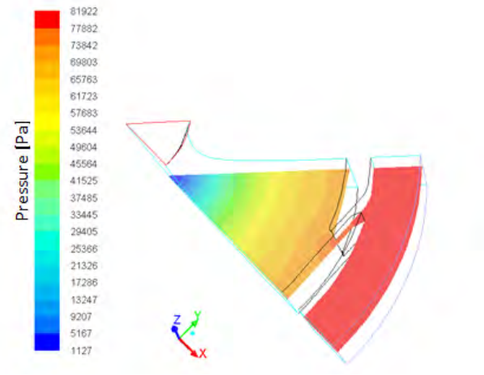


*Figure 5: Pressure profile across axial plane at z=10 mm. gas flow rate= $10^{-2}$ kg $s^{-1}$, T=842 K*

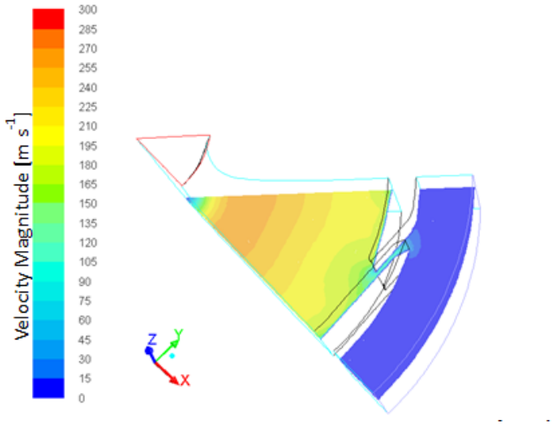


*Figure 6 : Velocity magnitude across axial plane at z=10 mm. gas flow rate= $10^{-2}$ kg $s^{-1}$, T=842 K*

As can be seen in Figure 7, the tangential velocity component is the dominant contribution to the total gas velocity. The radial velocity is low compared to the tangential velocity, except for in the slots. This confirms that the flow inside the reactor is swirl-dominated. The relative maximum in radial velocity near the reactor outlet will result in a maximum of radial drag force and will be important for particle entrainment in gas-solid operation.

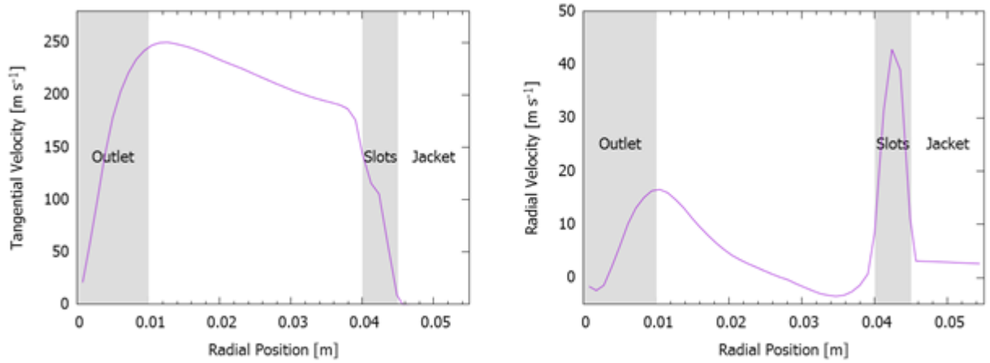


*Figure 7 : Profile of tangential and radial velocity, gas flow rate: $10^{-2}$ kg $s^{-1}$ T= 842 K*

## 3. CONCLUSION

Gas-only simulations of the GSVR display promising trends in terms of using this reactor for the fast pyrolysis of biomass. The comparisons between various turbulence models revealed there is not much difference in the calculated parameters in the reactor. The pressure drop values across the slots and in the reactor are reasonable and coherent with the published literature in similar areas. Detailed gas-only simulations indicate that the tangential velocity is the dominant velocity component in the inner chamber of the reactor. However, the high tangential velocities induce an axial recirculation zone close to the central axis of the reactor. In a next phase, gas-solid simulations will be carried out to confirm the operating window of the geometry and to assess the bed stability at various operating conditions. Ultimately, the full pyrolysis process will be simulated, including chemical reactions.

## 4. ACKNOWLEDGEMENTS

The SBO project “Bioleum” (IWT-SBO 130039) supported by the Institute for Promotion of Innovation through Science and Technology in Flanders (IWT) is acknowledged. The research leading to these results has received funding from the European Research Council under the European Union’s Seventh Framework Programme (FP7/2007-2013) / ERC grant agreement n° 290793. PAR acknowledges financial support from a doctoral fellowship from the Fund for Scientific Research Flanders (FWO). LAV acknowledges financial support from the Fund for Scientific Research Flanders (FWO), in association with the PI-FLOW project. The computational resources and services used in this work were provided by the VSC (Flemish Supercomputer Center), funded by the Research Foundation Flanders (FWO) and the Flemish Government – department EWI.

## 5. REFERENCES

[01] Ashcraft, R.W., G.J. Heynderickx, and G.B. Marin, Modeling fast biomass pyrolysis in a gas–solid vortex reactor. Chemical Engineering Journal, 2012. 207-208: p. 195-208.
[02] Kovacevic, J.Z., et al., Bed stability and maximum solids capacity in a Gas–Solid Vortex Reactor: Experimental study. Chemical Engineering Science, 2014. 106: p. 293-303.
[03] Volchkov, E.P., et al., Aerodynamics and Heat and Mass Transfer of Fluidized Particle Beds in Vortex Chambers. Heat Transfer Engineering, 1993. 14(3): p. 36-47.

*Souman Rudra (University of Agder, Norway)*

# A computational fluid dynamics analysis for the effects of variable Equivalence Ratio (ER) on birchwood gasification

*K.G.R.M. Jayathilake, Souman Rudra*
*University of Agder*
*4879, Grimstad, Norway*
*kgjaya14@student.uia.no, souman.rudra@uia.no*

**KEYWORDS:** Biomass, gasification, CFD, simulation, syngas

## ABSTRACT

The main focus of this work was to model the gasification process of the gasifier available at University of Agder (UIA), Norway, in a CFD interface and to examine the behaviour of gasification parameters. The gasification parameters such as producer gas yield, syngas composition, cold gas efficiency and lower heating value of the syngas were examined with a variable equivalence ratio (ER) using Birchwood as the feedstock. In this work the equivalence ratio was varied from 0.2 to 0.5. In addition the model was validated using the experimental data which were obtained from the actual fixed bed downdraft gasifier.

For the simulation work Birchwood particle with a diameter of 11.5 mm was used as the feedstock. In addition both gas and solid phases were modelled and also both homogeneous and heterogeneous reactions were considered for the work. Simulation data has predicted the syngas composition very closely to the experimental results. The cold gas efficiency (CGE) has been predicted for a very accurate value with the experimental values as well as the syngas yield.

## 1. INTRODUCTION

The impacts of greenhouse gasses on the atmosphere have helped biomass emerge as a power source which emits no greenhouse gasses [1]. Apart from combustion, gasification is also a very useful way of energy production from biomass [2]. As gasification is a very complex process using an engineering tool such as Computational Fluid Dynamics (CFD) can be emphatically helpful as it is rather a feasible and easy to use way to analyse the gasification process [3]. Regarding gasification process many more gasification characteristics can be measured. This paper is presented on Computational Fluid dynamics analysis for the effects of Equivalence Ratio (ER) on birchwood gasification, using fixed bed downdraft gasification method.

The physical and chemical activities which are taken place during gasification are very close to the carbonaceous thermal decomposition. Simply, drying, devolatilization oxidation and reduction of the biomass is occurred inside the gasifier [4]. During the gasification as both gas and solid phases are present, in order to model the gasification process with a CFD code both homogeneous and heterogeneous reactions should be considered.
Downdraft gasifiers are been proved to perform well within the ER ratio of 0.25 [5]. But even within the ER ratio of 0.43 it has shown some good performances too [6]. So in this work Equivalence Ratio (ER) value from 0.2 to 0.5 have been considered. In addition here in this work the downdraft gasifier available at university of Agder, Norway was used. So the CFD model was developed as to emulate the actual gasifier used for the experiments.





## 2. EXPERIMENTAL SETUP AND FEEDSTOCK

### 2.1. Material used as the Feedstock

In this study birch wood is used as the feedstock. The results of the ultimate and the proximate analysis for the Birchwood have been listed down in the Table 2.1 below [5].

*Table 1: Proximate and ultimate analysis of Birchwood*

| **Proximate analysis (dry basis)** | | **Ultimate analysis (dry basis)** | |
|---|---|---|---|
| Moisture % | 7 | Carbon % | 50.4 |
| Volatiles % | 82.2 | Hydrogen % | 5.6 |
| Fixed Carbon % | 10.45 | Oxygen % | 43.4 |
| Ash % | 0.35 | Nitrogen % | 0.12 |
| LHV (MJ/kg) | 17.9 | Sulphur % | 0.017 |
| | | Chlorine % | 0.019 |

According to the above analysis results, moisture content of the birchwood is comparably low. In gasification perspective it is an important aspect [7]. In addition Birchwood shows a lower amount of ash, Cl, S and as well as a higher value volatile matter and calorific value. Less ash can lead to a conversion process with less slag. As it has high carbon content Birchwood has a higher calorific value. [5].

### 2.2. Experimental setup

A schematic diagram of the system is shown below in Figure 1.

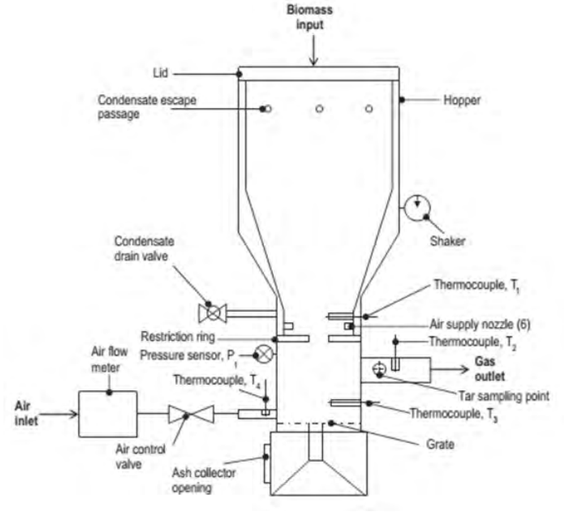


*Figure 2.1: Schematic diagram of the gasifier system [8]*

The hopper is a conical shaped stainless steel structure with a volume of 0.13 $m^3$ and with double-walled thick walls. It has a radius of 0.5 m. Through this hopper the biomass is fed and the connected electrical shaker can give vibrations every 15 s/min. So with this shaking process the common problems such as channelling and bridging can be reduced or avoided. In order to drain out the condensate moisture a drain valve also attached at the bottom of the hopper.
The reactor has a diameter of 0.26 m. It is 0.6 m in height. The air inlet system is consists of 6 equal nozzles with equal distance from each with a diameter of 5mm and they are located from 0.4 m of the bottom of the reactor. At the bottom of the reactor part, a reciprocally oscillating grate is connected and it takes out the ash to the bottom of the ash collector. The grate is oscillating 30 s/min. In order to measure the weight loss during the gasification process a weight scale is connected at the bottom of the gasifier system. In addition two pressure sensors and five K-type thermocouples are connected to the gasifier assembly to monitor and measure the parameters.

## 3. COMPUTATIONAL MODEL

For the computational model a 3-dimensional geometry of the gasifier was created. Segregated flow model was used to solve the transport equations. In addition Lagrangian particle modeling method was used for particle modeling. The following assumptions were made in order to simplify the system without any decrease in the accuracy.

- Flow is steady
- Particles are spherical shape and have an even distribution
- No slip condition was applied to the reactor walls

The developed 3D model was meshed with a base size of 0.01 m. But in order to obtain more accurate results the cell size was refined to 0.001m at air inlets and for the air fuel mixing region.

## 4. NUMERICAL SCHEME

In the numerical scheme Reynolds averaged Navier Stokes (RANS) equations are solved using an Eulerian- Lagrangian reference frame. The gas phase is solved as a reacting gas phase and the solid (particle) phase is solved using Lagrangian particle models. For turbulence modeling standard k-ε model was used. In addition in this model both eddy dissipation and finite rates are used for the reactions.

### 4.1. Governing Equations

The equation for mass conservation is [9],

$$\frac{\partial \rho}{\partial t} + \frac{\partial \rho v_i}{\partial x_i} = 0 \qquad (1)$$

Where ρ the density of the fluid is, $v_i$ represents the velocity tensor in the compact form in Einstein notation, t is the time and $x_i$ represents the special first order tensor.

The momentum conservation equation is,

$$\rho \frac{\partial u_i}{\partial t} + \rho u_j \frac{\partial u_i}{\partial x_j} = \rho g_i - \nabla P + \frac{\partial}{\partial x}\left[\mu\left(\frac{\partial v_i}{\partial x} + \frac{\partial v_j}{\partial x}\right)\right] \qquad (2)$$

Where $g_i$ represents the gravity force and p is the density of the fluid. P represents the pressure while $\mu$ represents the dynamic viscosity.





The energy equation is [9],

$$\rho\left(\frac{\partial h}{\partial t} + u_i \frac{\partial h}{\partial x_i}\right) = \frac{\partial P}{\partial t} + u_i \frac{\partial P}{\partial x_i} + \frac{\partial}{\partial x_j}(k.\nabla T) + \tau'_{ij}\frac{\partial u_i}{\partial x_j} \qquad (3)$$

Where p represents the density of the fluid P represents the pressure, k represents the thermal conductivity and $\tau'_{ij}$ represents the viscous stress tensor.

### 4.2. Energy model for Lagrangian particles

Using the Nusselt number ($Nu_p$) the heat transfer coefficient can be found for the Lagrangian particle which is energy model for the Lagrangian particle.

$$h_p = \frac{Nu_p}{D_p}.k \qquad (7)$$

Where, k represents the thermal conductivity of the phase and $D_p$ is the particle diameter. Nusselt number ($Nu_p$) is expressed in the following Eq (8) where it is calculated by the Ranz- Marshall correlation which is expressed below in Eq (9).

$$Nu_p = 2\left(1 + 0.3Re_p^{\frac{1}{2}} Pr^{\frac{1}{3}}\right) \qquad (8)$$

Where, Re represents the Reynolds number while the expression Pr expresses the prandtl number.

$$N_u = h\frac{d_p}{k} = a + c\,Re^m\,Pr^n \qquad (9)$$

Where, $N_u$ has represented the Nusselt number, h has represented the heat coefficient, $d_p$ has represented the particle diameter, k has represented the thermal conductivity of the gas, Re has represented the Reynolds number, Pr has represented the prandtl number while a, c, m and n are numerical constants which are determined by the flow field. According to the Ranz- Marshall correlation, it is explained that at fluid velocity (V), equals to zero, the heat transfer can be affected only by conduction. So then the values of a, c, m and n are become 2, 0.6, 0.5, and 0.33, respectively [10].

## 5. REACTIONS MODELLING

For a realistic modeling of the gasification of the Birchwood a qualitative analysis is required to determine the conversion of wood into syngas. So in Birchwood the volatile decomposition is happens according to the following reaction (It is assumed that Birchwood is consisted with only C, H and O).

$$CH_{1.69}O_{0.81} \longrightarrow 0.5605CO + 0.2306CO_2 + 0.1945CH_4 + 0.0144H_2 \qquad (10)$$

The following homogeneous reactions are considered for the modeling work. Both kinetic and eddy dissipation rates have been used for the reactions.

$$CO_{(g)} + H_2O_{(g)} \longleftrightarrow CO_{2(g)} + H_{2(g)} \qquad (11)$$
$$2CO_{(g)} + O_{2(g)} \longrightarrow 2CO_{2(g)} \qquad (12)$$
$$2H_{2(g)} + O_{2(g)} \longrightarrow 2H_2O_{(g)} \qquad (13)$$
$$CH_{4(g)} + 2O_{2(g)} \longrightarrow CO_{2(g)} + 2H_2O_{(g)} \qquad (14)$$

And, the following heterogeneous reactions are considered for the modeling work. Eddy dissipation rates have been used for these reactions.

$$C_{(s)} + O_{2(g)} \longrightarrow CO_{2(g)} \quad (15)$$

$$C_{(s)} + CO_{2(g)} \longrightarrow 2CO_{(g)} \quad (16)$$

$$C_{(s)} + H_2O_{(g)} \longrightarrow CO_{(g)} + H_{2(g)} \quad (17)$$

## 6. RESULTS AND DISCUSSION

### 6.1. Effect of ER on gas composition

When ER is changed the variation of CO mass fraction in both experiment and simulation model have been presented in the following figures 6.1. According to below figure 6.1 computational model has under predicted CO mass fractions. But in the lower ER values both experimental and simulation values have been scattered closely.

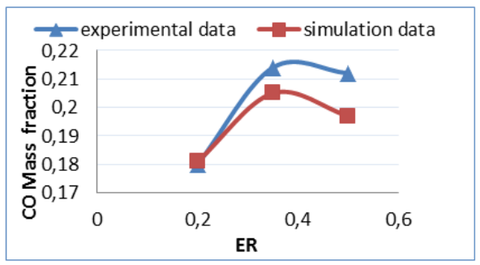


*Figure 6.1: Variation of CO mass fraction as an effect of ER*

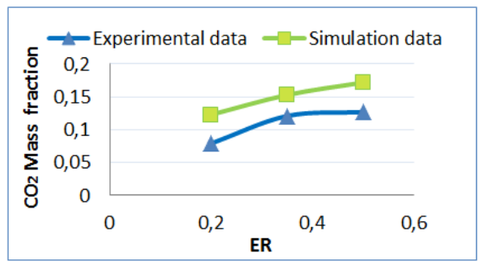


*Figure 6.2: Variation of CO2 mass fraction as an effect of ER*

When ER is changed the variation of $CO_2$ mass fraction in both experimentally and simulation model have been presented in the above figures 6.2. So, the simulation data has over predicted the $CO_2$ mass fractions slightly. When ER is changed the variation of $H_2$ mass fraction in both experimentally and simulation model has been presented in below figure 6.3. According to that $H_2$ mass fractions have shown a slight decrease in the simulation values with comparison to the experimental values.

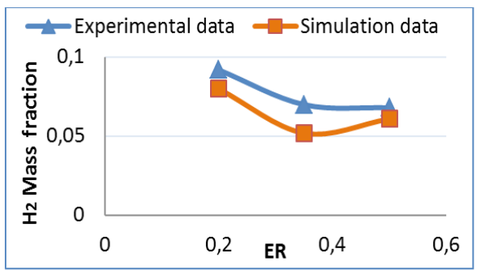


*Figure 6.3 : Variation of H2 mass fraction as an effect of ER*

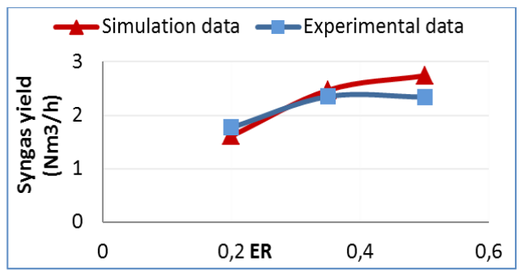


*Figure 6.4 : Variation of syngas yield as an effect of ER*

### 6.2. Effect of ER on syngas yield

When the ER is changed the variation of syngas yield in both experimental and simulation model has been presented above in Figure 6.4. According to the above figure simulation values have shown a very close correlation to the experimental values throughout the whole distribution.

### 6.3. Effect of ER on Cold Gas Efficiency (CGE)

When the ER is changed the variation of CGE in both experimental and simulation model has been presented below in Figure 6.5 So, according to figure 6.5 the CGE value in both experimental and simulation scenarios have shown a great similarity in their values throughout the distribution.

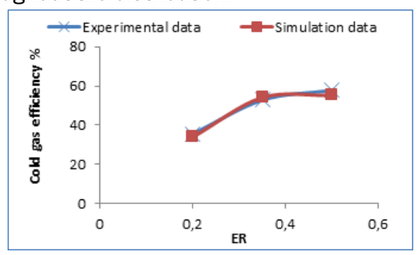


*Figure 6.5 : Variation of CGE as an effect of ER*

## 7. CONCLUSION

According to above results the simulation model has given really close values to the experimentally measured values. Mainly in gas compositions, experimental results have given slightly different values than the simulation values. But according to figure 6.4 and 6.5 simulation values for syngas yield and CGE have given really close values to the experimental values.

- For the experiment, as feedstock, Birchwood chips were used while for the simulations a spherical particle was used which has the diameter as the average length of the actual woodchip. So this might have an effect on the results.
- In the experiment the air in flow rate and the feedstock feeding rates were not constant always. So this might have an impact also.

## 8. REFERENCES

[01] Fletcher et al.(2000).A CFD based combustion model of an entrained flow biomass gasifier. Applied Mathematical Modelling. 24(3):165.

[02] Prabir Basu. (2010) Biomass Gasification and pyrolysis Practical Design and Theory. ELSEVIER. (ISBN- 0080961622)

[03] Petr A. Nikrityuk, Bernd Meyer. (2014).Gasification Processes- Modelling and Simulation. Wiley-VCH. (ISBN-9783527335503).

[04] I.Janajreh et al. (2013).Numerical and experimental investigation of downdraft gasification of wood chips," Energy Conversion and Management.65:783.

[05] S.Sarker et al. (2015.Preliminary fixed-bed downdraft gasification of birch woodchips. International journal of environmental science. 12:2119.

[06] Zainal Z. A.et al. (2001).Prediction of performance of a downdraft gasifier using equilibrium modeling for different biomass materials. Energy Conversion and Management.42:1499.

[07] Atnaw S.M et al. (2014).Influence of Fuel Moisture Content and Reactor Temperature on the Calorific Value of Syngas Resulted from Gasification of Oil Palm Fronds. The Scientific World Journal, Hindawi Publishing Corporation. Article ID 121908, http://dx.doi.org/10.1155/2014/121908

[08] Shiplu Sarker et al. (2015).Assessing the gasification potential of five woodchips species by employing a lab-scale fixed-bed downdraft reactor. Energy Conversion and Management.103:801.

[09] J Blazek. (2001).Computational Fluid Dynamics principles and applications. ELSEVIER. (ISBN-008-0432093)

[10] Abderrahmane et al.(2015).Ranz And Marshall Correlations Limits On Heat Flow Between A Sphere And Its Surrounding Gas At High Temperature.THERMAL SCIENCE.19:1521.

*Nuno Couto (University of Porto, Portugal)*

# A dual-stage approach to simulate Portuguese substrates for gasification purposes

*Nuno Couto[1], Valter Silva[1], Daniela Eusébio[1]*
*[1]Faculty of Engineering, University of Porto*
*Rua Dr. Roberto Frias, Campus da FEUP, 400, 4200-465, Porto, Portugal*
*nunodiniscouto@hotmail.com, vsilva@inegi.up.pt, deusebio@inegi.up.pt*

*Paulo Brito[2]*
*[2]Interdisciplinary Center for Research and Innovation, Polytechnic Institute of Portalegre*
*Lugar da Abadessa, Apartado 148, 7301-901 Portalegre, Portugal*
*pbrito@estgp.pt*

*Abel Rouboa[1,3,4]*
*[3]University of Trás-os-Montes and Alto Douro*
*Quinta de Prados 5000-801, Vila Real, Portugal*
*rouboa@utad.pt*
*[4]MEAM Department, University of Pennsylvania*
*PA 19020, Philadelphia, USA*
*rouboa@seas.upenn.edu*

**KEYWORDS:** Thermodynamic dual stage model, carbon boundary point, syngas quality indices, gasification

**ABSTRACT**

A thermodynamical dual stage model was used to study the effect of the gasification temperature and steam to biomass ratio on several syngas quality indices: $H_2$/CO ratio, $CH_4$/$H_2$ ratio and cold gas efficiency by using vineyard pruning residues as feedstock. Vineyard pruning residues were found to be a promising substrate for fuel cell and integrated gasification systems applications. Also, this feedstock shows good results under different syngas quality indices being versatile to be used in different applications.

## 1. INTRODUCTION

Equilibrium models are very important tools to study the influence of most parameters for any biomass system because of their gasifier design independence. Among the several approaches to develop equilibrium models, dual stage models imply several advantages [1]. The use of a dual stage approach makes an advantageous use of the carbon boundary point (CBP) allowing a more detailed understanding of the gasification phenomenon. The introduction of the CBP divides the gasification process in two different stages. The first stage considers a heterogeneous equilibrium where all the compositions are found below and at the CBP. At this stage there is the presence of unconverted solid carbon. Its total depletion occurs only at the CBP. The second stage considers a homogeneous equilibrium where all the compositions are in the gaseous state without any unconverted solid carbon. These models can be applied to evaluate the potential of biomass feedstocks for syngas generation. Portugal is one of the main wine producers in the world generating about 700 millions of $dm^3$ of wine per year. There is a great interest by Portuguese entities to study the best ways to valorize the residues and sub products generated by this industry. This paper aims at presenting a dual stage thermodynamical model applied to the gasification of biomass. The use of vine pruning residues is studied concerning the quality of syngas based on different indices including $H_2$/CO ratio, $CH_4$/$H_2$ ratio and cold gas efficiency.





## 2. MATHEMATICAL MODEL

A thermodynamical dual stage model was used to compute different syngas quality indices. The numerical model was firstly developed and detailed in [2]. It is divided in two main stages: the heterogeneous and the homogeneous equilibrium.
As mentioned before the CBP separates the homogeneous and the heterogeneous equilibrium. The equations describing the homogeneous equilibrium as well as numerical procedures can be found in the literature [2].

The global gasification reaction can be written as follows:

$$CH_xO_yN_z + wH_2O + m(O_2 + 3.76N_2) = n_{H_2}H_2 + n_{CO}CO + n_{CO_2}CO_2 + n_{H_2O}H_2O + n_{CH_4}CH_4 + \left(\frac{z}{2} + 3.76m\right)N_2 + n_{Char}Char \quad (1)$$

Where x, y and z are the number of atoms of hydrogen, oxygen, and nitrogen per number of atom of carbon in the feedstock, and w and m are the amount of moisture and oxygen per kmol of feedstock, respectively. The subscripts x, y and z are determined from the ultimate analysis of the biomass.
At the heterogeneous equilibrium, the mass balance considers the carbon, hydrogen and oxygen species, respectively:

$$n_{CO} + n_{CO_2} + n_{CH_4} + n_{Char} - 1 = 0 \quad (2)$$

$$2n_{H_2} + 2n_{H_2O} + 4n_{CH_4} - x - 2w = 0 \quad (3)$$

$$n_{CO} + 2n_{CO_2} + n_{H_2O} - w - 2m - y = 0 \quad (4)$$

The chemical reactions considered are the exothermic methane formation, the endothermic water-gas and Boudouard reactions, respectively:

$$C + 2H_2 = CH_4 \quad (5)$$

$$C + H_2O = CO + H_2 \quad (6)$$

$$C + CO_2 = 2CO \quad (7)$$

The equilibrium constants for each one of these reactions are computed using the following equation:

$$K(T) = exp\left(\frac{\Sigma_i \vartheta_i g_i^0}{RT}\right) \quad (8)$$

Where $R$ is the universal gas constant 8.314 J·kmol-1·K-1, $\vartheta_i$ is the stoichiometric coefficient, and $g_i^0$ is the molar specific Gibbs function at the reference state.

Finally, the global energy balance equation below and at the CBP can be defined as follows for a 1 kg of biomass:

$$Q + LHV_{biomass} + \Delta h_{air} \times n_{air} + \Delta h_{water} \times n_{water} = \left(\Delta h_{gas} + LHV_{gas}\right) \times n_{gas} + \left(\Delta h_{carbon} \times C_{p,carbon}\right) n_c\, Char \quad (9)$$

Where $Q$ is the heat addition to the gasification process, $C_{p,carbon}$ is the heat capacity of solid carbon (in kJ·kmol-1·K-1) and h is the gas enthalpy difference at any given T and at 298 K. The correlations for computing the HHV (high heating value) of the fuel and the LHV (lower heating value) of the gas can be obtained in the literature, respectively [3, 4].

## 3. RESULTS AND DISCUSSION

Syngas quality can be defined based on parameters such as $H_2$/CO ratio, $CH_4/H_2$ ratio and cold gas efficiency, among others. The thermodynamical dual stage model was used to study the effect of different operating conditions and their interactions on the syngas quality.
The main application for a syngas with high $H_2$/CO ratio is related to the fuel cell technology. In general, syngas generated from biomass tends to have a relatively low $H_2$/CO ratio (<1). It can be observed from Figure 1 that vineyard pruning residues show a high $H_2$/CO ratio with values ranging approximately from 1.1 to 1.7.

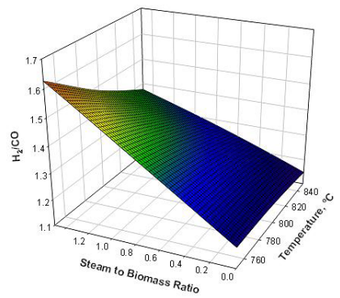


*Figure 1: $H_2$/CO ratio as a function of temperature gasification and steam to biomass ratio*

According to Le Chatelier's principle, endothermic reactions are favored by higher temperatures. This leads to increase in the hydrogen content due to strengthening of the endothermic reaction. In fact, since both $H_2$ and CO tend to increase with gasification temperature this operation condition doesn't affect significantly the $H_2$/CO ratio. Increasing the steam to biomass ratio (SBR) leads to an increase on $H_2$ content but consumption of CO (water/gas shift reaction) [5] and therefore $H_2$/CO ratio increases. The $H_2$/CO ratio in volatile matter is constant, so this ratio increase is related to the chemical reactions that are being developed along the gasification process. At low values of SBR both carbon and methane are reformed leading to the formation of $H_2$ with its concentration increase. At SBRs higher than 1, the hydrogen increases slowly and after 1.5 there is no increase effect. This implies that the surplus of steam is not reacting and that adding more steam is not efficient.
For domestic purposes, it is preferable to obtain a syngas with higher $CH_4/H_2$ ratio. In Figure 2 is depicted the Syngas $CH_4/H_2$ molar ratio as a function of the temperature and SBR for vineyard pruning.

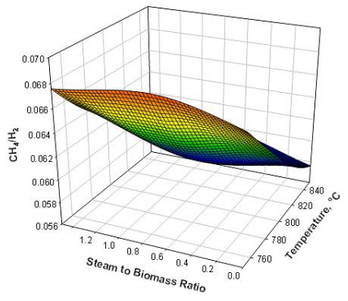


*Figure 2: $CH_4/H_2$ ratio as a function of gasification temperature and steam to biomass ratio*

As previous stated hydrogen increases with temperature and since methane is a small fraction (compared with hydrogen fraction) and its variation doesn't produce significant change to the ratio the $CH_4/H_2$ ratio decreases with temperature. Because of this the SBR effect was very slight on $CH_4/H_2$ ratio.





Maximizing the operating conditions in order to obtain a syngas with higher cold gas efficiency has to be a priority so that gasification can replace fossil fuels. The cold gas efficiency (CGE) is defined as the percentage of the heating value of biomass converted into the heating value of the product gas. In Figure 3 CGE is presented as a function of the steam to biomass ratio and temperature gasification.

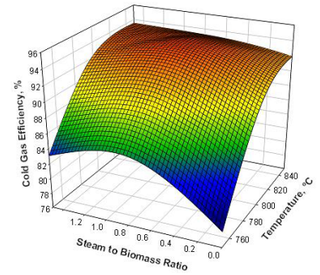


*Figure 3: Cold gas efficiency as a function of the temperature gasification and steam to biomass ratio*

CGE increases with SBR until $H_2$ formation starts to decrease slowly (after SBR =1). What this implies is that the surplus of steam is not reacting so supplying extra steam will only cost efficiency to the system. In fact, CGE will actually decrease due to this reason. Also, CGE increases with the gasification temperature. High gas efficiencies are suitable for IGCC (integrated gasification combined cycles) applications.

## 4. CONCLUSIONS

Syngas quality indices are essential to determine the best application to a given biomass. In order to investigate the influence of certain operating conditions on syngas quality indices for vineyard pruning residues a thermodynamical dual stage model was used.
Temperature gasification from 750 ºC up to 850 ºC as well as steam to biomass ratio from 0 to 1.5 were used to study the effects of operating conditions on both $H_2$/CO and $CH_4/H_2$ ratios along with cold gas efficiency. The model was able to predict with accuracy all the trends for the performed simulations. Vineyard pruning residues showed good versatility to be used in different applications, especially for fuel cell and integrated gasification systems.

## 5. ACKNOWLEDGMENTS

We would like to express our gratitude to the Portuguese Foundation for Science and Technology (FCT) for the support to the grant SFRH/BD/86068/2012 and the projects PTDC/EMS-ENE/6553/2014 and IF 01772.

## 6. REFERENCES

[01] Silva V, Rouboa A. Optimizing the gasification operating conditions of forest residues by coupling a two-stage equilibrium model with a response surface methodology. Fuel Process Technol 2014; 122; 163-9.
[02] Silva V, Rouboa A. Using a two-stage equilibrium model to simulate oxygen air enriched gasification of pine biomass residues. Fuel Process Technol 2013; 109; 111-17.
[03] Channiwala S.A, Parkih P.P. A unified correlation for estimation HHV of solid liquid and gaseous fuels, Fuel 2002; 81; 1051–63.
[04] Karamarkovic R, Karamarkovic V. Energy and exergy analysis of biomass gasification at different temperatures, Energy 2010; 35; 537–49.
[05] Silva V, Monteiro E, Couto N, Brito P, Rouboa A. Analysis of syngas quality from Portuguese biomasses: An experimental and numerical study. Energy and Fuels 28 (2014) 5766-5777.

*Thomas Plankenbühler (Friedrich-Alexander-University Erlangen-Nuremberg, Germany)*

# Numerical simulation and experimental investigation of slagging in biomass combustion

*Thomas Plankenbühler, Dominik Müller, Jürgen Karl*
*Chair of Energy Process Engineering, Friedrich-Alexander-University Erlangen-Nuremberg*
*Fürther Straße 244f, 90429 Nürnberg, Germany*
*thomas.plankenbuehler@fau.de, dominik.mueller@fau.de, juergen.karl@fau.de*

**KEYWORDS:** Biomass combustion, ash, slagging, power plant

## ABSTRACT

The Chair of Energy Process Engineering at Friedrich-Alexander-University Erlangen-Nuremberg (FAU-EVT) developed a prediction tool for slagging and fouling in biomass boilers in the megawatt range. The long-term goal of our work is the enhancement of the fuel flexibility in biomass boilers. Towards this goal, we devised a CFD simulation methodology for ash-related phenomena including particle combustion, the formation of slag and its wall adhesion.
After plant operators' experience, high fine particle content in the biomass feedstock one of the prevailing factors for the emergence of ash depositions. These fine particles are carried away from the fuel bed, thus burn in the flue gas duct, locally exceeding melting temperatures. Hereinafter, on wall contact, the nascent ash sticks, leading to depositions. Therefore our slagging prediction model is premised on biomass particle combustion with special regard to ash properties like the elemental composition, viscosity and surface tension. The resulting methodology is used as a post-processor for CFD simulations of biomass firings.
Exerting this prediction tool, we performed simulations of gas phase combustion and slagging indicator for different biofuels in various combustion chambers – grate firings and fluidised beds – in the megawatt range. The obtained results are in good agreement with operator experiences and observations during power plant maintenance.
In addition to CFD simulations, we performed experiments of particle combustion and slagging behaviour in a 100 kW fluidised bed facility at FAU-EVT. An extra inlet for a fuel fine particle fraction above the fluidised bed allows controlled combustion in the freeboard area, provoking higher amounts of slagging. An isothermal probe based on the heat pipe principle collects these depositions. The experimental results supply necessary boundary conditions for the CFD model.

## 1. INTRODUCTION

Ash-related phenomena like slagging and fouling are major obstacles in solid biomass combustion [1]. Inorganic matter deposits on boiler walls and heat transfer surfaces, leading to costly maintenance works, shorter operating cycles and sharply accelerated corrosion processes.
Especially alternative biomass feedstock like forest residues, landscape conservation material and herbaceous material show particularly unfavourable slagging behaviour due to various reasons [2]. First of all, these biomaterials usually evince an unpropitious elemental composition, featuring high alkali (e.g. potassium and sodium) concentration as well as elevated silicon and phosphorous content (in comparison to log wood). In addition, biomass feedstock usually suffers from a high proportion of fine particles, consisting of fuel particles conjointly with foreign matter like soil. These properties lead to increased amount of ash and slag depositions. Eventually, existing biomass firings were often conceived and constructed for traditional biomass feedstock, operators thus lack of experience in the utilization of alternative biofuels.
However, the enhancement of fuel flexibility of existing biomass furnaces must be strived for future economic and ecologic plant operation. CFD simulations are a potent tool for the pre-assessment of the (slagging) behaviour of new biofuels as well as for the determination of suitable operational conditions for their utilization.
Therefore, the Chair of Energy Process Engineering at the Friedrich-Alexander-University Erlangen-Nuremberg (FAU-EVT) developed a methodology for combustion simulation of biomass power plants in the megawatt range.





Special focus lays on the prediction of ash deposition and slagging emergence. This conference contribution describes our CFD modelling strategy as well as its application on existing biomass power plants. Eventually, we describe our experimental setup used for the validation of the model's assumptions.

## 2. SIMULATION PRINCIPLES

### 2.1. Slagging modelling

Slagging and fouling can, in theory, occur due to a variety of different mechanisms like thermophoresis, condensation or (eddy) diffusion. However, inertial deposition on boiler walls and heat transfer surfaces accounts usually for the largest share of contaminations [3](2. The other mechanisms dominate only for ash particle diameters smaller than 1 µm - and often only during the first hours of plant operation. Since our model focusses on slagging due to burning fuel fine particles in the flue gas duct, inertial deposition is the most relevant.
When a molten – thus sticky – ash particle collides with a solid interface, the formation of slagging can be described by a statistic approach proposed by Walsh [4]:

$$p_{stick}(T_P, T_S) = p_{Particle}(T_P) + \left(1 - p_{Particle}(T_P)\right) \cdot p_{Surface}(T_S) - p_{Erosion} \quad (1)$$

The sticking probability $p_{stick}$ depends on an intrinsic particle stickiness $p_{Particle}$ and a certain surface sticking probability $p_{Surface}$. In the simplest case, these parameters are only a function of particle and wall temperature, like in equation (1). This is addressed by temperature-dependent formulation of fuel, ash or wall properties like viscosity, surface tension. Besides that, dimensionless correlations like Weber- and Stokes-number [5]from the injection position to the deposit surface, the information about the char combustion rate is essential. Of particular importance is determination (through measurements are often included as additional slagging criteria.

For the hereby presented work, we rely on an approach based those numbers combined with thermodynamic calculations performed with FACTSAGE™. This procedure bases on fuel ashes' elemental composition and their temperature-dependent equilibrium liquid fraction $Y_{melt}$. This value can be connected to the particle sticking probability $p_{Particle}$ by the following expression:

$$p_{Particle} = \frac{Y_{melt}(Tp) - 0.1}{0.7 - 0.1} \quad \text{für} \quad 0.1 \leq Y_{melt} < 0.7 \quad (2)$$

Figure 1 displays exemplary temperature dependent melting curves for straw pellets and wood chips.

### 2.2. Simulation of gas phase combustion

The described methodology for slag formation monitoring is combined with CFD gas-phase combustion simulations of biomass combustion chambers like grate firing and fluidized-bed furnaces. Inlet boundary conditions are derived from in-house calculation tools like [6] and operational data. Ansys FLUENT™ 16.2 serves as simulation environment.

Gas phase combustion is described with a lumped species approach together with CO oxidation reaction using an EDM/finite-rate reaction model. Turbulence is resolved using k-ε-realizable model with scalable wall functions and RSM for validation purposes. For radiation depiction, we use the Discrete Ordinates model.
In addition to Eulerian gas phase, we use a Discrete Phase Model (DPM) – thus a Lagrangian approach – for the additional calculation of burning fuel fine particles. Devolatilization and particle combustion are, together with the occurring transformation of particle properties, implemented via User Defined Functions (UDF). The rate determining step for char conversion under prevalent conditions is oxygen (boundary layer) diffusion [7], [8].

When a trajectory hits a wall boundary, another UDF calculates the particle stream's intrinsic sticking probability with regard to particle and wall properties by the described method.
This value is compared to a random number provided by a RNG; hereinafter, the corresponding wall face registers a certain amount of slag formation. Calculation of trajectories occurs during post-processing after a steady-state gas-phase solution.

## 3. SIMULATION RESULTS AND DISCUSSION

For this conference contribution, we studied the combustion and slagging behavior of two different biomass power plants, one 50 MW fluidized bed furnace and a 25 MW grate firing. Both combustion chambers were mapped until the economizer passage by structured meshes including geometric details like nozzles and important internal heat transfer surfaces.
The power plants use wood chips and landscape conservations materials as feedstock. Figure 1 shows – in the upper part – the temperature distribution obtained from the described combustion simulation methods. In both cases, the maximum temperature occurs in the area of secondary combustion next to the air nozzles. In general, the simulated values are in good agreement with operational data from the process control system. Furthermore, energy conservation is fulfilled regarding the overall heat balance.

Below the temperature field, figure 1 displays the predicted amount of slagging due to fine particle combustion for both power plants in a typical full load scenario. The coloring as "specific slagging" – with 1 being the highest amount of contamination – is area- and thermal load-weighted and time averaged. This allows comparison of different boiler geometries and different operational scenarios.
For both power plants, slagging occurs in the first boiler pass, peaking in the area of secondary combustion. The high amount of depositions in that area can be explained by the presence of oxygen due to the air supply, which enhances both gas phase and particle combustion, leading to high particle stickiness.
The abrupt end of contaminations in the upper part of the first pass locally fits the end of refractory. This leads to lower wall temperature and corresponding flue gas cooling, resulting in a sharp decrease of sticky particles. This phenomenon could be observed under realistic conditions in the actual power plant during maintenance works.
In general, our simulations are in a good agreement with observations and plant operators' experience. Furthermore, a recent survey performed by FAU-EVT among operators 100+ biomass heat and/or power plants emphasize the high influence of fuel fine particles on the slagging behavior of biomass feedstock [8].

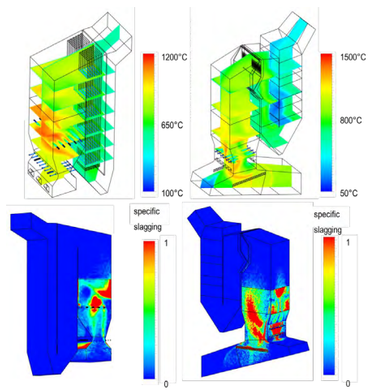


*Figure 1: CFD simulation results of the temperature field (up) and deposition prediction (low) in a 50 MW fluidized bed firing (left) and a 25 MW grate furnace (right) using wood chips as fuel [8]*





## 4. EXPERIMENTAL INVESTIGATIONS

The presented methodology, especially the postulate of significant influence of the fuel fine particles were investigated in a lab experiment carried out at FAU-EVT. For this purpose, we performed slagging experiments using a 100 kW fluidized bed combustion facility. Ash depositions are collected at the surface of an isothermal slagging probe built as heat pipe. After a defined duration of operation, the collected contaminations can be scraped off, weighted and further analyzed [9].
Wood chips and different kinds of pellets serve as primary fuel. An additional thermal load of up to 20 kW can be provided by grinded particle in the range up to 2 mm, injected into the freeboard area through a separate nozzle. Figure 2 displays the experimental setup.

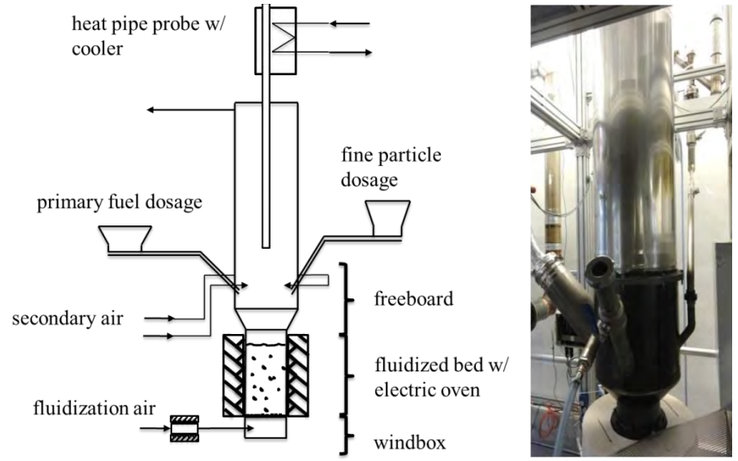


*Figure 2: Experimental setup used for slagging investigations (adapted from [10])*

The experiments show a highly elevated amount of collected depositions after 8 hours of operation when fuel is introduced as fine particles instead of pellets or wood chips. Therefore our experimental investigations affirm the modelling methodology focusing on the simulation of burning fine particles (Fig 3).

Eventually, the obtained slag properties were further studied using SEM/EDS and laser diffraction size analysis.

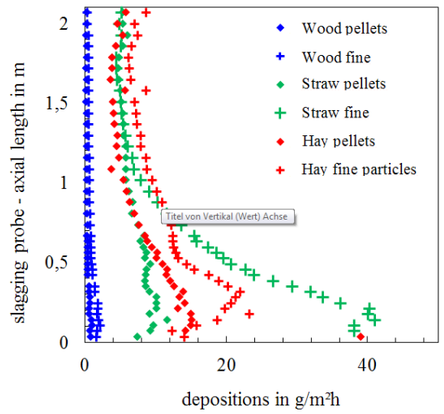


*Figure 3: Collected depositions on slagging probe using pellets and fine particles as fuel*

## 5. CONCLUSION

In this conference contribution, we present recent developments towards an efficient and convincing CFD model in order to predict slagging in biomass firings in the megawatt range. The model focuses on fine fuel particle as the main reason for the occurrence of ash depositions. The CFD results – here shown in two different kinds of boiler technologies – can be used to evaluate alternative biomass feedstock. Furthermore, this methodology allows engineering and development of ameliorated operating strategies.

## 6. ACKNOWLEDGEMENTS

This work has been supported by the Bundesministerium für Wirtschaft und Energie (BMWi) under the grant „Energetische Biomassenutzung“ (03KB069).

## 7. REFERENCES

[01] J. Karl, Dezentrale Energiesysteme: Neue Technologien im liberalisierten Energiemarkt. Oldenbourg Verlag, 2012.
[02] B. Gatternig, “Predicting Agglomeration in Biomass Fired Fluidized Beds,” 2015.
[03] C. Wieland, B. Kreutzkam, G. Balan, and H. Spliethoff, “Evaluation, comparison and validation of deposition criteria for numerical simulation of slagging,” Appl. Energy, vol. 93, pp. 184–192, 2012.
[04] P. M. Walsh, A. N. Sayre, D. Loehden, J. M. Beer, and A. F. Sarofim, “Pilot scale simulation of ash deposition on an isolated convective tube: the effect of temperature on deposit growth,” no. 21, 1988.
[05] R. Weber, M. Mancini, N. Schaffel-Mancini, and T. Kupka, “On predicting the ash behaviour using Computational Fluid Dynamics,” Fuel Process. Technol., vol. 105, pp. 113–128, 2013.
[06] D. Müller, T. Plankenbühler, and J. Karl, “Numerical simulations of staged fluidized bed boilers based on heat release measurements,” Proc. 2nd Int. Work. Comput. Fluid Dyn. Biomass Thermochem. Convers., vol. 2, 2016.
[07] T. Plankenbühler, D. Müller, and J. Karl, “Numerical simulation and experimental investigations of slagging in biomass combustion,” in Proceedings of the 24th European Biomasse Conference, 2016, pp. 450–456.
[08] T. Plankenbühler and J. Karl, “Erweiterung des Brennstoffbandes moderner Biomassefeuerungen - BMWi-Projektworkshop ‘FuelBand,’” in Workshop Erweiterung des Brennstoffbandes moderner Biomassefeuerungen, 2016.
[09] T. Plankenbühler and J. Karl, “Influence of fuel fine particles on slagging of commercial size biomass boilers,” in Proceedings of the 22nd European Biomasse Conference, 2014.
[10] T. Plankenbühler and J. Karl, “Numerische Simulation und experimentelle Untersuchung der Verschlackungsneigung biogener Brennstoffe,” VDI Berichte - Dtsch. Flammentag, vol. 2267, 2015.





*Dominik Müller (Friedrich-Alexander-University Erlangen-Nuremberg, Germany)*

# Numerical simulations of staged fluidized bed boilers based on heat release measurements

*Dominik Müller, Thomas Plankenbühler, Jürgen Karl*
*Chair of Energy Process Engineering, Friedrich-Alexander-University Erlangen-Nuremberg*
*Fürther Straße 244f, 90429 Nürnberg, Germany*
*dominik.mueller@fau.de, thomas.plankenbuehler@fau.de, juergen.karl@fau.de*

**KEYWORDS:** Fluidized bed combustion, bed model, industrial scale boilers

## ABSTRACT

The determination of inlet boundary conditions for the gas phase simulation of bubbling fluidized bed boilers in respect to the conservation equations of mass, energy and species is a quite difficult problem. This paper presents the application of an adapted model for grate furnaces in combination with the experimental observed results for the heat release within a fluidized bed in order to gain the composition of a syngas. This syngas contains a modelled volatiles species and carbon-monoxide as flammable components and can directly be used in ANSYS Fluent. The simulation of a 43 MW fluidized bed boiler proofs its suitability also for industrial scale power plants. Temperatures and heat transfer can be predicted in a very good accordance to operating data.

## 1. INTRODUCTION

The focus of the project “FuelBand - Erweiterung des Brennstoffbandes moderner Biomassefeuerungen”, founded by the German Federal ministry for Economic Affairs and Energy, was to develop a model for predicting slagging probabilities in biomass boilers [1]. With this tool, it is expected to evaluate the slagging behaviour for still unused fuels with lower qualities, which due to their low costs can have a strong economic impact for the operator. Compared to well-known wood chips, such fuels contain an increased content of ash and fine particles. The central issue is the combustion behaviour of these fine particles, they are carried away by the flue gas and burn along the freeboard of the furnace where they exceed their typically low ash melting temperatures and accumulate at heat exchangers or other components. In order to extend the range of fuels for such power plants it is necessary to predict the slagging probability as a function of fine particles, ash-melting temperature and particle residence time. This approach needs experimental evaluations of the slagging behaviour as well as CFD simulations for the validation with experiences from the operators. One of these power plants is the bubbling fluidized bed boiler located in Heiligenkreuz/Austria. It has a fuel input of 41 MW wood chips with a staged combustion management. It is able to provide 50 t/h of steam at 520 °C and 100 bars.
A special difficulty lies on the generation of boundary conditions for this boiler. A staged combustion means, that the fuel will be only partially burned ($\lambda$ = 0.6...0.8), while there is a second combustion zone within the freeboard of the furnace after the injection of secondary air. For the simulation of the gas phase of fluidized bed boilers, it is necessary to determine a gas composition at the surface of the fluidized bed which contains a certain amount of flammable gases.
This paper will present a methodology for deriving an appropriate gas composition which fulfils the conservation equations of mass, energy and species based on measurements of the heat release for fluidized beds.

## 2. METHODOLOGY

The choice of a chemical equilibrium at the surface of the fluidized bed would assume that a sufficient residence time as well as an entire mixture within the fluidized bed is guaranteed. According to the experiences with fluidized bed combustion, combustion reactions take place even above the surface, which means, that not the complete heat of reaction is transferred within the fluidized bed. Especially for operating conditions with excess air at $\lambda$ = 1.0...1.5, the chemical equilibrium would predict a heating value of 0, while still a significant part of the entire combustion occurs in the freeboard.

The reason is that a uniform mixture cannot be guaranteed due to the low density of the fuel particles, which leads to segregation of the fuel and pyrolysis mechanisms at the surface with a gas release directly to the freeboard [2, 3].

### 2.1. Experimental measurements of the heat release

In 2015, the authors presented a methodology [4] for the measurement of the so-called heat release of fluidized bed combustion

$$\eta_{WS} = \frac{\dot{Q}_{FB}}{\dot{Q}_{fuel}}, \qquad (1)$$

which is defined as the ratio of the in-bed released heat to the heat input of the fuel. It is based on a transient measurement procedure, where the differences of the time-dependent gradients of the bed temperature for fuel-fired conditions as well as for a cool-down run are representing the heat-release. These tests were performed at a 100 kW fluidized bed combustion chamber at the Chair of Energy Process Engineering. Compared to a steady state determination of the heat release over a adequate period, this method allows experiment durations of about 2 hours for each operating condition.

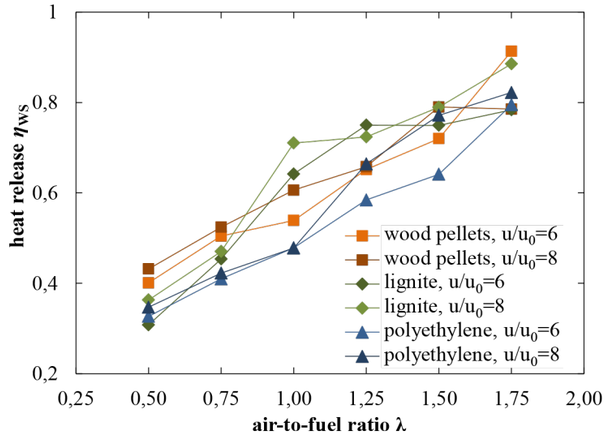


*Figure 1: Experimental determined heat release for the combustion of different fuels at different air-to-fuel ratios λ and fluidization numbers $u/u_0$*

Figure 1 presents the results for three different fuels, each with special properties. Wood pellets as a well-known biofuel with a high volatile matter, lignite with a dominant content of fixed carbon and polyethylene consisting entirely of volatile matter. It can be seen, that the air-to-fuel ratio λ has the pre-dominant effect on the heat release and that fuel and fluidization number $u/u_0$ have minor influence.
At stoichiometric conditions the amount of in-bed released heat is about 50-60%, while a nearly complete heat release would require a high excess of air due to the mixing behaviour of the fluidized bed.

### 2.2. Modelling of inlet boundary conditions

In [5] a model for the simulation of grate furnaces was developed according to literature [6, 7] at the Chair of Energy Process Engineering. It is an experience-based model where the grate is divided into typically five or more discrete zones. Each zone is characterized by a user-defined rate of drying, pyrolysis und combustion of fixed carbon of a fuel with known proximate und ultimate analyses.





Drying means an endothermal release of $H_20$ due to its evaporation, pyrolysis products are modelled as volatiles (“lumped species”) $C_xH_yO_lN_m$ and the combustion of fixed carbon is an exothermal reaction towards carbon-monoxide or – when considering a temperature dependent approach – even towards carbon-dioxide. The heating value of the volatiles is then the heating value of the fuel reduced by the heating value of the amount of fixed carbon. An iterative coupling with the CFD toolkit allows a back coupling of radiative heat transfer for the reactions on the grate in order to close the energy conservation and to determine the conversion rate of combustion reactions already taking place within the bulk.
For the presented simulation it can be assumed, that the entire reactions of drying, pyrolysis and combustion of fixed carbon must take place within the fluidized bed, which means that the number of zones is reduced to one. The result is a composition of a flammable gas (called syngas), while the content of volatiles and carbon-monoxide has to correlate with the remaining heating value according to the heat release measurements. This can be influenced with the conversion rate of the combustion reactions within the modelled zone.

## 3. SIMULATION SETUP

As already mentioned, the boiler operates with a fuel input of nearly 43 MW at staged combustion. Its relevant operating conditions are listed in table 1.

*Table 1: Operating conditions of the fluidized bed boiler*

| | |
|---|---|
| fuel | wood chips (w = 0.4) [8] |
| bed temperature | 700 °C |
| bed material | quartz sand (0.7-1.0 mm) |
| air-to-fuel ratio λ primary air | 0.5 |
| air-to-fuel ratio λ global | 1.3 |

### 3.1. Geometry and mesh

Figure 2 presents the structured mesh of the fluidized bed boiler, it contains 3.3 million cells. The surface of the fluidized bed (3.8 x 6.5 m) represents the inlet boundary, the recirculation gas and the remaining combustion air are injected within a distance 10 meters of the first boiler pass, which is built as a evaporator with finned walls. Further heat exchangers are located in the second and third pass of the boiler, they are modelled as porous zones with negligible resistances in order to represent a simplified heat sink.

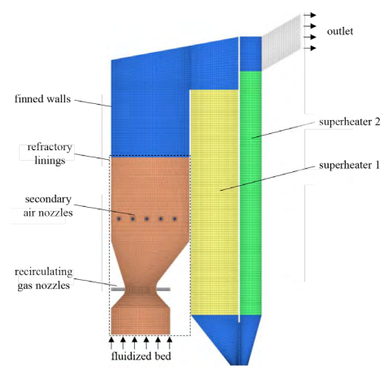


*Figure 2: Mesh of the fluidized bed boiler*

### 3.2. Boundary conditions

Due to the admixture of recirculated flue gas the air-to-fuel ratio within the fluidized bed is increased to λ = 0.6. According to figure 1 this corresponds to a heat release of approximately 42 % when choosing wood pellets as representative due to its comparable fuel properties. The boundary conditions for this setup can be calculated with the previously described model just from mass flows, fuel composition and the specified heat release (figure 3).

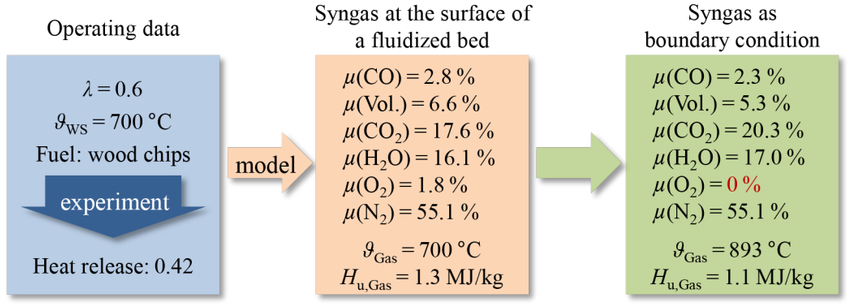


*Figure 3: Calculation methodology for the boundary conditions of a fluidized bed boiler simulation*

Due to a limited heat release, there is still some oxygen in the modelled syngas which – in reality – corresponds to visible flames in the freeboard of the boiler. Unfortunately this is not suitable as boundary condition as it would lead to a combustion reaction within the first cells in a numerical treatment. For this reason, the combustion with this remaining oxygen is already handled in the described model with an equivalent combustion of volatiles and carbon monoxide in order to reach an oxygen content of zero. Of course this has to results in an increase inlet temperature and a decrease of the heating value in order to ensure energy conservation.
Further boundary conditions of walls and kinetics and radiation are similar to the simulation of grate furnaces, why they were chosen according to literature [5]

## 4. RESULTS

Figure 4 presents the temperature distribution within the fluidized bed boiler obtained with ANSYS Fluent. The increase of the temperature due to the combustion reactions starts with the injection of recirculation gas as well as with secondary air. At the end of the refractory linings, the combustion is finished and the heat transfer to the evaporator becomes predominant.

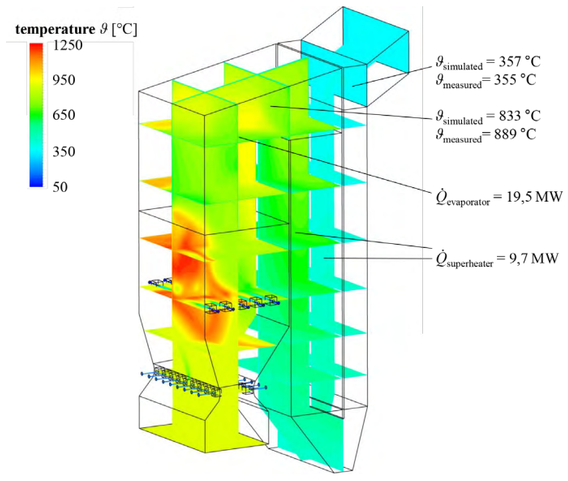


*Figure 4: Simulated temperature distribution within fluidized bed boiler and its comparison with operator's data*

When comparing the simulated temperatures with data from the operator, it gets clear that the differences are within the uncertainty of temperature measurements, which especially for high temperatures are quite difficult. Even the hot spot on the front wall was confirmed by the operator. In addition, the reported data from the operator were only snapshops, especially the heat input differs with varying moisture contents as well as temperatures are relatively subdued as a consequence of the boilers' high heat capacity.

## 5. CONCLUSION

The presented model is an application of a modified experience-based model for grate furnaces. Together with experimental data for the heat release in fluidized bed boilers is able to predict boundary conditions for the simulation of a staged fluidized bed boiler. Simulations are in very good agreement with the measurements and the experiences of the operator. This methodology also allows simulating projected boilers where it is not possible to calculate an energy balance in order to determine the released heat within the fluidized bed. Furthermore, the methodology of measuring the heat release at a laboratory scale and the obtained results are also valid for power plants in the MW range. The simulation of the flow field can now serve as base for simulation of burning particles with the DPM in order to determine the slagging behaviour for the combustion of solid biofuels as presented in [9].

## 6. ACKNOWLEDGEMENTS

This work has been supported by the German Federal ministry for Economic Affairs and Energy (BMWi) under the grant „Energetische Biomassenutzung" (03KB069).

## 7. REFERENCES

[01] Plankenbühler, T.; Karl, J.: "Erweiterung des Brennstoffbandes moderner Biomassefeuerungen - BMWi-Projektworkshop 'FuelBand,'" in: Workshop Erweiterung des Brennstoffbandes moderner Biomassefeuerungen, 2016.
[02] Karl, J.: Dezentrale Energiesysteme: neue Technologien im liberalisierten Energiemarkt. Oldenbourg, 2006.
[03] Scala, F.; Salatino, P. 2004. Modelling fluidized bed combustion of high-volatile solid fuels. Chemical Engineering Science. 57, 7 (Apr. 2004), 1175–1196.
[04] Müller, D.; Karl, J.: Bestimmung der Wärmeentbindung in biomassegefeuerten Wirbelschichten, Forschungskolloquium Bioenergie, Straubing, 11./12.02.2015.
[05] Gring, D.: Numerische Simulation eines biomassegefeuerten Kraftwerkskessels mit Vorschubrost im Leistungsbereich 20 MW, Master thesis, 2013.
[06] C. Yin, L. Rosendahl, S. K. Kær, S. Clausen, S. L. Hvid und T. Hille, „Mathematical Modeling and Experimental Study of Biomass Combustion in a Thermal 108 MW Grate-Fired Boiler," Energy & Fuels 22, pp. 1380-1390, 2008.
[07] Scharler, R.; Obernberger, I.: Numerical Modelling of Biomass Grate Furnances. In: Proceedings of the 5th European Conference on Industrial Furnances and Boilers, Porto, 2000.
[08] BioBib, TU Wien, http://cdmaster2.vt.tuwien.ac.at/biobib/fuel309.html. (date: 01.08.2013)
[09] Plankenbühler, T.; Müller, D.; Karl, J.: Numerical simulation and experimental investigation of slagging in biomass combustion. In: 2nd edition of the international workshop on CFD and biomass, Leipzig, 2016.

*Mohammadhadi Nakhaein (Technical University of Denmark, Denmark)*

# CFD simulation of a full-scale RDF-fired calciner

*Mohammadhadi Nakhaei, Hao Wu, Peter Glarborg, Kim Dam-Johansen*
*Technical University of Denmark, Department of Chemical and Biochemical Engineering*
*Lyngby Campus, 2800, Kgs. Lyngby, Denmark*
*Mnak@kt.dtu.dk, haw@kt.dtu.dk, PGL@kt.dtu.dk, KDJ@kt.dtu.dk*

*Damien Grévain, Lars Skaarup Jensen*
*FLSmidth A/S, Cement R&D*
*Vigerslev Allé 77, 2500 Valby, Denmark*
*DAG@flsmidth.com, LaSJ@ flsmidth.com*

**KEYWORDS:** CFD, MP-PIC, cement calciner, RDF, combustion

## ABSTRACT

Fuel cost is a major operating expense in cement production. In recent years, there has been an extensive attempt in reduction of the fuel cost in cement production by using alternative fuels, such as refuse derived fuels (RDF), in cement calciners. However, as RDFs differ significantly from conventional fossil fuels in terms of physical, chemical, and combustion properties, problems related to incomplete burnout of RDF particles may arise. In this study, CFD simulation of a full-scale calciner is conducted in order to gain insights of the flow patterns, gas-solid interactions, and reactions inside the calciner using Barracuda VR® solver. The gas flow is solved using large eddy simulation (LES) turbulence model in the regions away from the wall, and a k-ε wall function model in the wall proximity. The raw meal and fuel particles are tracked in a Lagrangian frame using multiphase particle-in-cell (MP-PIC) method. In the CFD simulation, the RDF particles go through drying, devolatilization, and char oxidation reactions after injection, while the released volatiles are oxidized in the gas phase. The raw meal particles are fed to the calciner from two positions and the related calcination reaction is included in the simulation. The simulations are carried out for three test cases; two simulations with coal and RDF being the only solid-fuel used in the calciner, respectively; and one simulation with a mixture of coal and RDF. For each fuel particle species, the corresponding conversion degree is reported. The calciner performance and fuel burnout are compared for the studied cases. Finally, from the simulation results, some strategies are proposed for improvement of the simulation.

## 1. INTRODUCTION

Calcination reaction is the most energy demanding process in cement production and around 55 to 65 percent of the plant's fuel is used in the calciner. In the past few years, there has been an increased interest toward using alternative fuels especially refuse derived fuels (RDF) in cement calciners. The main motivations for this replacement are low fuel cost and environmental aspects, e.g. $CO_2$ emission reduction and waste disposal.
RDF is produced from combustible fraction of municipal solid waste and industrial waste using sorting and shredding [1]. The main components of RDF are plastic, paper, textile, wood, and inert materials such as metal and glass particles. RDF particles are significantly different from conventional fuel particles such as coal and petcoke both in physical and chemical properties. Compared to the conventional fuel particles, RDF particles are generally quite heterogeneous (made from different types of materials), larger, and they have a higher amount of volatiles and moisture. One of the important issues to consider when burning RDF in calciners is the amount of moisture content of the fuel. The endothermic drying process may postpone and/or inhibit the oxidation of volatiles and RDF char. This would impose a decrease in the gas temperature which consequently leads to inadequate calcination of raw meal particles and also reduced potential of NOx reduction in in-line calciners (ILC). Apart from the mentioned issues, the final degree of fuel burnout at the exit of the calciner is also important. Incomplete combustion of RDF particles in the calciner may cause local combustion of unburnt particles inside the last stage cyclone and also in the rotary kiln. This would lead to negative effects on the kiln operation stability and the quality of cement product [2].





CFD simulation of cement calciners has been conducted previously in the literature with the main objectives being improvement of knowledge about the reactive gas-solid flow inside the calciner, reduction of emissions, etc. (for example see [3] and [4]). However, previous CFD research about firing alternative fuels in a full-scale calciner is rare. In the current study, CFD simulations of a full-scale calciner at different conditions are conducted to better understand the changes in the operating conditions of the calciner when RDF is used as the fuel. In the first section, the gas flow behavior of a coal-fired calciner is studied. Afterwards, the results of RDF-fired calciner are presented and described.

## 2. RDF CHARACTERISTICS

The main focus in this paper is firing RDF in a cement calciner and to study the subsequent calciner performance. In this section, the physical and chemical properties of RDF particles and corresponding CFD sub-models for their conversion in calciner conditions are described.

### 2.1. RDF Physical properties

The RDF that is used in the simulations is provided by a European cement plant. This RDF is composed of different types of materials, mainly plastic, paper, wood, metal, etc. The RDF particles are categorized into six groups according to their terminal velocity using a wind sieve. This wind sieve is composed of a vertical hollow tube. Air passes through the tube with a predetermined bulk velocity. The particles are fed from the middle of the tube and are separated into light and heavy fractions based on their behavior inside the wind sieve. The corresponding mass fraction of each group is shown in Figure 1. It can be seen that around half of the particles have a terminal velocity smaller than 4 m/s.
It is possible to estimate the average size of particles in each RDF group by using the information about aerodynamic behavior of RDF particles at terminal conditions. For this purpose, the Ganser drag model for non-spherical particles [5] is used. Also a constant value for the shape factor (sphericity) and the density of particles are assumed. The assumed value for the sphericity is in the range of 0.15-0.75 with the lowest value corresponding to the lightest particles (Fraction group 6). The sphericity of particles is approximated according to their morphology in each group. All RDF particles are considered to have the same density of 1100 kg/m$^3$.

### 2.2. RDF Chemical properties

The proximate analysis of the sample is presented in Table 1. Also provided in this table is the proximate analysis of a medium-rank bituminous coal that is used for simulations. As expected, the volatile content and the moisture content of the RDF are significantly higher than the ones for the coal.
For RDF particles, heating, drying, devolatilization, and char oxidation processes are considered as conversion stages. The heating model for non-spherical RDF particles is assumed to be the same as for isothermal spherical particles [6] except for the addition of the effect of external surface area. The particles drying is based on a shrinking core model. The evaporation takes place at an active layer inside the particle and water vapor diffuses through a shell of dried material to the outer space.
The particles size may have a significant effect on the devitalization rate of large alternative fuel particles. This is because this process largely depends on the heating rate of particles (for example see [7]). However, due to lack of literature studies, the results of RDF devolatilization in low heating rates using TGA experiments are used [8]. The devolatilization model for RDF particles is considered as four independent parallel first order Arrhenius–type reactions corresponding to devolatilization of hemicellulose, cellulose, lignin, and plastics. Fractions of each mentioned volatile material and the corresponding devolatilization kinetics are based on averaged values reported by [8]. The gaseous species from released volatiles are methane and carbon monoxide. The ratio of the amount of carbon monoxide to methane is obtained according to energy and mass balance calculations. It should be noted that during the devolatilization process, the size of particles remains constant while their density is decreased as the volatile matters are released.

*Table 1: Proximate analysis, heating value, and physical properties of RDF sample and medium-rank coal used for simulations*

| Proximate analysis, wt. %, as received | | |
|---|---|---|
| | RDF | Coal |
| Volatile Matter | 61.0 | 29.0 |
| Fixed carbon | 13.0 | 54.0 |
| Ash | 10.9 | 15.0 |
| Moisture | 15.1 | 2.0 |
| LHV (kJ/kg) | 18,664 | 25,100 |
| Mean diameter (μm) | 7348 | 17.2 |
| Density (kg/m$^3$) | 1100 | 1266 |

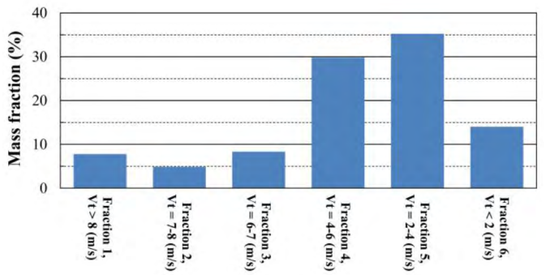


*Figure 1: Percentage of mass fraction for each group of RDF particles being in the same range of aerodynamic terminal velocity.*

The char yield of coal and RDF particles is considered to be the same as the amount of fixed carbon reported in Table 1. For RDF particles, the char yield is mostly from biomass particles such as paper, wood, textile, etc. The model for char oxidation is based on averaged reaction kinetics of [9] for tested biomass particles. The kinetic rates were obtained using TGA. However, in order to consider the effect of high heating rate on particles, the char for different materials were produced using a high temperature reactor. More details about the RDF char oxidation model can be found in [9]. It should be noted that the drying, devolatilization, and char oxidation models for coal particles are different from the ones used for RDF particles. These models as well as calcination reaction model are not explained in this study.

## 3. COMPUTATIONAL METHOD AND SIMULATION CONDITIONS

Full 3-D Navier-Stokes equations for compressible flow are solved to simulate the gas flow inside the calciner using Barracuda virtual reactor solver. The fuel and raw meal particles are tracked in a Lagrangian frame using Multiphase Particle-In-Cell (MP-PIC) method [10]. Large Eddy Simulation (LES) with classic Smagorinsky model combined with a k-ε wall function model for regions close to the walls are used to consider the effect of turbulence in the flow [10]. For the raw meal, coal, and RDF particles, the EMMS drag model [11], Stokes drag model, and non-spherical Ganser drag model [5] are used, respectively.

A schematic representation of the calciner geometry is depicted in Figure 2 along with the specific boundary conditions for the current simulations. The flue gas from the kiln enters the calciner from the bottom. In the riser, the fuel and also a fraction of the raw meal are fed. The tertiary air duct is connected tangentially to the calciner in the conical section. In the calciner section, the rest of the raw meal is fed. More information about fluid and solid boundary conditions is presented in Table 2. It should be noted that the values presented in this table are for a case when coal is fired in the calciner. When the fuel type is changed, the amount of fuel and also properties of tertiary air may change according to the fuel properties. However, the same inlet boundary condition for tertiary air is used for all cases in this study.

The computational grid contains 296,751 hexahedral elements for simulations of gas-solid flow in the first compartment of the calciner. The simulations are carried out for 90s while the temporal averaging is done for the last 45s when the flow and particles inside the calciner have reached a steady state condition. Numerical simulations of the full-scale calciner are carried out for three different cases summarized in Table 3. The computational grid is the same for all cases. In the first test case, C1, only coal is used in the calciner as the fuel and it is considered as the base case. The test cases C2 and C3 are chosen to study the effect of burning RDF in the calciner on its performance.





*Table 2: Calciner inlet boundary condition properties for case C1*

| Boundary (type) | Mass flow rate (kg/s) | Gas/solid Temperature (K) | $O_2$ vol. % |
|---|---|---|---|
| Kiln flue gas inlet (fluid) | 44.4 | 1323 | 4.2 |
| Tertiary air inlet (fluid) | 58.9 | 1177 | 21.0 |
| Raw meal to riser (solid) | 57.7 | 1047 | - |
| Raw meal to calciner (solid) | 86.5 | 1047 | - |
| Fuel, coal (solid) | 5.5 | 323 | - |

*Table 3: The test cases studied for numerical simulation of full-scale calciner*

| Test case | C1 | C2 | C3 |
|---|---|---|---|
| RDF energy input fraction | 0 | 1 | 0.8 |
| Coal energy input fraction | 1 | 0 | 0.2 |

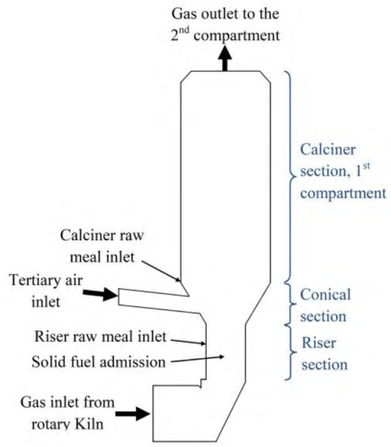


*Figure 2: Schematic representation of calciner geometry used for simulations as well as the flow and particle boundaries.*

## 4. RESULTS AND DISCUSSIONS

### 4.1. Flow Structures and temperature distribution

In order to investigate the gas-solid flow behavior of the base case, C1, the time-averaged gas velocity and temperature contours are presented in Figure 3. The profiles of gas velocity and temperature depend directly on the distribution of raw meal and coal particles. In the riser, the gas velocity is decreased in regions where coal and raw meal particles are fed to the calciner. On the other hand, areas with high upward gas velocity, corresponding to regions of high gas temperature, are due to partial oxidation of released volatile materials from coal particles. As the gas temperature rises, the velocity also increases due to reduced density.

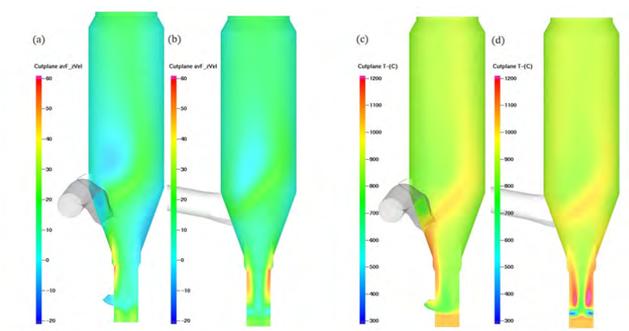


*Figure 3: Time-averaged upward gas velocity (a, b) and gas temperature (c, d) contours of case C1. Front view (a, c) and side view (b, d)*

Downstream of the riser, the tertiary air is added to the calciner. Along the tertiary air trajectory, there is an increase in the gas temperature because of the volatiles oxidation and char oxidation reactions. Accordingly, the gas velocity is also higher in regions with higher gas temperature. The upward gas velocity and temperature profiles become nearly uniform before the gas leaves the first compartment of the calciner.

### 4.2. Calciner performance

Two important aspects of calciner performance that are studied here are fuel conversion and calcination degree. The fuel conversion and calcination degree along the calciner height are presented in Figure 4. Also provided in this figure (right side) is the time-averaged gas temperature along the calciner height. The reported fuel conversion includes evaporation, devolatilization, and char oxidation processes. For the base case, C1, the final fuel burnout is 71.2% at the end of the first compartment. However, these values decrease for the other two cases. The lowest fuel conversion is for case C2 and is around 47.9% while the amount of conversion for the last case, C3, lies in between. The higher value for fuel conversion for C3 compared to C2 is due to the contribution of coal conversion rather than RDF. The final RDF conversion is nearly the same for C2 and C3 cases even though the gas temperature is higher for case C3. The increase in the gas temperature for case C3 compared to case C2, slightly increases the particles heating, drying, and devolatilization rates. However, for this case, the gas volume flow rate is higher than the one for case C2 due to the higher amount of product gases from calcination and fuel conversion reactions. This leads to slightly shorter residence times for almost all groups of RDF particles (not shown here). Accordingly, for case C3 and compared to case C2, the effect of higher temperature on the RDF conversion rate is nearly canceled out by shorter residence time of particles in the calciner. Apart from the mentioned issues, it should be noted that RDF particles are fairly large and particle size have a significant effect on the time needed for completion of particles conversion. Hence, the effect of gas temperature on the RDF conversion may be of less importance.

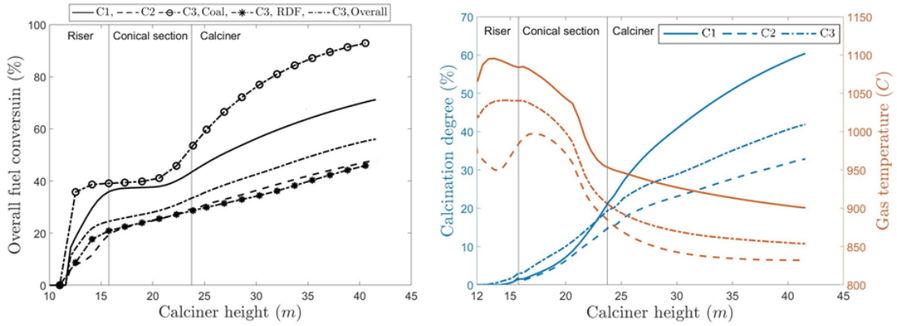


*Figure 4: The fuel burnout degree (left) and calcination degree of raw meal fed to the riser (right) along the calciner height. The time-averaged gas temperature is also depicted in the right figure*

An important issue to consider while interpreting RDF conversion is the effect of endothermic evaporation phase. During evaporation, the gas temperature reduces which suppresses both calcination and fuel conversion rates. In the first part of the riser, the reduction of gas temperature for case C2 can be seen in Figure 4. This can be attributed to the evaporation of small RDF particles (fraction 6 mainly). In the second part of the riser, however, the gas temperature for this case increases due to the start of devolatilization and char oxidation processes for the dried particles. For case C3, this behavior is not observed and the gas temperature increases in the riser. This can be explained by the presence of coal particles and partial oxidation of volatile materials released from coal which compensates for the contribution of endothermic drying of RDF particles. The drying of smaller RDF particles, i.e. fraction 6 in Figure 1, is almost completed before particles leave the riser.

For case C1, the final calcination degree of the raw meal fed to the riser is around 60.4%. The calcination degrees for cases C2 and C3 are somewhat lower than this value. The decrease in progress of calcination reaction can be explained by the reduction in the gas-temperature and subsequently reduction in the chemical reaction rate for calcination. As the raw meal particles are fairly small, the chemical reaction rate of calcination is highly dependent on the gas temperature.

## 5. CONCLUSION

In recent years, cement producers are more inclined toward using alternative fuels especially RDF because of economical purposes. In order to improve the knowledge about burning RDF in calciner systems, CFD simulations of a full-scale calciner are conducted using Barracuda virtual reactor solver. Large Eddy Simulation is used to solve the fluid domain while particles are tracked in a Lagrangian frame. The calciner performance and working conditions are compared for three test cases. For two test cases, only coal and RDF were used as the fuel while in the third one, a mixture of coal and RDF was considered. It has been observed that when coal is partly/completely replaced by RDF, the gas temperature and the degree of calcination are reduced along the calciner height. The RDF conversion degree is nearly independent of the gas temperature. This behavior was explained by considering the change in the particles residence time inside the calciner. Also it is expected that the size of particles has a significant impact. For the future work, as the particles physical properties have an important impact on the conversion rate of RDF particles, the size, shape, and density of particles chosen for calculations should be validated and/or modified using a different method. Possible practices would be using 2D/3D image analysis, weight measurements, etc. Conversion sub-models such as devolatilization and char oxidation can be improved after making sure that physical properties are estimated accurately.

## 6. REFERENCES

[01] Luis FD et al. (2005). Solid waste management. Vol. 1. UNEP/Earthprint. (ISBN 9789280726763).
[02] Nørskov LK (2012). Combustion of solid alternative fuels in the cement kiln burner. PhD thesis. Technical University of Denmark.
[03] Mikulčić H et al. (2013). Numerical analysis of cement calciner fuel efficiency and pollutant emissions. Clean Technologies and Environmental Policy, 15(3): 489-499.
[04] Fidaros DK et al. (2007). Numerical modelling of flow and transport processes in a calciner for cement production. Powder Technology. 171(2):81-95.
[05] Ganser GH (1993). A rational approach to drag prediction of spherical and nonspherical particles. Powder Technology. 77(2):143-152.
[06] Ranz WE and Marshall WR (1952). Evaporation from drops. Chem. Eng. Prog. 48(141):173-180.
[07] Larsen MB et al. (2006). Devolatilization characteristics of large particles of tyre rubber under combustion conditions. Fuel 85(10-11):1335–1345.
[08] Grammelis P et al. (2009). Pyrolysis kinetics and combustion characteristics of waste recovered fuels. Fuel. 88(1):195-205.
[09] Pedersen PN (2015). Single particle combustion of refuse derived fuel. Technical report. Technical University of Denmark, Department of Chemical and Biochemical Engineering.
[10] Snider DM and ORourke PJ (2011). The Multiphase Particle-in-Cell (MP-PIC) Method for Dense Particle Flow. Computational Gas-Solids Flows and Reacting Systems. IGI Global.
[11] Yang N et al. (2004).. Simulation of heterogeneous structure in a circulating fluidized-bed riser by combining the two-fluid model with the EMMS approach. Ind. and Eng. Chemistry Research, 43(18): 5548-5561.

POSTER





*Abdelbaki MAMERI (Université Larbi Ben Mhidi, Algeria)*

# MILD combustion of hydrogenated biogas in opposed jet configuration

*Abdelbaki MAMERI[1] , Fouzi Tabet[2] , Yassmine AGGAB[1] and Youssouf ZAOUIA[1]*
*[1]Faculté des sciences et sciences appliquées, Département de Génie Mécanique, Université Larbi Ben Mhidi, Oum El Bouaghi, BP 358, 04000, Algeria*
*[2] DBFZ Deutsches Biomasseforschungszentrum gemeinnützige GmbH, Torgauer Straße 116 D-04347 Leipzig, Germany*
*mameriabdelbaki@yahoo.fr*

**KEYWORDS:** Opposed jet flame, hydrogenated biogas, MILD combustion

## ABSTRACT

Flameless combustion is applied first to suppress thermal NOx by preheating combustion air. This technique is then used in large number of applications such as: heat-treating and heating furnaces in the steel industry, gas turbines, bio gas burners, burners for hydrogen reformers, and burners for CHP units ... Some of these applications are still at a research stage. In conventional combustion, when the mixture of fuel and air is ignited, the temperature rises quickly close to the adiabatic temperature which is enough higher to produce NOx. In MILD combustion, the burned products are recycled to preheat the combustion air to a temperature higher than the fresh mixture ignition one. In addition, in this mode of combustion small amounts of oxygen are used to feed combustion. The fuel is completely burnt and the exhaust carbon monoxide and NOx are close to zero. In this work, MILD combustion benefits are associated with biogas ones (biogas is a renewable and biodegradable fuel) to optimize combustion system. To characterize fuel and oxidizer composition effects on combustion two biogases were considered BG40 and BG60 with 40% and 60% $CO_2$, hydrogen volume added to biogas is varied from 0% to 20% and finally the $O_2$ volume contained in oxidizer is varied from 2% to 10%. To simplify equations and combustion characterization, the opposed flow geometry is chosen. Injection temperatures for fuel and oxidizer are $T_f$=300K and $T_{ox}$=1200K respectively, ambient pressure is kept constant and equals to 1 atm. The Grimech 3.0 mechanism is used to describe combustion kinetics and full diffusion transport equations are solved. The Chemkin Oppdiff program is adopted to solve the equations. Results showed that $CO_2$ volume increasing dilutes the fuel, reduces the flame temperature and the emissions. Hydrogen addition produces chain carrier radicals and stabilizes the flame, non-reacting mixture burns with small amounts of hydrogen addition. Reduced volume of oxygen in oxidizer stream reduces flame temperature and emissions to very low limits.

## 1. INTRODUCTION

The growth of human activity during recent decades induced global warming and depletion of fossil energy resources. To overcome these problems, it is crucial to develop more efficient energy utilization technologies and also to find new sources of clean energy. The moderate or intense low-oxygen dilution (MILD) combustion is one of the optimum solutions for the reduction of environmental problems caused by combustion. In MILD combustion, minimum and maximum temperatures are controlled. Precisely, MILD combustion is defined as follows: “A combustion process is named Mild when the inlet temperature of the reactant mixture is higher than mixture self-ignition temperature whereas the maximum allowable temperature increase with respect to inlet temperature during combustion is lower than mixture self-ignition temperature (in Kelvin)”[1]. Several aspects of MILD combustion have been explored, particularly transition from conventional to MILD combustion, sustainability conditions and emissions. J. Ye et al. [2] have experimentally explored the transition from conventional to MILD combustion in ethanol flames. It has been found from experience that the transition can be made by preheating the oxidizer and decreasing the $O_2$ coflow level and/or the use of $N_2$ as a carrier gas. To identify the sustainability domain of MILD combustion, M. de Joannon et al. [3] studied the influence of fuel percentage and pressure on high temperature oxidizer combustion. A combustion diagram is obtained for each pressure and MILD-HDDI (Hot-Diluted-Diffusion-Ignition) limits were clearly identified. C.A.O. Zhenjun et al. [4] investigated numerically the effect of exhaust recirculation gas (EGR) in

MILD combustion on ignition delay. The authors found that when equivalence ratio or $CO_2$ is increased, the ignition delay time increases, this is mainly attributed to the decrease of H, O and OH radicals. From the above, the dilution is crucial in MILD combustion, the well-known naturally diluted, renewable and biodegradable fuel is the biogas. S. E. Hosseini et al. [5] have numerically investigated the biogas flameless combustion; they found that in flameless combustion, NOx formation reduces due to elimination of hot spots and low level of oxygen. For very high concentration of $CO_2$ species in biogas flameless products, better radiation heat transmission and higher heat capacity are observed. To enhance biogas properties, hydrogen is added in relatively small amounts; S. Chen et al. [6] explored a counter flow diffusion flame of hydrogen-enriched biogas under MILD condition. The authors found that MILD combustion is sustained for extremely low-oxygen concentration in the oxidizer flow, there is no necessity to add much hydrogen. Also, MILD combustion of biogas from landfills is better sustained with lower oxygen concentration in the oxidizer flow than higher one.

The lake of informations about hydrogen doping of biogas under MILD combustion makes sense to this work. In this study, the effect of several parameters on the MILD combustion of hydrogenated biogas and emissions are investigated. Two biogas are explored (BG40: 40% $CH_4$, 60% $CO_2$ and BG60), the hydrogen content volume is varied from 0% to 20% and the volume of oxygen in the oxidizer ranges from 2% to 10%.

## 2. GEOMETRY AND SIMULATION DETAILS

The opposed jets configuration was used to analyse the structure of the reaction zone developing in a steady unidimensional diffusive layer. The flow geometry is schematized in Fig. 1, the fuel conditions refer to a hydrogen doped biogas while the oxidizer one refers to preheated and diluted air by $CO_2$. Distance between injectors is D=2cm, velocity injection is the same for fuel and oxidizer [6].

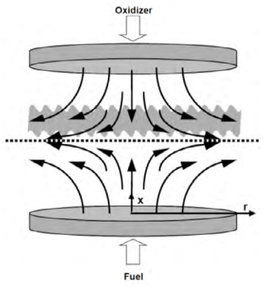


*Figure 1: Opposed flow geometry in cylindrical coordinates*

The boundary conditions for the fuel and oxidizer streams at the nozzles are:

- Injection velocity is computed by keeping a constant strain rate a=200 $s^{-1}$ from the relation :

$$a = \frac{2(-v_O)}{L}\left[1 + \frac{v_F}{(-v_O)}\sqrt{\frac{\rho_F}{\rho_O}}\right] \quad (1)$$

With a the strain rate, $v_0$, $p_0$ and $v_F$, $p_F$ are respectively the oxidizer and fuel streams velocity and density.

- Injection temperature for the fuel is $T_F$=300 K and for oxidizer $T_0$=1200K.
- Injection fuel composition is:

$$(1-\beta)\alpha CH_4 + (1-\beta)(1-\alpha)CO_2 + \beta H_2 \quad (2)$$

Where α is the fraction of methane in biogas and β is the hydrogen fraction added to biogas.

- Injection oxidizer composition is given by:

$$(0.21-\delta)O_2 + \delta CO_2 + 0.79N_2 \quad (3)$$

With δ the fraction of oxygen in oxidizer.

The differential equations and boundary conditions form a boundary value problem, which is resolved by CHEMKIN [7]. The differential equations are solved assuming multicomponent diffusion transport for all species participating in the chemical mechanism. Radiative heat loss is modelled by the optically thin body model. Combustion kinetics is described by the GRImech 3.0 mechanism [8], which is formed by 325 reactions involving 53 species. Two biogas are considered BG40 and BG60 with several doping volumes of $H_2$. Computations are performed at ambient pressure over a range of $H_2$ molar ratio from 0 to 0.2, $O_2$ molar fraction is varied from 0.03 to 0.09 and strain rate is kept constant and equal to 200 $s^{-1}$ .

## 3. RESULTS AND DISCUSSIONS

The Figures 7 to 10 show profiles of combined effects of oxygen and hydrogen concentrations in oxidizer and fuel respectively. Here, MILD combustion of BG40 biogas is showed with a volume of hydrogen varied from 0% to 20% in the fuel and a volume of oxygen increased from 2% to 10% in the oxidizer flow. The ambient pressure is kept constant and equal to 1 atm. Figure 7 presents the combustion temperature, it can be seen in figure 7 (a) that for 0% hydrogen addition in the fuel with 2% and 6% $O_2$ in the oxidizer, the mixture doesn't burn. In figures 7 (b) and (c), while the volume of hydrogen is increased to 10% and 20%, the combustion occurs. The temperature is reduced with oxygen decreasing in the oxidizer and increased with hydrogen added to the fuel. In case of 10% hydrogen the maximum temperature decreases from 1743K for 10% oxygen to 1241K for 2% of oxygen. For the case of 20% hydrogen addition, the maximum temperature decreases from 1788K for 10% of oxygen to 1293K for 2% of oxygen. Also, it can be noticed that with oxygen addition the maximum temperature position is shifted toward the fuel and it doesn't depend on hydrogen blending.

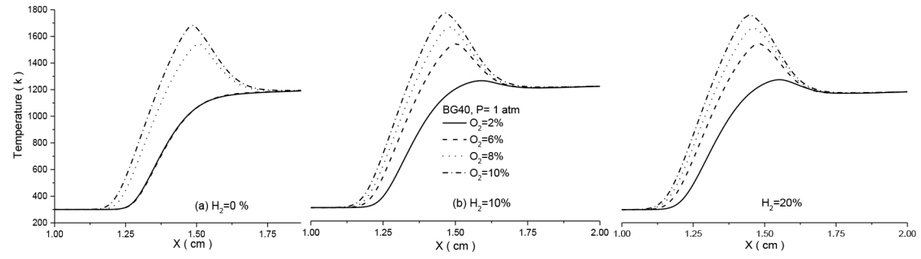


*Figure 7: Effects of oxygen and hydrogen concentration on combustion temperature*

The CO molar fraction profiles are presented in figure 8. For the case of $H_2$=0% in the fuel and $O_2$=2% and 6% in the oxidizer there is no reaction as seen before, so no CO or other species are produced from combustion. It can be seen from figure 8, that CO mole fraction is enhanced by hydrogen addition to the fuel and depressed by oxygen reduction in the oxidizer. It is noticed that effect of oxygen is more pronounced than hydrogen one. For the case of $O_2$=10%, when adding 20% of hydrogen to the fuel, the maximum of the CO mole fraction is increased by about 50%. Whereas for the case of $H_2$=20%, when adding 10% of oxygen to the oxidizer, the maximum of the CO mole fraction is increased by about five times. It can be seen that the maximum of the CO mole fraction is located at the same position of the maximum temperature and it is shifted in the same way.

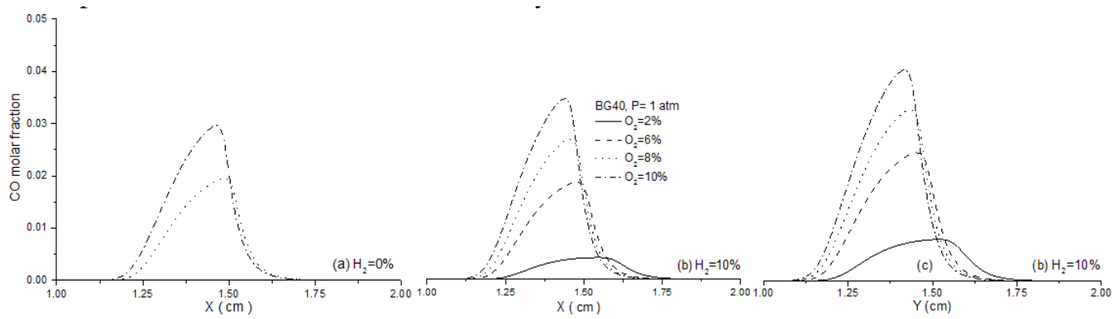


*Figure 8: Effects of oxygen and hydrogen concentration on CO mole fraction*

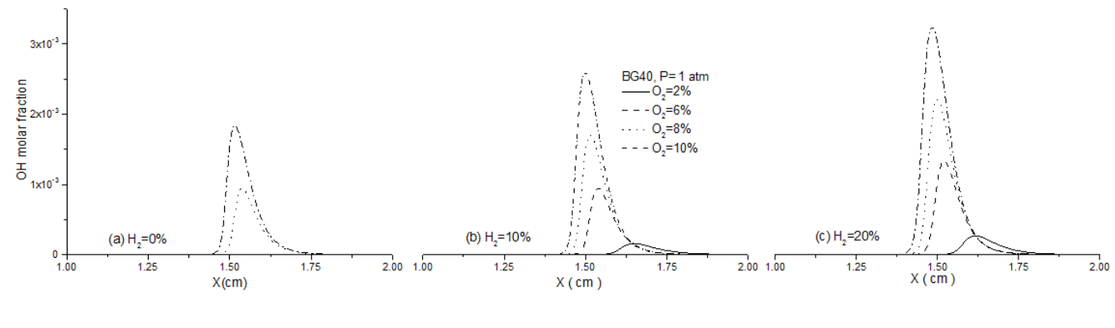


*Figure 9: Effects of oxygen and hydrogen concentration on OH mole fraction*

In figure 9 the OH molar fraction profiles are presented, it can be noticed that OH mole fraction is increased with hydrogen addition to the fuel and reduced by the oxygen decreasing in the oxidizer. Like CO mole fraction, it is seen that effect of oxygen is more pronounced than hydrogen one. For the case of $O_2$=10%, when adding 20% of hydrogen to the fuel, the maximum of the OH mole fraction is increased by about 80%. Whereas for the case of $H_2$=20%, when adding 10% of oxygen to the oxidizer, the maximum of the CO mole fraction is increased by about twelve times. The location of the maximum of the OH mole fraction is slightly shifted towards the oxidizer side compared to the maximum of temperature. This position is shifted to the fuel when oxygen in added.

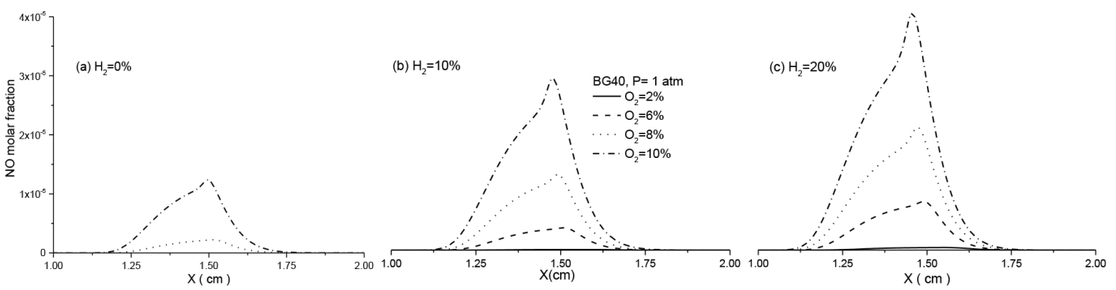


*Figure 10: Effects of oxygen and hydrogen concentration on NO mole fraction*

Figure 10 shows the NO mole fraction profiles, the same remarks can be done concerning the evolution of this species. The mole fraction of NO is augmented with hydrogen and oxygen increasing in the fuel and the oxidizer streams respectively. Whereas, increasing of NO mole fraction by oxygen addition is more pronounced than it by hydrogen. For the case of $O_2$=10%, when hydrogen increases from 0% to 20%, the NO mass fraction increases by about three times. In the case of $H_2$=20%, when $O_2$ increases from 2% to 10%, the mole fraction of NO increases by about ninety times. The positions of the maximum of the NO mole fractions shows the same behaviour of maximum temperature.

## 4. CONCLUSION

The present paper presents the effects of dilution of pre-heated oxidizer and hydrogen blending of the fuel (biogas) in a MILD combustion. The oxidizer is preheated at a temperature of 1200K while the fuel is kept at 300K; the oxygen volume in the oxidizer is increased from 2% to 10% and hydrogen in the biogas is augmented from 0% to 20%. The following conclusions can be drawn:

- Used biogases BG40 and BG60 and doped biogases with hydrogen have all lower calorific heat values than methane.
- In MILD combustion the heat released is lower than that released in conventional combustion, which considerably reduces the emissions.
- When oxygen is reduced in MILD combustion, temperature and all emissions are reduced drastically. At low oxygen volume which is characteristic of MILD combustion, temperature and emissions are very low.
- At low oxygen volume concentration in the oxidizer (2%), the mixture does not burn until adding hydrogen. In biogas at low oxygen concentration in the oxidizer, MILD combustion can be sustained by doping fuel with hydrogen.
- In MILD combustion of biogas, the effect of oxygen increasing on temperature and emissions is more noticeable than the effect of hydrogen one.

## 5. REFERENCES

[01] Antonio Cavalierea, Mara de Joannonb, Mild Combustion, Progress in Energy and Combustion Science 30 (2004) 329–366

[02] Jingjing Ye , Paul R. Medwell , Bassam B. Dally , Michael J. Evans, The transition of ethanol flames from conventional to MILD combustion, http://dx.doi.org/10.1016/j.combustflame.2016.05.020

[03] M. de Joannon a, P. Sabia b, G. Sorrentino b, A. Cavaliere b, Numerical study of mild combustion in hot diluted diffusion ignition (HDDI) regime, Proceedings of the Combustion Institute 32 (2009) 3147–3154

[04] CAO Zhenjun and ZHU Tong, Effects of CO2 Dilution on Methane Ignition in Moderate or Intense Low-oxygen Dilution (MILD) Combustion: A Numerical Study, Chinese Journal of Chemical Engineering, 20(4) 701-709 (2012)

[05] Seyed Ehsan Hosseini, Ghobad Bagheri, Mazlan Abdul Wahid, http://dx.doi.org/10.1016/j.enconman.2014.02.006

[06] Sheng Chen, Chuguang Zheng, http://dx.doi.org/10.1016/j.ijhydene.2011.09.002

[07] CHEMKIN-PRO 15131, Reaction Design: San Diego, 2013

[08] Smith GP, Golden DM, Frenklach M, Moriarty NW, Eiteneer B, Goldenberg M, et al. GRI Mech-3.0. Available from: http://www.me.berkeley.edu/grimech/

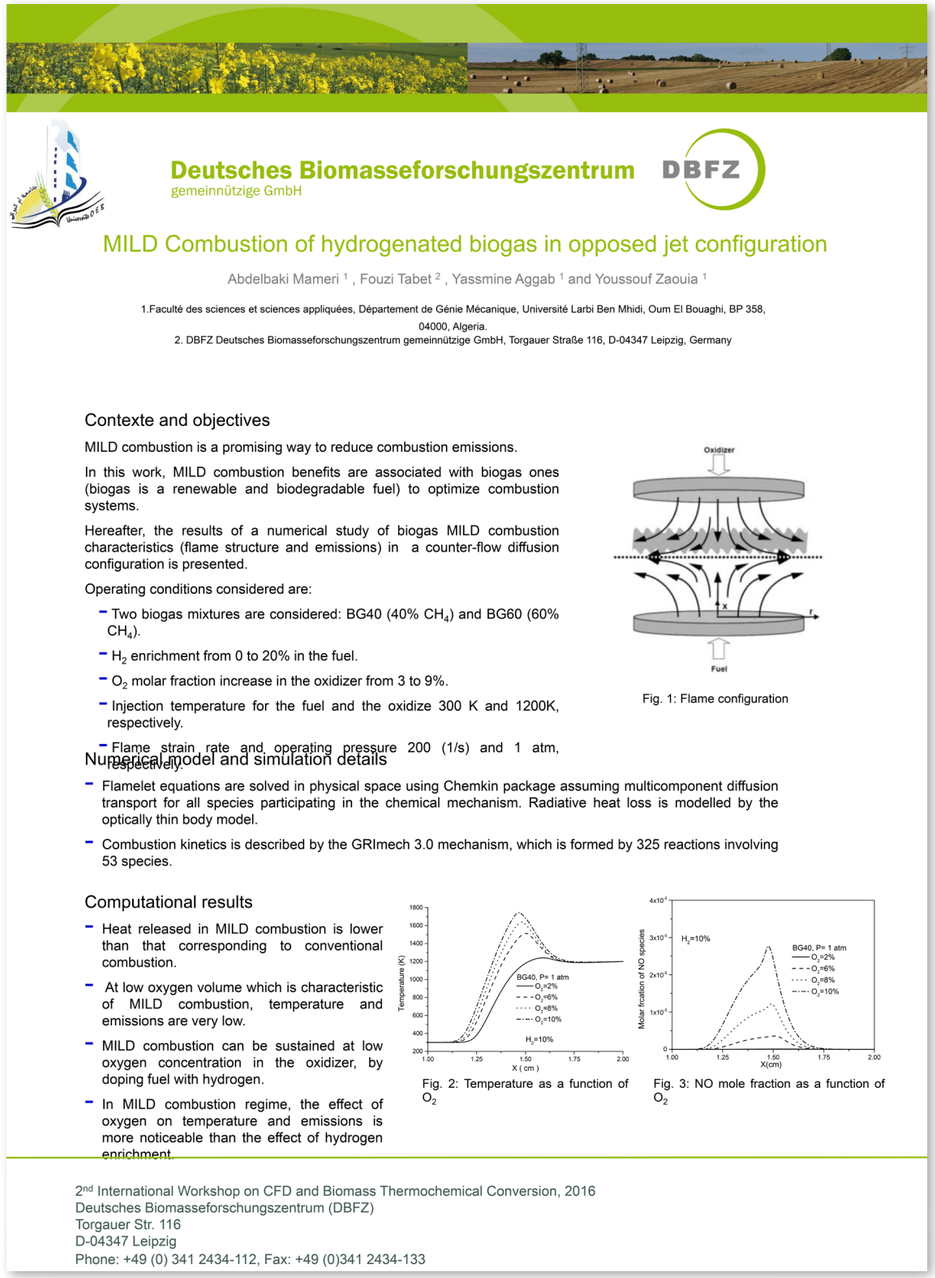

Deutsches Biomasseforschungszentrum
gemeinnützige GmbH

DBFZ

MILD Combustion of hydrogenated biogas in opposed jet configuration

Abdelbaki Mameri [1] , Fouzi Tabet [2] , Yassmine Aggab [1] and Youssouf Zaouia [1]

1.Faculté des sciences et sciences appliquées, Département de Génie Mécanique, Université Larbi Ben Mhidi, Oum El Bouaghi, BP 358, 04000, Algeria.
2. DBFZ Deutsches Biomasseforschungszentrum gemeinnützige GmbH, Torgauer Straße 116, D-04347 Leipzig, Germany

Contexte and objectives

MILD combustion is a promising way to reduce combustion emissions.

In this work, MILD combustion benefits are associated with biogas ones (biogas is a renewable and biodegradable fuel) to optimize combustion systems.

Hereafter, the results of a numerical study of biogas MILD combustion characteristics (flame structure and emissions) in a counter-flow diffusion configuration is presented.

Operating conditions considered are:

- Two biogas mixtures are considered: BG40 (40% $CH_4$) and BG60 (60% $CH_4$).
- $H_2$ enrichment from 0 to 20% in the fuel.
- $O_2$ molar fraction increase in the oxidizer from 3 to 9%.
- Injection temperature for the fuel and the oxidize 300 K and 1200K, respectively.
- Flame strain rate and operating pressure 200 (1/s) and 1 atm, respectively.




Fig. 1: Flame configuration

Numerical model and simulation details

- Flamelet equations are solved in physical space using Chemkin package assuming multicomponent diffusion transport for all species participating in the chemical mechanism. Radiative heat loss is modelled by the optically thin body model.
- Combustion kinetics is described by the GRImech 3.0 mechanism, which is formed by 325 reactions involving 53 species.

Computational results

- Heat released in MILD combustion is lower than that corresponding to conventional combustion.
- At low oxygen volume which is characteristic of MILD combustion, temperature and emissions are very low.
- MILD combustion can be sustained at low oxygen concentration in the oxidizer, by doping fuel with hydrogen.
- In MILD combustion regime, the effect of oxygen on temperature and emissions is more noticeable than the effect of hydrogen enrichment.




Fig. 2: Temperature as a function of $O_2$




Fig. 3: NO mole fraction as a function of $O_2$

2nd International Workshop on CFD and Biomass Thermochemical Conversion, 2016
Deutsches Biomasseforschungszentrum (DBFZ)
Torgauer Str. 116
D-04347 Leipzig
Phone: +49 (0) 341 2434-112, Fax: +49 (0)341 2434-133





*Abdallah Elorf (ICARE CNRS, France; LETSMP Université d'Ibn Zohr, Maroc)*

# Numerical analysis to study excess air ratio (EAR) effects on combustion characteristics of pulverized biomass

*Abdallah Elorf[1,2]*, Brahim Sarh[1], Stéphane Bostyn[1], Veronica Belandria[1], Toufik Boushaki[1], Iskender Gökalp[1], Jamal Chaoufi[2]*
*[1] ICARE CNRS, 1C, Avenue de la Recherche Scientifique, 45071 Orléans Cedex 2, France*
*[2] LETSMP Université d'Ibn Zohr, Faculté des Sciences – B.P 8106, Agadir, Maroc*
**Corresponding author: Abdallah ELORF*
*Abdallah.elorf@cnrs-orleans.fr*

**KEYWORDS:** Biomass, CFD, combustion, numerical simulation, Excess Air Ratio (EAR)

## ABSTRACT

The aim of this work is to study the effect of excess air ratio (λ) on the combustion dynamics of pulverized olive cake (OC) in a vertical furnace using CFD modelling. This study belongs to the "VERA" project which is developed in ICARE-CNRS, France, in order to design a new efficient burner which works with OC as a biomass fuel. The OC used is a Moroccan biomass. For cases namely (a), (b), (c) and (d) for the air inlet conditions with different excess air ratio (EAR) (λ=1.7, 2.3, 2.7 and 3.2 respectively) are studied. The numerical approach is based on Reynolds Average Navier-Stokses (RANS) equations. The chosen turbulence closure model is the k–ε model. For turbulence-chemistry interactions of the non-premixed combustion, a mixture fraction/PDF approach is used. The particles of OC are injected perpendicularly to the central axe of furnace near the lower base. This injection mode increases the particle residence time in the furnace. The mean size particle diameter is 70 μm. A comparison is done between all cases for, flow topology, velocity contours, temperature distribution and specie concentration profiles in several locations along the flow. Results show that increasing the excess air ratio decreases the emission of CO and $CO_2$ inside to the furnace and lowered the temperature in the furnace exit.

## 1. INTRODUCTION

It has been widely recognized that biomass has the potential to fulfill the increasing energy demands and strict regulations on $CO_2$ emissions [1]. An understanding of the physical and chemical processes involved in biomass combustion is important for any application in which biomass combustion is required, including stoves, boilers, and large-scale burners [2].
Substituting for traditional fossil fuel with biomass large scale combustion facilities is not only of significant importance for meeting society's energy needs, but can also make a huge contribution towards the reduction of greenhouse gases emitted into the atmosphere. Furthermore, the development of new technologies for utilization of biomass raises new opportunities for economic re-vitalization and growth [3-5]. The combustion behavior of biomass is different from that of coal because the biomass yields a much higher fraction of volatiles through and the low density of biomass results in the higher oxidation rate of biomass char. [6]
This work is a part of VERA (Energetic Valorisation of Agricultural Residues) project conducted between France and Morocco. He concerns the valorisation of olive cake (OC) biomass. OC, which is a waste of olive oil-mill, is an important biomass produced in Mediterranean countries in large quantities, available at a very low cost. OC can be considered as alternative fuels, which do not contain sulfur [7]. Efficient use of OC in energy production solves the two problems in one step: clean energy production and acceptable disposal of olive-mill wastes. OC can be burned alone or can be combined with other combustible materials, like low calorific value lignite coals [8].
The biomass used in this work is a Moroccan OC. The olive tree represents over 50% of the surface occupied by trees growing in Morocco. Its cultivation mobilizes an intense agricultural activity with more than 11 million working days per year (55 000 employed). In addition, it creates an intense industrial activity providing for 16 000 traditional mills (Maâsras), 260 modern units of olive mill, and around 50 olive canning plants. However, olive growing in Morocco does not benefit from suitable farming techniques and the oil extraction process is, for most part, still

traditional [9]. Annually, about 1.5 million tons of olive is used in olive oil production and approximately 675,000 tons of OC are produced in morocco. The calorific value (LHV) of this OC is about 12,500– 22,000 kJ/kg. It is comparable with the calorific values of wood and soft coal, which are 17,000 and 23,000 kJ/kg, respectively [10]. The sulfur content of OC is about 0.05– 0.1 wt%. Therefore, it is of prime importance to be able to burn this waste in producing clean energy in the regions where olive trees are raised. However, an appropriate technology must be employed to avoid the production of pollutants and other problems while maximizing process efficiency [8-10]. Murat et al. [11] studied the experimental effect of excess air ratio in the emission characteristics of co-combustion of a low calorie and high sulfur-lignite coal and woodchips in a circulating fluidized bed combustor. It's shown that increasing the excess air lowered temperature but mixing in the combustor was improved.
In this work, the development and application of a CFD model for pulverized olive cake combustion is presented. The Discrete Phase Model (DPM) of the commercial CFD software FLUENT 14 available in the laboratory, originally developed for the combustion of pulverized coal, was investigated regarding its capability to predict pulverized biomass combustion in general and especially olive cake presented in this paper. For burning biomass in particle form, the particles were described as a discrete phase in great number of works, for this, DPM is used for tracks the motion of individual (discrete) particles. Note that the same principles apply whether the object is a solid particle, or, a liquid droplet.

## 2. GOVERNING EQUATIONS

### 2.1. Continuous gas phase (gas flow)

The gas phase transport is described by the standard equations of fluid dynamics: the continuity, momentum, energy transport and species transport equations. A Fluent k-ε model was chosen for the turbulence model, as this is the most appropriate model when turbulence transfer between phases plays an important role in gasification in the combustion chambers. For the chemical reaction modeling, the PDF/mixture fraction model is used. The equilibrium system for biomass (OC) combustion consists of 20 species (C, C(s), H, $H_2$, O, $O_2$, N, $N_2$, CO, $CO_2$, OH, $H_2O$, $CH_4$, $C_2H_2$, $CH_3$, $HO_2$, $C_2H_4$, $C_2N_2$ and $C_2H_6$). Being a conserved scalar quantity, the value of f at each point in the flow domain is computed through the solution of the conservation equation for mean (time-averaged) value of $f$ in the turbulent flow field, $f$ [12]:

$$\frac{\partial}{\partial x_i}(\rho u_i f) = \frac{\partial}{\partial x_i}\left(\frac{\mu_t}{\sigma_t}\frac{\partial \overline{f}}{\partial x_i}\right) + S_M \qquad (1)$$

In addition to solving the conservation equation for the mean mixture fraction, a conservation equation for the mixture fraction variance, $f'^2$ is also solved:

$$\frac{\partial}{\partial x_i}(\rho u_i \overline{f'^2}) = \frac{\partial}{\partial x_i}\left(\frac{\mu_t}{\sigma_t}\frac{\partial \overline{f'^2}}{\partial x_i}\right) + C_g \mu_t \left(\frac{\partial \overline{f}}{\partial x_i}\right)^2 - C_d \rho \frac{\varepsilon}{k}\overline{f'^2} \qquad (2)$$

The values of constants $\sigma_t$, $C_g$ and $C_d$ in this Equation will be taken depending on simulations and situation, respectively. If a secondary stream is included in a non-adiabatic system, the instantaneous values will depend on the instantaneous fuel mixture fraction, fuel, the secondary partial fraction, $p_{sec}$ and the enthalpy, $H^*$

$$\Phi_i = \Phi_i^*\left(f_{fuel}, p_{sec}, H^*\right) \qquad (3)$$

Here $H^*$ is given by:

$$H^* = \sum_{i'} m_{i'} H_{i'} = \sum_{i'} m_{i'}\left[\int_{T_{ref,i'}}^{T} C_p + h_{i'}^0(T_{ref,i'})\right] \qquad (4)$$

More details about solution could be referred from Ref. [13]





### 2.2. Equation for particle motions

The Discrete Phase Model (DPM) tracks the motion of individual (discrete) particles. Note that the same principles apply whether the object is a solid particle, or as in this case, a liquid droplet.
In this case the particles (droplets) are inert; however the DPM does support much more complex cases where the particles may evaporate and/or combust.
The discrete solid particle phase is solved in a Lagrangian frame of reference. The injection diameter follows a Rosin-Rammler distribution. This phase consists of spherical particle with mean diameter $D_{mean}$=*70 µm*.
Their trajectory is predicted by integrating the force balance on the particle. This force balance equates the particle inertia with the forces acting on the particle and can be described as:

$$\frac{d\vec{u}_p}{dt} = F_D(\vec{u} + \vec{u}_p) + \vec{g}(\rho_p - \rho)/\rho_p \qquad (5)$$

More details about solution could be referred from Ref. [14]

### 2.3. Geometry and mesh construction

The pilot-scale furnace configuration is developed in the laboratory ICARE. A schematic view of the system furnace is shown in Figure 1. The combustion chamber is a cylindrical tube with inner diameter of *500 mm* and total length of *1500 mm.* The air inlet diameter d = *80 mm* is used to calculate the non-dimensional data presented in the paper and is divided in two diameters primary and secondary air inlet. The particles of OC are injected perpendicularly to the central axe of burner near the lower base in four particles injections presented in the furnace.

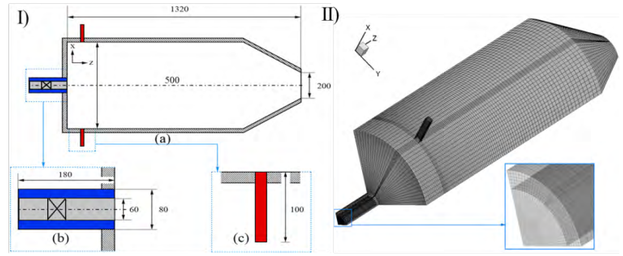


*Figure 1: I) Schematic view of the furnace-burner system: (a) the furnace; (b) the axial swirl burner; (c) particles inlet (unit: mm). II) Computational mesh*

## 3. RESULTS AND DISCUSSION

The OC proprieties used in this study are presented in table 1. A ratio of axial and tangential velocities *w/u=0.9* is introduced to give the flow the desired swirling velocity for the all cases. Four cases are studied with different excess air ratioΦ = 0.5Φ = 0.5 at atmospheric pressure, the OC mass flow rate $\dot{m}_{OC} = 0.566\ g/s$ is used to generate a power of 50 kW. The used total mass flow rates at the inlet air for each case are presented in the table 2.

*Table 1: Fuel compositions*

| **Proximate Analysis** | | **Ultimate analysis** | |
|---|---|---|---|
| Volatile Matter | 64 | Carbon (C) | 59 |
| Fixed Carbon | 23.2 | Hydrogen (H) | 8.5 |
| Ash | 6.5 | Nitogen (N) | 1.5 |
| Moisture | 6.3 | Sulphur (S) | 0 |
| | | Oxygen (O) | 31 |

*Table 2: Case details*

| Case | Exess air λ | Total air mass flow (g/s) |
|---|---|---|
| (a) | 1.7 | 8.67 |
| (b) | 2.3 | 10.18 |
| (c) | 2.7 | 11.69 |
| (d) | 3.2 | 13.87 |

Figure 2 illustrates axial velocity contours and streamlines along to the furnace for all studied cases. The flow structure takes the same behavior for all case, and it composed of two main regions. The first is the swirling jet region which locates near the center line of the furnace. The second region is the recirculation zone (RZ) which locates near the wall between the particles inlet and the converging section of the furnace. It can be seen that the size of the recirculation zone is greatly affected by the total mass flow rate of the air. When the mass flow rate of the air increases, the recirculation zone increases too, as expected in sudden expansion burners. In addition, the increase of the air mass flow rate leads to increase both negative and positive axial velocities which are related to the recirculation zones and the swirling jet region, respectively.

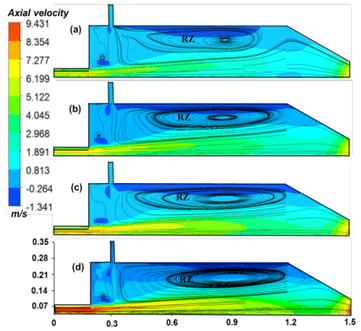


*Figure 2: Axial velocity and streamlines along the furnace for all cases in (X-Z) plan*

Temperature distributions along the furnace for different air-fuel excess ratios are shown in figure 3. The maximum temperatures are located in the shear layer regions between the recirculation zones and the swirling jet regions, which confirm the stabilization of the flame in regions where no high velocity gradient is present. The maximum temperature reached is about 1600 K, it's a common value for this type of combustion system as reported in the literature. The increase of the air mass flow rate leads to increase the flame temperature from the lowest air-fuel excess ratio case (a) to the highest air-fuel excess ratio case (d).

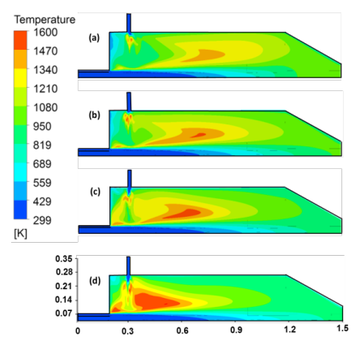


*Figure 3: Temperature distribution along the furnace for all cases*





Figure 4 presents averaged temperature and averaged $O_2$ concentration values for different air-fuel excess ratios in two transvers planes (X-Y) along the furnace Z/d=9.375 and Z/d=18.750, respectively. For both locations close to the furnace exit, the increase of the excess air ratio is accompanied with an increase of the $O_2$ concentration and a decrease of the average temperature. The OC combustion in the furnace with low excess air ratio (case (a)) provides the maximum average temperature in planes, 1071 K and 966 K at Z/d= 9.375 and Z/d=18.750 respectively. Contrary to the case (d) at high excess air ratio the average temperature reaches its minimum values in both planes. This is due to the flame position which is very close to the furnace inlet at this condition.

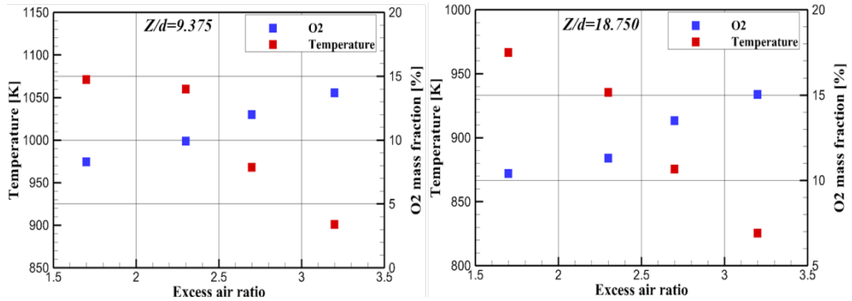


*Figure 4: Average temperature profiles and averaged $O_2$ concentration for all cases*

Figure 5 shows average mass fractions of $CO_2$ and CO combustion products at two transvers planes along to the furnace. The first plane locates at Z/d=5.625 and the second at Z/d=9.375. It is shown that more excess air decreases the emission of CO and $CO_2$ level respectively from 1.9% and 12% at λ=1.7 to 0.6 % and 9% in Z/d=5.625. In plan Z/d=9.375 distant to the reaction zone, the emission of CO and $CO_2$ decreases to a minimum values noticed in high excess air ratio (λ=3.2). Emissions of gaseous hydrocarbon compounds and CO are a result of incomplete combustion. Large emissions of CO indicate unsatisfactory combustion conditions. In the present cases, higher excess air ratio (more oxygen available) will lead to an almost complete combustion. Consequently, the maximum CO level corresponds to the lowest excess air ratio or the more fuel rich condition. As observed in figure 5 for two plans along to the furnace the maximum of CO and $CO_2$ concentration level corresponds to the lowest excess air ratio λ=1.7 and the minimum CO and $CO_2$ concentration level corresponds to the high excess air ratio λ=3.2

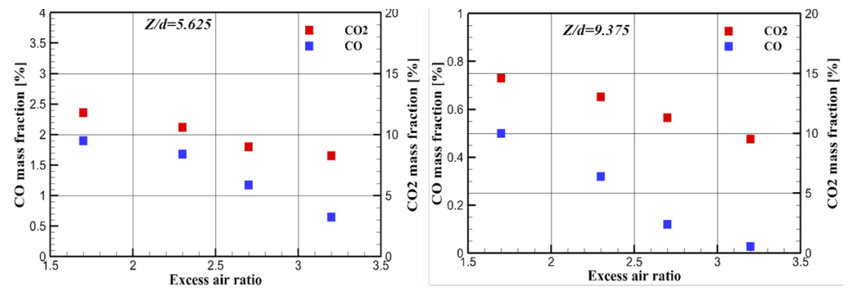


*Figure 5: Average mass fraction radial profiles of the $CO_2$ and CO for all cases*

## 4. CONCLUSION

Computational fluid dynamic investigation is performed to analyze combustion characteristics of pulverized olive cake (OC) in a 3D vertical furnace with various excess air ratios. A comparison is done between (a), (b), (c) and (d) configurations by interesting to flow structure, velocity contours, temperature distribution, $O_2$ concentration and species concentrations of CO and $CO_2$ profiles in several location along the furnace. The results show that the increase of the air mass flow rate leads to increase both negative and positive axial velocities. Consequently leads to increase the flame temperature from the lowest air-fuel excess ratio case (a) to the highest air-fuel excess ratio

case (d) and reaches a maximum value of 1600 K obtained for (d) case. It is shown that maximum CO and $CO_2$ levels correspond to the lowest excess air ratio or the more fuel rich condition. However more excess air decreases the emission of CO and $CO_2$ levels.

## 5. ACKNOWLEDGEMENTS

The authors wish to acknowledge the funding support from Region Centre Val de Loire (VERA Project)

## 6. REFERENCE

[01] M. Hogan, J. O. Sveaskog, R. M. Södra, J. Wilde, available at <http://www.europeanclimate.org/documents/biomass_report_-_final.pdf>
[02] K. A. Al-attab, Z. A. Zainal, Applied Energy. 88 (2011) 1084-1095
[03] C.Yin, A. R. Lasse, K. K. Søren, (2008). Prog. Energ. Combust., 34 (2008) 725-754.
[04] Z. Xinhui, G . Mohsen, R. Albert, Biomass bioenerg. 56 (2013) 239-246.
[05] I. S. Ravi, B. Anders, H. Mikko, Appl. Therm. Eng. 52 (2013) 585-614.
[06] G. Lu, Y. Yan, S. Cornwell, M. Whitehouse, G. Riley, Fuel 87 (7) (2008) 1133-1140
[07] T. Hüseyin, T. A. Aysel, D. Ali, Fuel 82 (2003) 1049-1056.
[08] T. A. Aysel, T. Hüseyin, Fuel, 83 (2004) 859-867.
[09] M. Rahmani, Guide des bonnes pratiques de production de l'huile d'olive: unités traditionnelles et industrielles. Institut Agronomique et Vétérinaire, Rabat, Morocco 1996. p. 36
[10] S. Leverge at <http://www.afidoltek.org/index.php/Valorisation_%C3%A9nerg%C3%A9tique_des_grignons>
[11] M. varol, A. T. Atimatay, H. Olgun, H. Atakul, Fuel 117 (2014) 792-800
[12] A. M. Eaton, L. D. Smoot, S. N. Hill, C. N. Eatough, Prog. Energy Combust. Sci. 25 (1999) 387–436
[13] ANSYS. (2012) ANSYS Fluent User's Guide Release 14.0. ANSYS. Inc, Canonsburg PA, USA.
[14] S. A. Morsi, A. J. Alexander, journal of fluid mechanics 55(2)(1972) 193-208





# Numerical analysis to study excess air ratio (EAR) effects on combustion characteristics of pulverized biomass

A. Elorf[1][2][3]*, B. Sarh[1][2], S. Bostyn[1][2], V. Belandria[1][2], T. Boushaki[1][2], I. Gökalp[1], J. Chaoufi[3]

[1] ICARE, UPR 3021 du CNRS, Université d'Orléans, France [2] Université d'Orléans IUT – 16 rue d'Issoudun Orléans Cedex 2, France
[3] LETSMP Faculté des sciences, Université Ibn Zohr, Agadir, Maroc * Abdallah.elorf@cnrs-orleans.fr

This research was supported by Région Centre, France

## I. Context

- Biomass combustion with low pollutant émissions.
- Develop an environmental friendly technology for biomass usage in energy production.

## II. Objectifs

- This work present, a numerical study of combustion in a vertical furnace with olive cake (OC) as solid fuel. The aim of this work is modeling a pulverized OC combustion with 3D approach and study the EAR effects on combustion characteristics.

## III. Olive Cake analysis

- A thermogravimetric balance is used in this work to characterize OC fuels

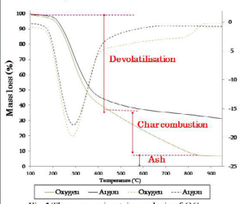


Fig.1 Thermogravimetric analysis of OC

| Proximate Analysis (Wt%, dry) -DAF | |
|---|---|
| Volatile Matter | 64 |
| Fixed Carbon | 23.2 |
| Ash | 6.5 |
| Moisture | 6.3 |
| Ultimate analysis (Wt %, dry) | |
| Carbon | 59 |
| Hydrogen | 8.5 |
| Nitogen | 1.5 |
| Sulphur | 0 |
| Oxygen | 31 |
| HHV (kJ/kg) | 21000 |

Table.1 Olive cake properties (used for CFD modeling)

## IV. Numerical simulation

### IV.1 Geometry and mesh generation

- A commercial CFD model, FLUENT 14.0 was used.
- A CFD model has been applied to combustion of pulverised olive cake in a 50 kW combustion facility.
- The 3D geometry and mesh of the furnace was developed with Gambit.

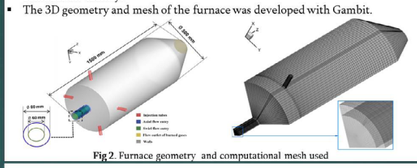

Fig 2. Furnace geometry and computational mesh used

### IV. 2 Simulation description

➢ We simultaneously compute : turbulent flow, energy transfer, P-1 radiation, PDF/mixture fraction and non-premixed combustion

- The $k$ $\varepsilon$ model was used for modeling gas phase turbulence
- The transport equations for mass and momentum are assembled and solved as a fully coupled system
- The transport equation for the P-1 approximation determines the distribution of the incident radiation throughout the domain
- The combustion simulation with the generalized finite rate chemistry model, referred to as the reacting flow with the mixture fraction PDF/equilibrium chemistry model, referred to as the PDF model is studied and calculated.

### IV. 2 Simulation description

➢ Input condition and particles proprieties

- OC are burned with different excess air, the case details studied in this work are presented in table 2.
- OC particles assumed enter the furnace with a Rosin Rammler distribution
- The trajectories of particles are computed in a Lagrangian frame / Exchange (couple) heat, mass, and momentum with Eulerian frame gas phase.

| Case details | Total air mass flow rate (g/s) |
|---|---|
| Case (a): λ=1.7 | 8.6 |
| Case (b): λ=2.3 | 10.1 |
| Case (c): λ=2.7 | 11.6 |
| Case (d): λ=3.2 | 13.8 |

Table2. Case details

| | |
|---|---|
| Olive cake flow rate (g/s) | 0.8 |
| Particle mean diameter (µm) | 70 |
| Temperature of the air (K) | 300 |
| Temperature of the injection (K) | 300 |
| Swirl number | 1.2 |

Table3. Injection conditions

## V. Simulation results

### V.1. Test methodology case

The validation of numerical model was performed by the comparison with the experimental data from Toporov et al.[1] and with numerical data from Kangwanpongpan et al.[2]

[1] Toporov, D. et al. (2008) Detailed investigation of a pulverized fuel swirl flame in CO2/O2 atmosphere. Combust. flame., 155, 605-618
[2] Kangwanpongpan, T. et al. (2012) Prediction of oxy-coal combustion trough an optimized weighted sum of gray gases model. Energy, 41, 244-251

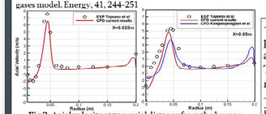

Fig.3. Axial velocity at two axial distance from the burner

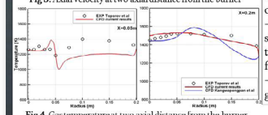

Fig.4. Gas temperature at two axial distance from the burner

-The results of the predicted radial profile of axial velocity have a good agreement with experimental data of Toporov et al.in axial sections: X=0.025 m and X=0.05 m (Fig. 5)
-In section X = 0.05 m, the comparison is carried out also with numerical results of Kangwanpongpan et al
-The temperature obtained in numerical simulation for the axial distance closest to the burner exit (X=0.05 m) differs from experimental data.
- The temperature at X=0.2 m have a good agreement with experimental data.

### V.2. Mesh study

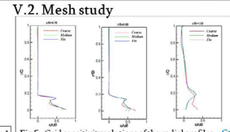

Fig 5. Grid sensitivity solutions of the radial profiles of the axial velocity at several locations

- The profiles of the coarse grid illustrate a significant difference in the location and the norm of the axial velocity peaks.
- The medium grid was chosen for all calculation in the present study.

Grid size: Fine (5460528) / Medium (3960000) / Coarse (1956384)

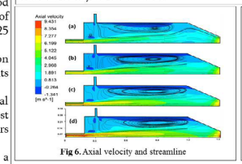

Fig 6. Axial velocity and streamline

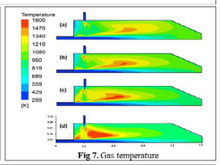

Fig 7. Gas temperature

### V.3. Results and discussion

-The increase of the air mass flow rate leads to increase both negative and positive axial velocities which are related to the recirculation zones and the swirling jet region, respectively (fig.6 ).
-The increase of the air mass flow rate leads to increase the flame temperature from the lowest air-fuel excess ratio case (a) to the highest air-fuel excess ratio case (d) (fig. 7).
- It is shown that more excess air decreases the emission of CO and $CO_2$ level respectively from 1.9% and 12% at λ=1.7 to 0.6 and 9% in Z/d=5.625. In plan Z/d=9.375 distantto the reaction zone, the emission of CO and $CO_2$decreases to a minimum values noticed in high excess air ratio (λ=3.2) (fig.8 and fig.9).

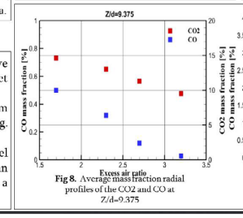


Fig 8. Average mass fraction radial profiles of the CO2 and CO at Z/d=9.375

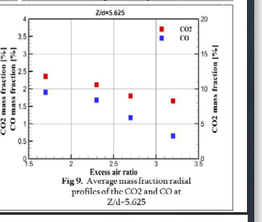


Fig 9. Average mass fraction radial profiles of the CO2 and CO at Z/d=5.625

## VI. Conclusion

Computational fluid dynamic investigation was performed to analyze combustion characteristics of pulverized olive cake (OC) in a 3D vertical furnace with various excess air ratios. The results show that the increase of the air mass flow rate leads to increase both negative and positive axial velocities. Consequently leads to increase the flame temperature from the lowest air-fuel excess ratio case (a) to the highest air-fuel excess ratio case (d) and reaches a maximum value of 1600 K obtained for (d) case. It's shown that maximum CO and $CO_2$ levels correspond to the lowest excess air ratio or the more fuel rich condition. However more excess air dilute the emission of CO and $CO_2$ levels.

# ANNEX





## The DBFZ

Organizer of the CFD-Workshop is the DBFZ Deutsches Biomasseforschungszentrum gemeinnützige GmbH.

### *Our Mission*

The DBFZ was established by the former German Federal Ministry of Food, Agriculture and Consumer Protection (BMELV) with the aim of establishing a central scientific research institution covering all the fi elds relevant to bioenergy, to bring together the findings of the highly diverse German research community in the sector. The scientific mission of the DBFZ is to support the efficient integration of biomass as a valuable resource for sustainable energy supply based on wide-ranging applied research. The mission incorporates technical, ecological, economic, social policy and energy business aspects all along the process chain, from production, through supply, to use. The DBFZ drives and supports the development of new processes, methodologies and concepts in close cooperation with industrial partners. It also maintains close links with public-sector research bodies in Germany in the agricultural, forestry and environmental sectors, as well as with European and global institutions. Working from this broad research base, the DBFZ is also tasked to devise scientifically sound decision-making aids for government policy-makers.

**DBFZ Deutsches Biomasseforschungszentrum gemeinnützige GmbH**
Torgauer Straße 116
04347 Leipzig
Phone: +49 (0)341 2434-112
Fax: +49 (0)341 2434-133
info@dbfz.de

# List of participants

| Nº | Name | First name | Institution |
|---|---|---|---|
| 1. | Dieguez Alonso | Alba | Technische Universität Berlin |
| 2. | Bujalski | Jakub | Yara International ASA |
| 3. | De la Cuesta de Cal | Daniel | Faculty of Engineering Technology CTW |
| 4. | Dernbecher | Andrea | DBFZ Deutsches Biomasseforschungszentrum gemeinnützige GmbH |
| 5. | Elorf | Abdellah | Institut de Combustion Aérothermique Réactivité et Environnement (ICARE) |
| 6. | Filipowicz | Mariusz | Akademia Górniczo-Hutnicza (AGH) |
| 7. | Gómez | Miguel | University of Vigo |
| 8. | Goryl | Wojciech | Akademia Górniczo-Hutnicza (AGH) |
| 9. | Kulkarni | Shekhar | Ghent University |
| 10. | Kwiatkowski | Kamil | Uniwersytet Warszawski |
| 11. | Mehrabian | Ramin | BIOENERGY 2020+ GmbH |
| 12. | Nakhaei | Mohammadhadi | Technical University of Denmark |
| 13. | Ortwein | Andreas | DBFZ Deutsches Biomasseforschungszentrum gemeinnützige GmbH |
| 14. | Plankenbühler | Thomas | Friedrich-Alexander-Universität Erlangen-Nürnberg |
| 15. | Roekaerts | Dirk | Delft University of Technology |
| 16. | Rudra | Souman | Universitetet for Agder |
| 17. | Schmalfuß | Silvio | Martin-Luther-Universität Halle-Wittenberg |
| 18. | Schneider | Jens | DBFZ Deutsches Biomasseforschungszentrum gemeinnützige GmbH |
| 19. | Struve | Marlen | DBFZ Deutsches Biomasseforschungszentrum gemeinnützige GmbH |
| 20. | Szubel | Mateusz | Akademia Górniczo-Hutnicza (AGH) |
| 21. | Tabet | Fouzi | DBFZ Deutsches Biomasseforschungszentrum gemeinnützige GmbH |
| 22. | Tavakkol | Salar | Engler-Bunte-Institut des Karlsruher Instituts für Technologie (KIT) |





# Scientific Committee

- Fouzi Tabet, DBFZ Deutsches Biomasseforschungszentrum gemeinnützige GmbH, Leipzig, Germany
- Andreas Ortwein, DBFZ Deutsches Biomasseforschungszentrum gemeinnützige GmbH, Leipzig, Germany
- D.J.E.M. Roekaerts, Delft University of Technology, Delft, The Netherlands
- Mariusz Filipowicz, AGH University of Science and Technology, Krakow, Poland
- Brahim Sarh, University of Orleans, Orleans, France

**Organization committee**

- Fouzi Tabet, DBFZ Deutsches Biomasseforschungszentrum gemeinnützige GmbH, Leipzig, Germany
- Katja Lucke, DBFZ Deutsches Biomasseforschungszentrum gemeinnützige GmbH, Leipzig, Germany
- Andrea Dernbecher, DBFZ Deutsches Biomasseforschungszentrum gemeinnützige GmbH, Leipzig, Germany

## Organizer:

**DBFZ Deutsches Biomasseforschungszentrum gemeinnützige GmbH**
Torgauer Straße 116
D - 04347 Leipzig
Phone: +49 (0) 341 2434-112
Telefax: +49 (0) 341 2434-133
E-Mail: info@dbfz.de
www.dbfz.de

With support from

Federal Ministry
of Food
and Agriculture

by decision of the
German Bundestag